Distribution and intensity of High-Temperature Low-Pressure metamorphism across the Pyrenean-Cantabrian belt: constraints on the thermal record of the pre-orogenic hyperextension rifting

Maxime Ducoux, Laurent Jolivet, Emmanuel Masini, Romain Augier, Abdeltif Lahfid, Matthias Bernet, Sylvain Calassou

▶ **To cite this version:**

HAL Id: insu-03428169
https://insu.hal.science/insu-03428169

Submitted on 15 Nov 2021

BSGF
Earth Sciences Bulletin

Available online at:
www.bsgf.fr

OPEN ⋑ ACCESS

Distribution and intensity of High-Temperature Low-Pressure metamorphism across the Pyrenean-Cantabrian belt: constraints on the thermal record of the pre-orogenic hyperextension rifting

Maxime Ducoux[1,*][iD], Laurent Jolivet[2][iD], Emmanuel Masini[1,3][iD], Romain Augier[4][iD], Abdeltif Lahfid[5][iD], Matthias Bernet[3][iD] and Sylvain Calassou[6][iD]

[1] M&U SAS, 3 rue des Abattoirs, 38120 Saint-Égrève, France
[2] Sorbonne Université, CNRS-INSU, ISTeP UMR 7193, 75005 Paris, France
[3] Institut des Sciences de la Terre (ISTerre), Université Grenoble-Alpes, Grenoble, France
[4] Université d'Orléans, ISTO, UMR 7327, 45071 Orléans, France
[5] BRGM, ISTO, UMR 7327, Orléans, France
[6] TOTAL SE, CSTJF, avenue Larribau, 64000 Pau, France

Abstract – Whereas a straightforward link between crustal thinning and geothermal gradients during rifting is now well established, the thermal structure of sedimentary basins within hyperextended domains remains poorly documented. For this purpose, we investigate the spatial distribution of rift-related High-Temperature Low-Pressure (HT/LP) metamorphism recorded in the preserved hyperextended rift basins inverted and integrated in the Pyrenean-Cantabrian belt. Based on Vitrinite Reflectance (R_o) data measured in 169 boreholes and more than 200 peak-metamorphic temperatures (T_{max}) data obtained by Raman Spectroscopy of Carbonaceous Material (RSCM) added to ~425 previously published T_{max} data, we propose a new map depicting the spatial distribution of the HT/LP metamorphism of the Pyrenean-Cantabrian belt. We also provide three regional-scale geological cross-sections associated with R_o and T_{max} data to constrain the distribution of paleo-isograds at depth. Based on these results, we show that the impact of rift-related metamorphism is restricted to the pre- and syn-rift sequence suggested by the depth profiles of R_o values measured in different tectonostratigraphic intervals (pre-, syn- and post-rift and syn-convergence sediments). However, a small strip of early orogenic sediments (Santonian in age) appears also affected by high temperatures along the North Pyrenean Frontal Thrust and above the Grand Rieu ridge, which we attribute to the percolation of hot hydrothermal fluids sourced from the dehydration of underthrust basement and/or sedimentary rocks at depth during the early orogenic stage. The map shows that the HT/LP metamorphism (reaching ~500 °C) is recorded with similar intensity along the Pyrenean-Cantabrian belt from the west in the Basque-Cantabrian Basin to the east in the Boucheville and Bas-Agly basins, for similar burial and rift-related structural settings. This thermal peak is also recorded underneath the northern border of the Mauléon Basin (calibrated by wells). It suggests that the high temperatures were recorded at the basement-sediment interface underneath the most distal part of the hyperextended domain. At basin-scale, we observe in the Basque-Cantabrian, Mauléon-Arzacq and Tarascon rift segments an asymmetry of the thermal structure revealed by different horizontal thermal gradients, supporting an asymmetry of the former hyperextended rift system. Using our results, we compare the Pyrénées to the Alps that also recorded hyperextension but no HT/LP metamorphic event and suggest that the high-temperature record within the basins depends on high sedimentation rate promoting a thermal blanketing effect and circulation of hydrothermal fluids.

Keywords: thermal evolution / hyperextended rifted margin / Pyrenean-Cantabrian belt / HT/LP metamorphism / RSCM Method / Vitrinite Reflectance

Résumé – Distribution et intensité du métamorphisme haute-température basse-pression de la chaîne Pyrénéo-Cantabrique : des contraintes sur l'enregistrement thermique de l'hyperextension anté-orogénique. Bien que l'association de l'amincissement crustal et de gradients géothermiques élevés

*Corresponding author: maxime@mandu-geology.fr

lors du rifting continental soit largement reconnue, la structure thermique des bassins sédimentaires dans la partie distale des systèmes de rift reste mal documentée. Pour cela, nous étudions la distribution spatiale du métamorphisme Haute-Température/Basse Pression (HT/BP) enregistrée dans les bassins préservés du système de rift hyper-aminci, par la suite inversés et intégrés dans la chaîne Pyrénéo-Cantabrique. Basé sur la réflectance de la Vitrinite (R$_o$) mesurée dans 169 puits et plus de 200 données de pic de température lié au métamorphisme (T_{max}) obtenues avec la méthode de Spectroscopie Raman de la Matière Carbonée (RSCM) ainsi que plus de 425 T_{max} provenant d'études précédentes, nous proposons une nouvelle carte de la distribution spatiale du métamorphisme HT/BP de la chaîne Pyrénéo-Cantabrique. Nous proposons également trois coupes géologiques regionales, sur lesquelles nous avons placé les données de T_{max} et de R$_o$ afin de contraindre la distribution des paléo-isogrades en profondeur. Basé sur ces résultats, nous montrons que l'impact du métamorphisme lié au rifting est restreint aux sédiments pré- et syn-rift, ce qui est suggéré par la tendance des profils des valeurs de R$_o$ en profondeur mesurées dans les différents intervalles tectonostratigraphiques (sédiments pré-, syn- et post-rift ainsi que syn-convergence). Cependant, une fine bande de sédiments syn-orogéniques (d'âge Santonien) est affectée par des températures relativement élevées au-dessus de la ride de Grand Rieu et le long du Chevauchement Frontal Nord Pyrénéen, que nous attribuons à la percolation de fluides hydrothermaux chauds provenant de la déshydratation du socle chevauché et/ou des sédiments profonds, lors du stade d'inversion précoce. La carte présentée montre que le métamorphisme (atteignant ∼500 °C) est enregistré avec la même intensité du bassin Basque-Cantabrique à l'ouest, aux bassins de Boucheville et du Bas-Agly à l'est, pour un enfouissement et un positionnement lors du rifting équivalents. Le pic thermique est également enregistré sous la bordure nord du bassin de Mauléon (calibré par des puits). Cela suggère que les hautes températures ont été enregistrées à l'interface socle-sédiments au niveau de la partie la plus distale du domaine hyper-aminci. À l'échelle des bassins, nous observons dans les segments Basque-Cantabrique, Mauléon-Arzacq et Tarascon une asymétrie de la structure thermique, révélée par différents gradients thermiques horizontaux, supportant une asymétrie de l'ancien système de rift hyper-aminci. En utilisant nos résultats, nous comparons les Pyrénées avec les Alpes qui ont également enregistré l'hyper-extension mais pas d'évènement métamorphique HT/BP, ce qui suggère que l'enregistrement des hautes températures dans les bassins dépend de taux de sédimentation élevés, favorisant un effet de couverture thermique et de circulations de fluides hydrothermaux.

Mots clés : évolution thermique / marge hyper-amincie / Pyrénées / métamorphisme HT/BP / méthode RSCM / reflectance de la Vitrinite

1 Introduction

One of the key characteristics of continental rifting is the development of hot geothermal gradients. At rift-scale, these transient thermal anomalies primarily result from the thinning of continental lithosphere under extensional tectonics (*e.g.* Buck *et al.*, 1988; Brune *et al.*, 2014; Elders *et al.*, 1972; Royden *et al.*, 1980). The observed structural variability between different rift systems is generally considered as mostly due to rifting intensity, localization and velocity with respect to the thermal conductivity of the rifted lithosphere (*e.g.* Allen and Allen, 2013; Hantschel and Kauerauf, 2009; Jolivet *et al.*, 2020; Lavier and Manatschal, 2006; Manatschal, 2004; Mohn *et al.*, 2010; Osmundsen *et al.*, 2016; Péron-Pinvidic and Manatschal, 2009; Péron-Pinvidic and Osmundsen, 2016; Sutra *et al.*, 2013). For incipient or early stages of rift systems, regional thermal predictions through time and space provided by basin modeling (*e.g.* Callies *et al.*, 2018; Lescoutre *et al.*, 2019; Nirrengarten *et al.*, 2020; Ungerer *et al.*, 1990), generally fit well the McKenzie-type pure-shear rifting models (McKenzie, 1978). Similar approaches were also applied for more mature rift cases corresponding to distal domains of hyperextended rift systems but failed to predict geological observations (Nirrengarten *et al.*, 2020; Peace *et al.*, 2017; Pross *et al.*, 2007). Unfortunately, boreholes used for these studies penetrated only basement highs and young syn-rift sedimentary units that are not documenting the syn-rift

thermal structure within deeper and thicker basins. It has been shown on both onshore and offshore records that hyper-extended domains of rifts usually display much higher and spatially variable syn-rift peak temperatures (T_{max}) in close association with indications for hydrothermal and/or magmatic processes (diagenetic, metasomatic or fluid inclusion datasets, spatial distribution of T_{max}, *e.g.* Jagoutz *et al.*, 2007; Larsen *et al.*, 2018; Manatschal, 2004; Nirrengarten *et al.*, 2020; Royden *et al.*, 1980). These observations strongly support the importance of syn-rift heat advection into distal rift domains. In this respect, the sedimentary blanket (either pre-, syn- or post-kinematic) may also strongly influence the basin thermal record by impacting fluid dynamics and therefore the advected heat (*e.g.* Callies *et al.*, 2018; Clerc *et al.*, 2015; Wangen, 1995). This is due to the petrophysical characteristics (conductivity and permeability) and spatial distribution of the sediment blanket. It is noteworthy that, so far, there is no available database describing the thermal record of a hyper-extended rift system at a sufficiently large scale (*i.e.* lithospheric scale), covering different structural domains of rifts from proximal to distal, with variable syn-rift sedimentary thicknesses and not overprinted by subsequent burial and/or tectonic phases such as lithospheric break-up, thermal and magmatic climax, or orogen-related.

At present, the alternative way to measure and describe the thermal record of lithospheric thinning and subsequent lithospheric break-up is to use fossil analogues that are
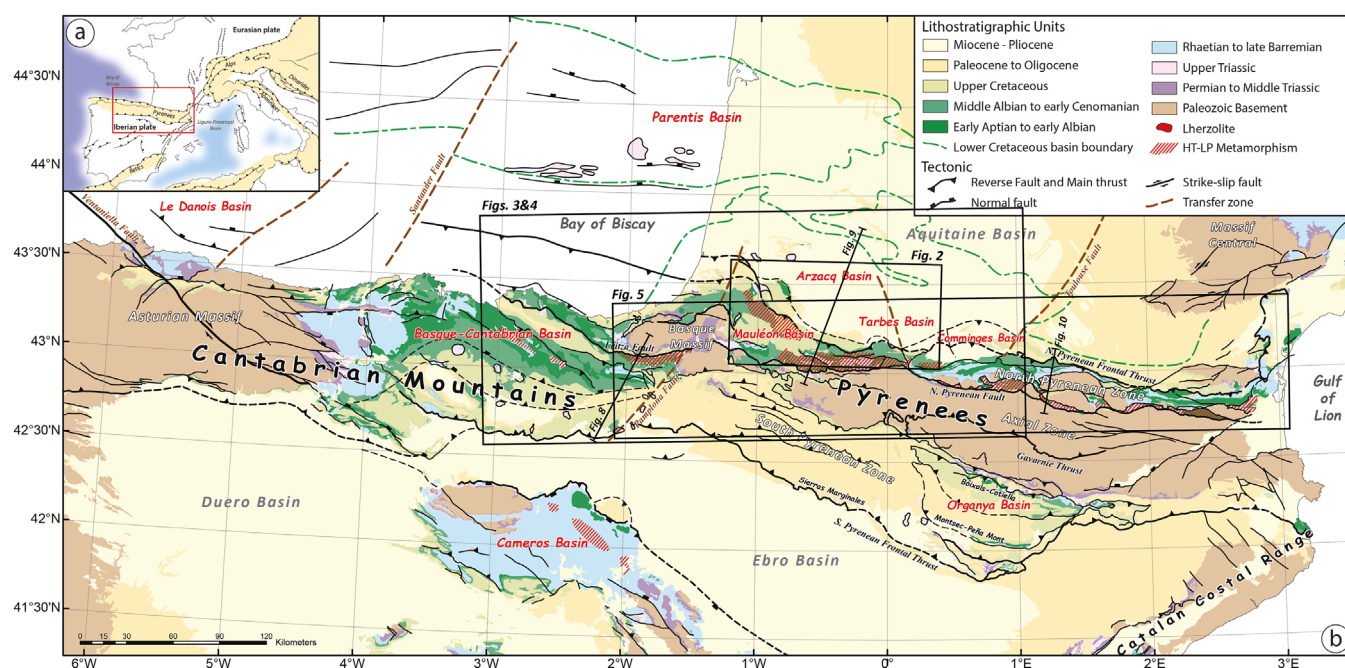
Fig. 1. Tectonic and geological framework of the Pyrenean-Cantabrian belt. (a) Main collision related geological features of the Western Mediterranean. (b) Geological map of the Pyrenean-Cantabrian collision belt (after 1 million-scale Geological Map of Spain and Geological Map of France, with RGF93 projection), with location of Figures 3 and 4.

currently cropping out in mountain belts (*e.g.* Taiwan: Conand *et al.*, 2020; Alps: Decarlis *et al.*, 2017; Gabalda *et al.*, 2009; Pinto *et al.*, 2015; Pyrénées: Clerc *et al.*, 2015; Ducoux *et al.*, 2019; Golberg and Leyreloup, 1990; Lescoutre *et al.*, 2019). This is what we intend to accomplish in this study, using the fossil Pyrenean rift record that was shown to preserve a rift-related thermal anomaly. The Pyrenean belt is an ideal candidate to study the thermal imprint of continental rifting, because: (i) this orogen is one of the typical examples of a mountain belt derived from an inverted hyperextended rift system (Clerc *et al.*, 2012, 2013; Jammes *et al.*, 2009, 2010a; Lagabrielle and Bodinier, 2008; Lagabrielle *et al.*, 2010, 2016; Masini *et al.*, 2014; Teixell *et al.*, 2016, 2018; Tugend *et al.*, 2014) and (ii) pre-and syn-rift sediments affected by HT/LP metamorphism not affected by subduction and collision metamorphic overprints. Owing to decades of industry (SNEAP, Elf Aquitaine, and TOTAL) and academic researches (*e.g.* RGF or OROGEN projects), we provide in this study a new compilation of T_{max} data documenting the spatio-temporal thermal record of hyperextension rifting across the entire Pyrenean segment of the belt. As measurements were performed on carbonaceous material coming from both surface and drillholes (Vitrinite Reflectance values and Raman Spectroscopy of Carbonaceous Material [RSCM] data), this unique dataset of a sedimentary rift system further enables to contextualize the so-called "Pyrenean HT/LP event" as well as to investigate the role of sediment burial in both time and space. Considering these results, we compare the Pyrenean-Cantabrian record to the Alps that show a generalized intense serpentinisation and brecciation of peridotites without significant HT/LP metamorphism of the syn-rift sediments. These differences are probably explained by a diversity of hyperextension architectures with variable extension rates,

the width of mantle exhumation domain and syn-rift sediment thicknesses. These various examples are thus perfect sites to study the thermal evolution of the ocean-continent transition (OCT) during hyperextension, a domain rarely attainable on present-day continental margins.

2 Geological setting

The Pyrenean-Cantabrian belt is a roughly 1000 km long fold and thrust belt, striking E-W from the Cantabrian belt in NW Spain to its eastern termination in the Pyreneo-Provençal belt in the south-east of France at the junction with the western Alps (Fig. 1a). Even though the precise Iberia-Eurasia kinematics scenario remains strongly debated (*e.g.* Barnett-Moore *et al.*, 2016; Jammes *et al.*, 2009; Neres *et al.*, 2013; Nirrengarten *et al.*, 2017; Olivet, 1996; Sibuet *et al.*, 2004; Srivastava *et al.*, 2000; Vissers and Meijer, 2012; Vissers *et al.*, 2016), it is well established that the Pyrénées first resulted from the Late Cretaceous to Miocene tectonic inversion of the former Cretaceous rifted domains (Clerc *et al.*, 2012, 2013; Jammes *et al.*, 2009, 2010a; Lagabrielle and Bodinier, 2008; Lagabrielle *et al.*, 2010, 2016; Masini *et al.*, 2014; Mouthereau *et al.*, 2014; Muñoz, 1992; Teixell *et al.*, 2016, 2018; Tugend *et al.*, 2014). Prior to the formation of the Pyrenean-Cantabrian belt, this area recorded several phases of extension after the Variscan orogeny. Post-Variscan extension was first recorded during the Permian and Triassic in the whole Western Europe by the development of several rift basins filled by continental clastic and volcaniclastic red sediments (Arche and López-Gómez, 1996; Autran and Cogne, 1980; Boillot, 1984; García-Mondéjar, 1996; Rat, 1988; Vissers, 1992; Winnock,

1974; Ziegler and Dèzes, 2006). The second event corresponds to the main divergence phase between Europe and Iberia, which occurred during Late Jurassic-Cretaceous times. In detail, two event can be differenciated (Nirrengarten *et al.*, 2018; Tavani *et al.*, 2018; Tugend *et al.*, 2015). A left-lateral transtensional rifting phase during the Late Jurassic-Early Cretaceous period mostly recorded in the Bay of Biscay and south of the Pyrénées into the Iberian Range (Boillot *et al.*, 1979; Cadenas *et al.*, 2018, 2020; Dérégnaucourt and Boillot, 1982; Ferrer *et al.*, 2008; García-Mondéjar, 1996; Jammes *et al.*, 2009; Montadert *et al.*, 1979; Tugend *et al.*, 2014, 2015). Then, a second phase of rifting, from Aptian to Cenomanian times, lead to the formation of rapidly subsiding rift basins in our study area (Brunet, 1984). Scattered exposures of sub-continental ultramafic rocks mainly reworked in or associated with Upper Triassic evaporites and/or Cretaceous syn-rift sediments (*e.g.* Clerc *et al.*, 2012, 2013; de Saint Blanquat *et al.*, 2016; DeFelipe *et al.*, 2017; Fabriès *et al.*, 1991, 1998; Lagabrielle and Bodinier, 2008; Lagabrielle *et al.*, 2016) demonstrate that this phase of rifting recorded hyperextension characterized by extremely thinned continental crust and local mantle exhumation (Asti *et al.*, 2019; Jammes *et al.*, 2009, 2010a; Lagabrielle and Bodinier, 2008; Lagabrielle *et al.*, 2010, 2019a, 2019b; Masini *et al.*, 2014; Pedrera *et al.*, 2017; Tugend *et al.*, 2014). Therefore, the Pyrenean rift systems contain pre-rift salt-bearing rocks (Mid-Upper Triassic), which are acting as a regional decoupling layer for Mesozoic extensional structures (Jammes *et al.*, 2009, 2010b; Labaume and Teixell, 2020; Lagabrielle *et al.*, 2010, 2019a, 2019b; Teixell *et al.*, 2016, 2018), and promoting salt-tectonics as well (Canérot, 1988, 1989; Canérot and Lenoble, 1993; Canérot *et al.*, 2005; Ducoux *et al.*, 2019; García-Senz *et al.*, 2019; Izquierdo-Llavall *et al.*, 2020; James and Canérot, 1999; López-Mir *et al.*, 2014; Saura *et al.*, 2016).

At variance with the Bay of Biscay that recorded breakup and an incipient seafloor spreading stage, all other rifted domains aborted at or before reaching a hyperextension stage like the Parentis Basin (Bois and Gariel, 1994; Ferrer *et al.*, 2009; Jammes *et al.*, 2010a, 2010c; Pinet *et al.*, 1987; Tomassino and Marillier, 1997), the Basque-Cantabrian Basin (DeFelipe *et al.*, 2018; Ducoux *et al.*, 2019; Lescoutre *et al.*, 2019; Pedrera *et al.*, 2017; Pedreira *et al.*, 2007; Roca *et al.*, 2011), the Cameros Basin (Casas-Sainz and Gil-Imaz, 1998; Rat *et al.*, 2019), the Columbrets Basin (Etheve *et al.*, 2018) as well as the North Pyrenean Zone (Clerc and Lagabrielle, 2014; Clerc *et al.*, 2012; Jammes *et al.*, 2009, 2010a; Lagabrielle and Bodinier, 2008; Lagabrielle *et al.*, 2010; Masini *et al.*, 2014; Tugend *et al.*, 2014) (Fig. 1). Extreme lithospheric thinning is commonly associated with a high-temperature and low-pressure (H*T*/L*P*) metamorphism referred to in this case as the Pyrenean Metamorphism (Azambre and Rossy, 1976; Bernus-Maury, 1984; Clerc and Lagabrielle, 2014; Clerc *et al.*, 2015; Dauteuil and Ricou, 1989; Ducoux *et al.*, 2019; Golberg and Leyreloup, 1990; Ravier, 1959). This H*T*/L*P* metamor-phism can be observed along E-W-striking narrow domains of the North Pyrenean Zone (NPZ) corresponding to the so-called Internal Metamorphic Zone (IMZ), in the Basque-Cantabrian Basin (BCB), and further to the south in the Cameros Basin (*e.g.* Rat *et al.*, 2019). In these domains, Mesozoic sediments recorded metamorphic temperatures up to 600 °C at pressures

as low as 4 kbar for the NPZ (Bernus-Maury, 1984; Clerc *et al.*, 2015; Golberg and Leyreloup, 1990; Vauchez *et al.*, 2013), 580 °C associated with pressure around 3–5 kbar for the BCB (Ducoux *et al.*, 2019; Martinez-Torres, 1989; Mendia and Gil Ibarguchi, 1991; Mendia, 1987), and up to 350 °C for the Cameros Basin (González-Acebrón *et al.*, 2011; Mantilla Figueroa *et al.*, 2002; Rat *et al.*, 2019). This apparent gradual increase of peak-temperature along the IMZ, from west to east is currently explained by non-cylindrical extensional defor-mation processes along the rift domain (Clerc and Lagabrielle, 2014; Clerc *et al.*, 2015). H*T*/L*P* metasediments of the IMZ also display an intense ductile foliation, first attributed to the Pyrenean collisional event (Choukroune 1972, 1976), subse-quently related to the pre-orogenic Cretaceous rifting event (Clerc and Lagabrielle, 2014; Clerc *et al.*, 2015; Golberg 1987; Golberg and Leyreloup, 1990; Lagabrielle *et al.*, 2010). The Variscan basement, cropping out in the Axial Zone and North Pyrenean Massifs was coevally affected by intense metaso-matism and magmatic albititic activity (Boulvais, 2016; 2006, 2007; Fallourd *et al.*, 2014; Pin *et al.*, 2001, 2006; Poujol *et al.*, 2010). Published geochronological data for this H*T*/L*P* metamorphic event, indicate ages ranging from Albian to Santonian (110–85 Ma) (Albarède and Michard-Vitrac, 1978a, 1978b; Casquet *et al.*, 1992; Chelalou *et al.*, 2016; Clerc *et al.*, 2015; Golberg and Maluski, 1988; Golberg *et al.*, 1986; Montigny *et al.*, 1986) among which the younger ages are coeval with the onset of Pyrenean shortening. The early stages of the tectonic inversion of the hyperextended rift system rapidly followed the end of the rifting phase during the late Santonian, with the deposition of a syn-orogenic sequence (*e.g.* Ford *et al.*, 2016; Gómez-Romeu *et al.*, 2019; Mouthereau *et al.*, 2014). This interpretation is supported by field observations in the South Pyrenean Zone (García-Senz 2002; Garrido-Megias and Rios 1972; McClay *et al.*, 2004; Mouthereau *et al.*, 2014; Muñoz, 1992; Teixell, 1998; Vergés and García-Senz, 2001; Vergés *et al.*, 1995), by seismic reflection data in the NPZ (Biteau *et al.*, 2006) and by kinematic reconstructions based on magnetic anomalies, (*e.g.* Macchiavelli *et al.*, 2017; Nirrengarten *et al.*, 2017; Olivet, 1996; Roest and Srivastava, 1991; Rosenbaum *et al.*, 2002). After a short period of tectonic quiescence during the early Paleocene (Desegaulx and Brunet, 1990; Dielforder *et al.*, 2019; Ford *et al.*, 2016; Grool *et al.*, 2018; Rougier *et al.*, 2016; Ternois *et al.*, 2019), the main collisional phase responsible for the present-day structure of the Pyrenean-Cantabrian belt occurred in Eocene-Oligocene times (Mouthereau *et al.*, 2014; Muñoz, 1992, 2002; Teixell *et al.*, 2018; Vergés *et al.*, 2002) and ended during the Chattian (Ortiz *et al.*, 2020). Thrust faults were however still active in the Southern Pyrénées until the early Miocene (Hogan and Burbank, 1996; Jolivet *et al.*, 2007; Labaume *et al.*, 2016; Millán Garrido *et al.*, 2000; Millán Garrido, 2006; Muñoz, 1992; Oliva-Urcia *et al.*, 2015; Roigé *et al.*, 2019; Teixell, 1996). After the main collisional event, the Eastern Pyrénées were affected by extensional deformation associated with the opening of the Valencia Trough and Gulf of Lion since the middle Oligocene (*e.g.* Etheve *et al.*, 2018; Gorini *et al.*, 1993, 1994; Jolivet *et al.*, 2020; Mauffret *et al.*, 1995, 2001; Roca, 2001; Roca *et al.*, 1999). The finite structure of the Pyrenean-Cantabrian belt shows an asymmetric double-verging tectonic wedge above the underthrusted Iberian continental lithosphere
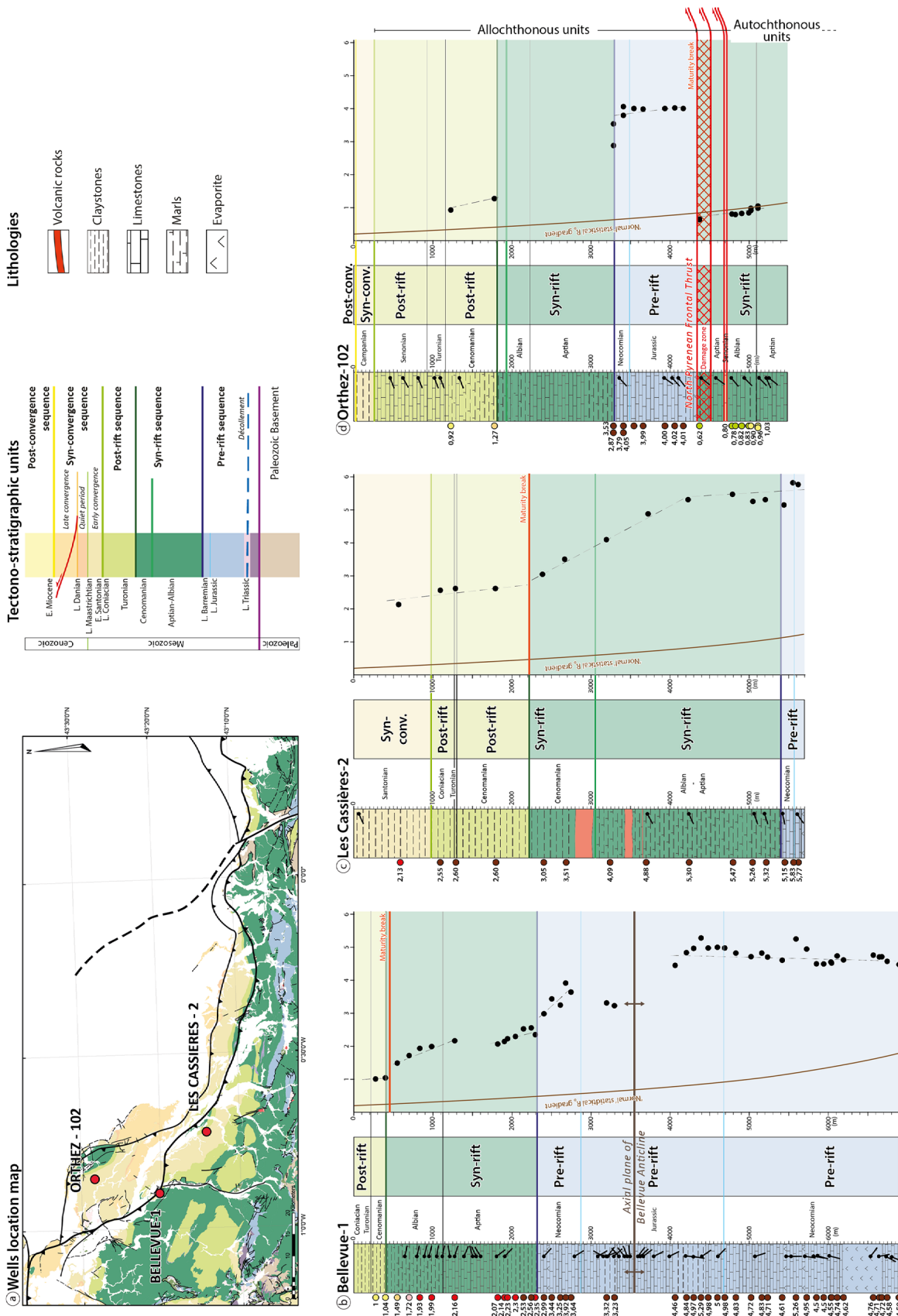
Fig. 2. Vitrine Reflectance (R_o) depth profiles along three wells located in the Western Pyrénées. (a) Geological map of the Western Pyrénées with the locations of the Les Cassières-2, Orthez-102 and Bellevue-1 boreholes. (b) Log of the Les Cassières-2 well with plotted Vitrinite Reflectance data along the depth profile. (c) Log of the Bellevue-1 well with plotted Vitrinite Reflectance and dip data along the depth profile. (d) Log of the Orthez-102 well with plotted Vitrinite Reflectance data along the depth profile. Each log is associated with graph showing the evolution of the thermal maturity of organic matter by Vitrinite Reflectance (R_o) *versus* depth. The brown curve represents the trend of R_o values related to normal statistical and steady geothermal gradient through time (Cardott and Lambert 1985). The orange line corresponds to a sharp shift of R_o data corresponding to a maturity break.

increasingly reworked by extensional tectonics toward the east (Beaumont *et al.*, 2000; Chevrot *et al.*, 2018; Jolivet *et al.*, 2020; Mouthereau *et al.*, 2014; Muñoz, 1992; Roure *et al.*, 1989; Teixell, 1998; Teixell *et al.*, 2016, 2018; Vergés *et al.*, 1995).

3 Data and methods

In order to constrain the distribution of the thermal record of the Cretaceous H*T*/L*P* metamorphism, we used two analytical methods: (i) the Vitrinite Reflectance (R$_o$) data as an indicator of the diagenetic thermal evolution of organic matter in the range of 50 to 400 °C that can be applied to areas with strong hydrothermalism and (ii) the Raman Spectroscopy of Carbonaceous Materials (RSCM) method as reliable indicator of peak metamorphic temperatures (from 200 °C until 640 °C). Except R$_o$ data obtained in boreholes, all T_{max} values are measured on rock sampled on the surface. Using finite thermal maturity data has limits, especially to determine the paleo-geothermal gradient, because T_{max} cannot be calibrated in age and depth.

3.1 Vitrinite reflectance

We provide a large set of unpublished Vitrinite Reflectance data (courtesy of SNEAP, Elf Aquitaine, and TOTAL R&D) in the Mesozoic sedimentary rocks measured in 169 wells drilled in the Western Pyrénées, including the Basque-Cantabrian, Mauléon, Arzacq and Tarbes basins (Figs. 2–4). Vitrinite Reflectance (R$_o$) analysis is the most commonly used organic indicator of thermal maturity in low to very low grade metasediments. It is generally used for oil-exploration in order to determine source-rock thermal maturity and maximum temperature (T_{max}) recorded in sedimentary rocks (Taylor *et al.*, 1998). In this study, we used the maturity evolution of R$_o$ values in boreholes along depth profiles to provide vertical constraints on the relative thermal maturity experienced by rocks from different tectono-stratigraphic levels. In order to fit with RSCM data calculated in this study, we provide a conversion of the Vitrinite Reflectance values to relative T_{max} based on the formulas published by Barker and Pawlewicz (1994) applied for hydrothermal metamorphism (Tab. S1–S4), but we also provide relative T_{max} calculated with formulas applied for classical burial heating. The formula for hydrothermal metamorphism is probably more appropriate for rift-related H*T*-metamorphism because heat seems not only produced by burial. Therefore, we used the formula for hydrothermal metamorphism in pre- and syn-rift sediments located in the NPZ, but we used the formula for burial heating in post-rift, syn- and post-convergence sediments. Evidence for intense metasomatism has been actually reported for both the sediments and basement rocks of the NPZ (*e.g.* Clerc *et al.*, 2015). For the Aquitaine Basin, only the formula for burial heating is used. However, it should be acknowledged that this conversion is informative and does not represent absolute temperature values as the T_{max} obtained with RSCM. It should be further noticed that we will use the Vitrinite Reflectance data in a comparative way, both vertically and laterally to discuss the time and space distribution of the H*T* event across the Pyrénées. For the purpose the Vitrinite Reflectance value to temperaure conversion itself is not a major issue.

3.2 Raman spectroscopy

Raman spectroscopy analyses were all performed using a Renishaw (Wotton-under-Edge, UK) InVIA Reflex micro-spectroscope at the BRGM (French Geological Survey) in Orléans equipped with a 514 nm Spectra Physics argon laser in circular polarization. The laser was focused on the sample by a DMLM Leica (Wetzlar, Germany) microscope with a 100× objective (NAD 0.90). The Rayleigh diffusion was eliminated by edge filters and the signal was dispersed using a 1800 g/mm grating before being analysed by a Peltier-cooled RENCAM CCD detector. Measurements were performed *in situ* on polished thin sections cut normal to the main planar fabrics and parallel to the stretching lineation when present (XZ structural planes). To avoid polishing induced damage, CM particles were systematically analyzed below a transparent adjacent mineral, usually calcite or quartz (Beyssac *et al.*, 2002b; Pasteris, 1989; Scharf *et al.*, 2013). Ten to twenty-five points were measured for each sample with 10 to 15 accumulations of 10 seconds acquisition periods. The measured Raman spectra of the carbonaceous material were decomposed for all Raman peaks of carbon by using the PeakFit (v4.06) software (Systat Software Inc®).

This analytical method allows to characterize the structural evolution of carbonaceous material (CM), reflecting a transformation from disordered to well-ordered CM during a metamorphic event (Wopenka and Pasteris, 1993). The irreversible reorganization and polymerization of these materials is reflected in their Raman spectrum by the decreasing width of the graphite G band and the gradual disappearance of the defect bands, first D3 and D4, then D1 and D2. The Raman spectrum of well-ordered CM (perfect graphite) contains only the G band. The link between this increasing graphitization and temperature was quantified, leading to a tool to determine peak temperatures attained by metamorphic rocks (Beyssac *et al.*, 2002a). Since graphitization is an irreversible process, the RSCM method gives the peak metamorphic temperatures (Beyssac *et al.*, 2002a; Pasteris and Wopenka, 1991). This is the basis of the RSCM geothermometer, which was calibrated in the range between 330 and 640 °C by Beyssac *et al.* (2002a). Due to uncertainties related to petrological data used for calibration, the RSCM geothermometer has an absolute precision of ±50 °C. Considering a range of measurements, the relative uncertainties on temperature are limited, around 10–15 °C (Beyssac *et al.*, 2004), allowing accurate estimation of field thermal gradients (Bollinger *et al.*, 2004). The RSCM calibration established by Beyssac *et al.* (2002a, 2002b) was extended towards low temperatures in the range of 200–330 °C with an absolute precision of ±25 °C (Lahfid *et al.*, 2010).

This geothermometer has been applied on 208 thin sections, sampled in Paleozoic to Upper Cretaceous carbonates and pelitic rocks, in order to characterize the distribution of the recorded peak metamorphic temperatures (T_{max}) in the study area. All results are presented in Table S5 (see Supplementary material) and Figures 5–7. A systematic sampling was performed in the metamorphic units to complete the previous H*T*/L*P* metamorphism map provided by Clerc *et al.* (2015).

4 Thermal record of Cretaceous rifting in the Pyrenean-Cantabrian belt

In addition to $425\,T_{max}$ measurements from previous studies focused on the H*T*/L*P* metamorphism, we provide in this paper 208 new T_{max} across the Pyrenean-Cantabrian belt, from the Basque-Cantabrian Basin to the west to the Bas-Agly syncline to the east. Twenty were measured in Paleozoic rocks and 188 in Mesozoic metasediments. Syn- to post-rift outcropping rocks in the Western Pyrénées seems to be colder (Clerc *et al.*, 2015; Saspiturry *et al.*, 2020). As they are only discriminant for the rocks exposed today at the surface, we used 169 measurements of Vitrinite Reflectance from boreholes to get insights on the vertical T_{max} evolution in this area. Gathering both of the surface and subsurface data allow to propose a new isometamorphic map as well as sections related to former rift basins, which shows the imprint of the paleothermal regime.

4.1 Thermal maturity measured with vitrinite reflectance

In this study, we used a large data set of vitrinite reflectance values collected over several decades of petroleum exploration and provided by TOTAL R&D (Tabs. S1–S4). These data are from samples mainly collected in the north Pyrenean foreland, especially in the Aquitaine Basin and the north-western part of the North Pyrenean Zone. In order to describe the thermal maturity of the pre- and syn-rift sediments which are not oucroping in the Western Pyrénées, we used the depth evolution of thermal maturity depth profile of the area along three key boreholes: Bellevue-1, Les Cassières-2 and Orthez-102 wells (Figs. 3 and 4). The observations performed along these wells were then generalized to the Western Pyrénées with a series of maps of vitrinite reflectance values for each tectono-stratigraphic unit from rifting (pre-, syn- and post-rift) to the subsequent collision (early- and late-convergence sequences).

4.1.1 Thermal maturity of organic matter along depth profiles

Bellevue-1, Les Cassières-2 and Orthez-102 boreholes, used as examples for describing the thermal maturity of organic matter along depth profiles and are consistently reaching the pre-rift layers. It should be noticed that, considering the thickness and nature of the syn-rift strata they penetrated, they are also respectively representing a distal to proximal trend on the northern side of the Mauléon Basin until the Arzacq Basin further north (Fig. 2). From both surface and subsurface data, this area is described as the highest thermal maturity area of the former hyperextended rift system in the Mauléon Basin (Lescoutre *et al.*, 2019).

The Bellevue-1 well is located within the northern Mauléon Basin and corresponds to the more distal palaeogeographic position (Fig. 2a). The post-/syn-rift boundary is documented by this well at 210 m in depth and the well reached the pre-rift successions at about 2300 m (Fig. 2b). Average R_o values measured in the post-rift deposits are about ~1%. Using the two formulas for burial heating and hydrothermal metamorphism of Barker and Pawlewicz (1994), such a R_o corresponds respectively to temperatures of ~135 °C eq (with burial heating formula) and of ~150 °C eq (with hydrothermal metamorphism formula, see Table S2). The maturity trend of organic matter shows a break across the post-rift and the top of syn-rift sediments with R_o values that slightly increased from 1.0 to 1.49%. From this maturity break, R_o values increase in depth from 1.49 to 2.56% (~200 to ~275 °C eq) until the base of the syn-rift sediments reached at 2320 m in depth at the exception of the central part of the well where a relative stability is recorded (likely due to a post-deposition deformation as it coincides with a change in the sedimentary bedding). Downsection, the pre-rift sediments starting with the Neocomian deposits were penetrated until the end of the borehole at 6909 m in depth. In the upper part, R_o values rapidly increase from 2.99 to 3.64% (~290 to ~325 °C eq) between 2400 to 2700 m depth. After a lack of data with only two lower R_o values (~3.30%) between 2875 to 4000 m depth, R_o displays a roughly constant trend ranging between 4.46 to 5.26%, corresponding to equivalent temperatures between 343 and 364 °C eq (Table S2). This gradient shift between 3300 to 4000 m depth starts from the axial plane of the Bellevue anticline revealed by dip directions (Fig. 2b). Then, the constant R_o trend in depth until the base of the well correspond to the steeply dipping limb of the Bellevue fold. In addition of the bedding, the fact that the same stratigraphic level (Barremian) was drilled along more than 2300 m in depth is further indicating this structural setting. As the R_o trend is following the bedding, this well further reveals that the thermal imprint was recorded before the folding at this location. This vertical stratigraphic level is consistent with the constant value of R_o along depth profile.

As for the Bellevue-1 borehole, Les Cassières-2 well is located within the northern Mauléon Basin corresponds to a less distal palaeogeographic position compared to the Bellevue-1 well (Fig. 2a). In details, the Les Cassières-2 borehole penetrated the early convergence, post- and syn-rift units and reached the Lower Cretaceous (Neocomian) pre-rift sediments at 5692 m depth (Fig. 2c). The thermal maturity is relatively high in this well, even in the earliest syn-convergence Santonian sediments with R_o values of 2.13%, corresponding to a temperature of ~200 °C eq (with burial heating formula, Table S1). It is noteworthy that RSCM measurements and the burial heating formula yield the same evaluation as a T_{max} in this area (Saspiturry *et al.*, 2020). From a petroleum system point of view, this value further indicates that the gas window was reached at this stratigraphic level (Tissot and Welte, 1984). Going downsection, R_o values slightly increased from 2.55 to 2.6%. These R_o recorded in the post-rift sequence are significantly higher than the equivalent measurements of the Bellevue-1 as the corresponding temperature (with burial heating formula) would be in the order of ~210 °C eq (Table S1). At 2200 m depth, maturity evolution rapidly increased, indicating an important break in the trend of maturity as R_o values rapidly increased from 3.05% (~300 °C eq) at 2400 m up to 5.30% (>350 °C eq) at 4200 m (Fig. 2c). Even though absolute values recorded in Les Cassières-2 well differ from the Bellevue-1 well, their vertical trends are similar and show the same maturity break at the top of the syn- to post-rift boundary (Cenomanian). From 4200 m downward, the lower part of the syn-rift sequence shows an

inflection break in the maturity trend which is almost stable until reaching the pre-rift cover. Then, R_o values are increasing to values ranging from 5.15 to 5.83% (∼360 to ∼380 °C eq) across the drilled pre-rift successions. At the scale of the entire well, this vertical trend of R_o values does show significant variations while the sedimentary bedding is constantly gently dipping southwards (Fig. 2c). It should be further noticed that it significantly diverges from a theoretical burial-related record as shown by the expected trend for a stable 30 °C/km geothermal gradient (brown curve in Fig. 2c, Cardott and Lambert 1985). We therefore conclude that the thermal record cannot be explained by the sedimentary burial only. Accounting for similar sedimentation rates between syn- and post-rift times (∼1 km/10 My), this shift between our observations and a constant thermal model therefore suggests a high syn-rift paleo-thermal gradient until post-rift times in this area. As R_o values within the syn-rift sediments systematically exceed the value of 3%, they indicate that the coalification of the organic matter reached the level of meta-anthracites and semi-graphite indicative for metamorphic conditions.

Compared to the above-described Les Cassières-2 and Bellevue-1 boreholes, the Orthez-102 borehole is located further north corresponding to a more proximal structural setting in respect of the rift palaeogeography. It actually penetrated a duplicated stratigraphy on each side of the south-dipping North Pyrenean Frontal Thrust (Fig. 2d). The drilled upper unit (hanging-wall) corresponds to a thin post-convergence sequence overlying the syn-convergence, post- and syn-rift sediments and terminated within the pre-rift strata. Paleo-geographically, this hanging-wall unit is derived from the northern margin of the Mauléon Basin. Beneath the North Pyrenean Frontal Thrust, the Orthez-102 well penetrated the autochthonous syn-rift sediments at ∼4500 m depth until 5489 m deep (Fig. 2d). Despite a lack of data in most of the syn-rift strata of the upper unit, the vertical interpolation of the data at the top and the base of the syn-rift strata suggests a roughly similar vertical maturity trend as in the Les Cassières well. Indeed, the measured R_o values range between 0.92 and 1.27% in the post-rift strata (late Cenomanian, Fig. 2d), which correspond respectively to temperatures of ∼130 and ∼155 °C eq (Table S3) and the R_o values of the pre-rift strata ∼1.3 km deeper are between 2.87 and 4.05% (287 to 331 °C eq). Most likely because of the lack of data, the thermal maturity break observed within the Les Cassières-2 and Bellevue-1 wells cannot be observed in the allochthonous syn-rift unit of the Orthez-102 well even though the underlying pre-rift sediments reached similar thermal maturities (Fig. 2d). In the footwall of the North Pyrenean Frontal Thrust, from 4350 m depth and deeper, in the maturity trend recorded by the autochthonous syn-rift units shows a signifantly steeper slope than within the hanging wall with values increasing downward from 0.62 to 1.03% (∼95 to 140 °C eq). It should be further noticed that these values show the same trend as the brown curve which represents the normal statistical R_o gradient for a normal burial-related thermal gradient of 30 °C/km. This indicates that the thermal maturity of organic matter in the autochthonous unit did not recorded a high-temperature event and therefore differs from the thermal record of the neighboring Mauléon Basin.

4.1.2 Mapping the thermal maturity of organic matter within each tectono-stratigraphic unit

Thermal maturity data obtained from the three previously described boreholes provide key information on the intensity, the vertical (*i.e.* timing) and spatial distribution of the HT Pyrenean event recorded mainly within the pre-rift and until the middle part of syn-rift sediments. With this information, we compare mean R_o values from 169 wells (Table S4) where thermal maturities were analyzed, for each tectonostratigraphic layer of the Western Pyrénées (pre-, syn-, and post-rift as well as early- and late convergence deposits). This comparison is illustrated in five maps showing the values for the different stratigraphic levels (Figs. 3 and 4).

Mean R_o values for the pre-rift unit were measured in Upper Triassic-Barremian sediments (Fig. 3a). Pre-rift sediments were affected by the rift-related and the subsequent convergence-related tectono-thermal events. Their thermal maturities were abundantly documented by R_o measurements. From this dataset, distinctive tectono-thermal domains can be identified within the NPZ and further west in the Basque-Cantabrian Basin. The northern Mauléon Basin systematically shows high thermal maturity with a range of mean R_o between 3 to 5.60%, corresponding to estimated temperatures between 300 and 370 °C eq, indicating that these rocks underwent metamorphic conditions (Tissot and Welte, 1984). Similar to the Mauleon Basin, the western part of the Basque-Cantabrian Basin shows very high thermal maturity of the organic matter for the pre-rift units located along its northern side. It should be however acknowledged that only a few measurements are available (Robert, 1971) with R_o values exceeding 6–7% corresponding to temperatures above 400 °C eq. Further east, along the Pamplona transfer zone, the thermal maturity remains significantly high with a R_o of 3.5% (Fig. 3a). However, further east across the pamplona transfer zone (*i.e.* South Pyrenean Zone), the thermal maturity of the pre-rift units, significantly decreases with R_o values <1%, suggesting an estimated temperature lower than ∼130 °C eq. Therefore, the high-temperature domain is restricted to the eastern Basque-Cantabrian Basin on the western side of the Pamplona transfer zone. Concerning the Aquitaine foreland Basin further to the NE, we define in its southern part an area of moderate to high thermal maturity with mean R_o values ranging between 1.09 and 3.56%. This area concerns the Arzacq Basin which was intensively drilled for petroleum exploration and has also recorded the Cretaceous rifting (Biteau *et al.*, 2006; Brunet, 1984). Further east, the Comminges Basin shows the same range of R_o values. Farther north, the pre-rift strata of the rest of the Aquitaine foreland shows a contrasting lower thermal maturity with R_o <0.9%.

As for the pre-rift, the map of mean R_o values for the syn-rift units (Aptian-Cenomanian) (Fig. 3b), shows the same spatial distribution of thermal maturities with slightly lower R_o values, except in the Comminges Basin where measured R_o values of the syn-rift unit are higher than in the pre-rift units.

The map of mean R_o values for the post-rift unit is restricted to few measurements in Turonian-Coniacian sediments acquired in the Mauléon and Comminges basins (Fig. 3c). These sediments were deposited after the end of rifting during the post-rift thermal relax. The northern part of the Mauléon Basin shows a moderate to high thermal maturity
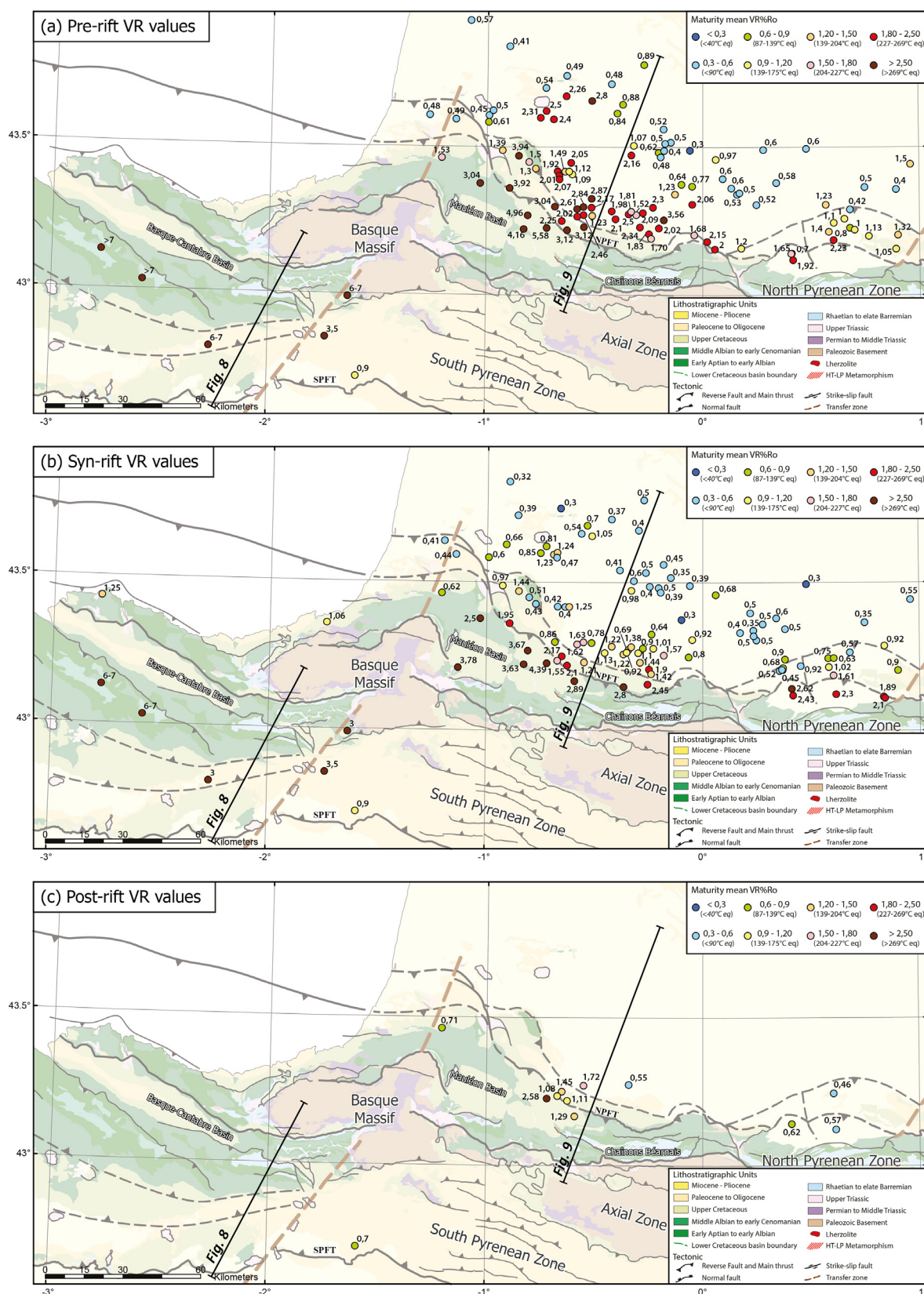
Fig. 3. Maps displaying the spatial distribution of R$_o$ data for each rift-related tectono-stratigraphic unit. (a) Average R$_o$ values measured in pre-rift sediments (Triassic to Barremian). (b) Average R$_o$ values measured in syn-rift sediments (Aptian to Cenomanian). (c) Average R$_o$ values measured in post-rift sediments (Turonian to Coniacian).
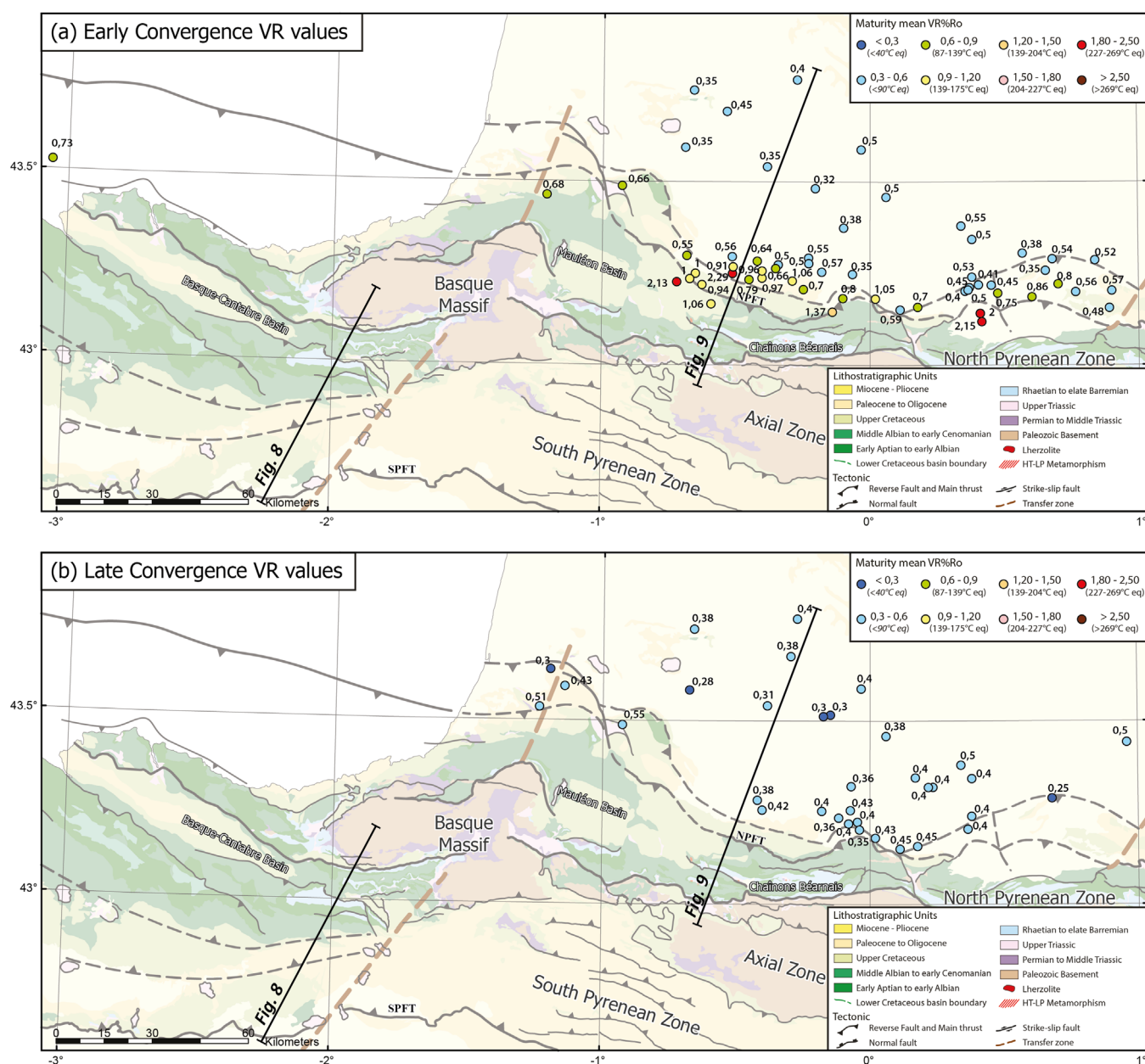
Fig. 4. Maps displaying the spatial distribution of R$_o$ data for each convergence-related tectono-stratigraphic unit. (a) average R$_o$ values measured in early-convergence sediments (Santonian to Maastrichtian). (b) average R$_o$ values measured in later-convergence sediments (Danian to Chattian).

of the post-rift unit with an average R$_o$ of 1.30% (~155 °C eq) and a higher value of 2.58% (~210 °C eq). R$_o$ is 0.71% in the western part of the Mauléon Basin, indicating a low thermal maturity of syn-rift sediments for this area that can be linked to a more limited sedimentary burial (Lescoutre and Manatschal, 2020). The Arzacq Basin located north of the North Pyrenean Frontal Thrust, and the Comminges Basin eastwards both show R$_o$ values <0.62 which indicate a low thermal maturity in these areas for the post-rift event. Similar values are recorded east of the Basque-Cantabrian Basin with R$_o$ of 0.7%.

Mean R$_o$ values for the early convergence unit is derived from measurements within the Santonian-Maastrichtian sediments (Fig. 4a). This period corresponds to the onset of inversion of the hyperextended rift system (Gómez-Romeu *et al.*, 2019). Two tectono-thermal domains can be distinguished based on the R$_o$ data. The first one represents an area with very low-grade thermal maturity with values of R$_o$ <1% indicating estimated temperatures <150 °C eq. This area is restricted to the Aquitaine foreland Basin and is limited in the south by the North Pyrenean Frontal Thrust. The second domain located further south, corresponding to the Mauléon Basin and

the NPZ, shows relatively higher R_o values exceeding 1% with a maximum value of 2.29% ($\sim$260 °C eq). These values are roughly similar to the underlying post-rift mean R_o values.

Mean R_o values for the late convergence unit (main orogenic collisional phase) is derived from the measurements within Paleocene-Eocene deposits (Fig. 4b). R_o is relatively constant in the overall late-convergence unit with values ranging between 0.28 to 0.51%. This range of R_o indicates estimated temperatures <60 °C eq, corresponding to very low thermal maturities reaching during the main collisional phase of orogeny despite of the sedimentary and tectonic burial.

4.2 Distribution of H*T*/L*P* metamorphism-related peak temperature of the Pyrenean-Cantabrian belt

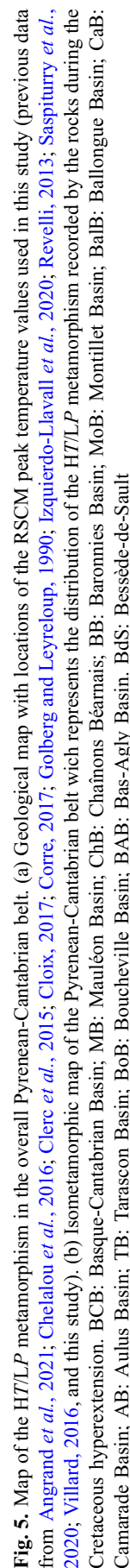### 4.2.1 Mapping the peak-temperatures using RSCM geothermometry

Using the RSCM geothermometer, we provide a rift-related maximum peak-metamorphic temperature map (Fig. 5). This map displaying different tectonostratigraphic units was built with 633 T_{max} from our dataset from which 208 are unpublished so far, in addition of 425 from the literature (Angrand *et al.*, 2021; Chelalou *et al.*, 2016; Clerc *et al.*, 2015; Cloix, 2017; Corre, 2017; Ducoux *et al.*, 2019; Golberg and Leyreloup, 1990; Izquierdo-Llavall *et al.*, 2020; Revelli, 2013; Saspiturry *et al.*, 2020; Villard, 2016). Most of the measurements were obtained by the analysis of sedimentary successions of the IMZ from the Basque-Cantabrian Basin in the west until the Agly area in the east (Fig. 5a). Some additional measurements were also retrieved using the Paleozoic metasediments belonging to the upper crustal basement rocks in respect of the Mesozoic rift history. In previous studies (Clerc *et al.*, 2015; Golberg and Leyreloup, 1990), the eastern part of the IMZ was considered to record the highest metamorphic conditions compared to the Central and Western Pyrénées. Actually, even though the Boucheville and Bas-Agly basins yielded a range of T_{max} values between 500 to 600 °C within the pre- and syn-rift sediments (Chelalou *et al.*, 2016; Clerc *et al.*, 2015; Golberg and Leyreloup, 1990). Such a range of T_{max} was also recorded farther west, close to the Bessède-de-Sault Paleozoic massif (>550 °C), within the southern margins of the Tarascon Basin (>600 °C), in the Aulus Basin where T_{max} exceed 600 °C and in the Montillet Basin where the mean T_{max} exceeds 550 °C (Fig. 5a). In more details, the Aulus and Tarascon basins from the Central Pyrénées show a range of T_{max} between 500 and 630 °C, within their pre- and syn-rift sediments. In this central part of the Pyrénées, the maximum values are generally obtained along the southern side of the North Pyrenean Zone within the Aulus Basin in close association with mantle rocks (*e.g.* Lherz, Clerc *et al.*, 2012; Bestiac: de Saint Blanquat *et al.*, 2016). A thermal break is observed in the post-rift sequence located along the southern edge of the North Pyrenean Fault (in red in Fig. 5a) with T_{max} generally $\sim$350 °C. Northwards, the northern margin of the Tarascon Basin lower moderate T_{max} $\sim$350 °C for the same stratigraphic levels at the interesting exception of the $\sim$570 °C yielded by an Upper Triassic pre-rift outcrop. The Trois-Seigneurs Paleozoic massif located between the Aulus and Tarascon basins consists in a rift palaeo-high as its basement is directly covered by post-rift sediments. These sediments yielded much lower temperatures <200 °C than the surrounding Aulus and Tarascon rift-related troughs (Fig. 5a). It was reported that the Camarade Basin located further north beyond the Arize massif did not recorded the H*T* metamorphic event (Clerc *et al.*, 2015). However, the analysis its pre- and syn-rift sediments contrasts with these interpretations as it provided T_{max} measurements ranging between 230 to 330 °C. Such a thermal record cannot be reported from the syn-convergence strata located north of the North Pyrenean Frontal Thrust where T_{max} were systematically lower than <200 °C.

Further west, there is a lack of data in most of the Ballongue Basin until its western border corresponding to Milhas-Arguenos area. There, measured T_{max} are similar to those observed in the Aulus Basin and are bracketed between 420 and 605 °C (Fig. 5a). As for the Aulus and eastern Tarascon basins this area of high T_{max} is characterized by several mantle outcrops (see Clerc *et al.*, 2012; de Saint Blanquat *et al.*, 2016; Lagabrielle *et al.*, 2010 for more information).

Some tens of kilometers to the west, our results show that the Montillet Basin located between the Axial Zone and the Barousse Massif does show T_{max} values among the highest reported from the Pyrénées (up to 625 ± 17 °C, Fig. 5a). The pre- and syn-rift sediments from the entire basin shows a range of T_{max} between 480 and 625 °C. South of the Montillet Basin beyond the North Pyrenean Fault, recorded T_{max} from post-rift sequences abruptly decrease under 330 °C, with values of 321 ± 6 and 317 ± 4 °C (Fig. 5a). North of the Montillet Basin within the Barronies Basin, the syn-rift sequence recorded a lower H*T*/L*P* metamorphism (314 ± 20 to 477 ± 29 °C, Fig. 5a). From the western border of the Montillet and Baronnies basins westwards, T_{max} values from the outcropping pre- and syn-rift sequences of the Western Pyrénées are globally decreasing. T_{max} measured in the Chaînons Béarnais area consistently range from 310 to 390 °C, except along the North Pyrenean Fault within pre-rift sediments where T_{max} values often exceed 430 °C and can even reach locally T_{max} >500 °C (Fig. 5a). It should be noticed that T_{max} are increasing in the vicinity of mantle outcrops with values exceeding 400 °C, except for the Saraillé and Urdach outcrops (Clerc *et al.*, 2015; Corre, 2017). T_{max} are also consistently higher within pre-rift sequence than in younger deposits as shown by the Tres Crouts area, located in the eastern Chaînons Béarnais (see Labaume and Teixell, 2020; Villard, 2016), with values ranging between 420 and 500 °C (Fig. 5a). Westwards, calculated T_{max} decrease under 300 °C in the central part of the Mauléon Basin even reaching values under 200 °C along its southern margin (Fig. 5a).

On the western side of the Basque Massifs, the pre- and syn-rift cover of the eastern Basque-Cantabrian Basin, corresponding to the Nappe des Marbres unit, is also affected by the H*T*/L*P* metamorphism (Fig. 5a). From this point of view, this basin constrasts with the neighbouring Mauléon Basin as it shows T_{max} ranging from 250 to 580 °C. Similarly to the Tarascon Basin located in the Central Pyrénées, the eastern Basque-Cantabrian Basin recorded a thermal N-S asymmetry. It should be however noticed that they are opposite in direction as higher T_{max} values are located along its northern border along the Leitza Fault and decrease southward until 250 °C. It is interesting to note that here again highest temperatures were likely associated with mantle rocks as reported by DeFelipe *et al.* (2017). See more details below.

Fig. 5. Map of the H*T*/L*P* metamorphism in the overall Pyrenean-Cantabrian belt. (a) Geological map with locations of the RSCM peak temperature values used in this study (previous data from Angrand *et al.*, 2021; Chelalou *et al.*, 2016; Clerc *et al.*, 2015; Cloix, 2017; Corre, 2017; Golberg and Leyreloup, 1990; Izquierdo-Llavall *et al.*, 2020; Revelli, 2013; Saspiturry *et al.*, 2020; Villard, 2016, and this study). (b) Isometamorphic map of the Pyrenean-Cantabrian belt wich represents the distribution of the H*T*/L*P* metamorphism recorded by the rocks during the Cretaceous hyperextension. BCB: Basque-Cantabrian Basin; MB: Mauléon Basin; ChB: Chaînons Béarnais; BB: Baronnies Basin; MoB: Montillet Basin; BalB: Ballongue Basin; CaB: Camarade Basin; AB: Aulus Basin; TB: Tarascon Basin; BoB: Boucheville Basin; BAB: Bas-Agly Basin. BdS: Bessède-de-Sault

4.2.2 Metamorphic gaps and limits of the H*T*/L*P* metamorphic domain

All of the $T_{\max}$ dataset presented in this paper is used and interpolated to build a regional isometamorphic map to display the spatial distribution of the rift-related H*T*/L*P* metamorphism (Fig. 5b). One of the main striking information that can be inferred from this map is that the metamorphic domain is continuously recorded across the entire belt. Based on different N-S distributions, we will however distinguish the Eastern/Central Pyrénées from the Western/Basque Cantabrian Pyrenean records. In the Eastern and Central Pyrénées first, we show that the highest $T_{\max}$ values (between 450 to 630 °C) were indifferentially collected along the IMZ from the Montillet Basin in the Central Pyrénées until the Boucheville Basin in the eastern termination of the belt. The southern part of the IMZ is consistently bearing the highest $T_{\max}$ values (>500 °C) and is sharply separated from the much colder late syn- to post-rift record of the Axial Zone (<350 °C) by the North Pyrenean Fault (red line in Fig. 5). Some higher $T_{\max}$ exceeding 350 °C were obtained from the Paleozoic basement rocks underneath the colder Mesozoic cover suggesting that it may be inherited from the Late Variscan regional metamorphism.

It is commonly assumed that the northern border of the IMZ is limited by the North Pyrenean massifs (Clerc *et al.*, 2015). However, it arises from our dataset that the metamorphism is actually strongly recorded within the Bas-Agly syncline and more moderately within the Camarades and Baronnies basins. Within the Bas Agly syncline, the metamorphic imprint is of the same order than in the Boucheville Basin with $T_{\max}$ exceeding 450 °C (*e.g.* Ducoux *et al.*, 2021a). This is the Bas-Agly north-directed basal thrust that marks the northern limit of the H*T*/L*P* metamorphism from which with $T_{\max}$ are lower than 250 °C. Even though the Camarades and Baronnies basins are in a similar structural situation than the Bas Agly syncline, the recovered Tmax values seem to show a less intense metamorphism. However, they are documenting the shallowest part of the syn-rift record from which the deeper levels are not described so far (Espurt *et al.*, 2019). Consequently, $T_{\max}$ measured at the surface may not reflect metamorphic conditions at the base of this basin.

In the Western Pyrénées, the westward lateral extension of the metamorphic domain is bounded by the North Pyrenean Frontal Thrust. The Chaînons Béarnais area and its equivalent and less deformed Mauléon Basin are less pervasively affected by Pyrenean deformations. The eastern part of the Chaînons Béarnais only is limited from the Axial Zone by the westward continuation of the North Pyrenean Fault. This major structure is actually replaced by the south-vergent thrust Lakhora thrust in the rest of the area that marks the new structural and thermal boundary of the IMZ with the Pyrenean Axial Zone (*e.g.* Labaume and Teixell, 2020; Teixell *et al.*, 2016). Towards the north, there is no outcropping equivalent of the North Pyrenean Paleozoic massif until the North Pyrenean Frontal Thrust that directly juxtaposes the Chaînons Béarnais and Mauléon Basin cover ontop of the Aquitaine Basin. A likely equivalent of the North Pyrenean Paleozoic massifs would be the buried Grand Rieu ridge (more details below). In this lateral extent of the IMZ, the metamorphic imprint seems less intense than in the Central and Eastern Pyrénées. However, as for the

Baronnies Basin, the deepest part of the rift basin corresponding to the pre- and early syn-rift layers are not exposed in this part of the Pyrénées and are buried beneath a thick pile of syn- and post-rift sediments, except within the Chaînons Béarnais area (Fig. 5). This is where the highest $T_{\max}$ values were recovered from the pre-rift strata (>450 °C). These values are comparable to those obtained from the Montillet and Aulus basins of the Central and Eastern Pyrénées. We will partially answer to the missing record of the base of the rift basin using the drillhole data in the following.

As for the Chaînons Béarnais and Tarascon Basin, the highest metamorphic record from the eastern Basque-Cantabrian Basin at the southwest border of the studied area is located in the northern border of the IMZ and is limited by a north-vergent thrust corresponding to the Leitza Fault. This limit corresponds to a severe thermal gap between the metamorphic domain and the late syn- to post-rift sequences located in its footwall, that recorded $T_{\max}$ <200 °C (Fig. 5). The metamorphic domain is not limited to the south by a major fault but shows a progressive decrease of the metamorphic temperatures instead (Ducoux *et al.*, 2019).

4.2.3 Peak-temperatures distribution at basin-scale

According to our new results on the H*T*/L*P* metamorphism, we show that the IMZ has reached high $T_{\max}$ values >450 °C across the entire Pyrenean rift system, with numerous areas exceeding 550 °C. The IMZ is bounded by first order Pyrenean faults suggesting that they may have been important rift-related limits as the H*T*/L*P* metamorphic event predates the Pyrenean orogenesis. Studying the $T_{\max}$ distribution in each rift basin is generally complex, because: (i) these rift basins were affected by pervasive orogenic deformations, (ii) the dataset is neither dense enough nor equally distributed to determine precisely the pre-orogenic thermal structure. Nevertheless, using surface data, two favorable areas can be used to describe the spatial record of the H*T*/L*P* metamorphism at basin scale (Figs. 6 and 7) as the Eastern Basque-Cantabrian Basin (Nappe des Marbres) and the Central Pyrénées. For the first one the pre- and syn-rift sequences crop out and a dense coverage of surface data $T_{\max}$ measurements as published by Ducoux *et al.* (2019). Aside from the folded structure of the basin documented by this previous study, the regional thermal structure clearly shows a complex 3D pattern. First of all, isograds are E-W-elongated but present-day surface $T_{\max}$ values decrease toward the east and the south (Fig. 6). The highest $T_{\max}$ values significantly exceed 500 °C and are recorded within the pre- and syn-rift sediments located south of the Leitza Fault. This north-directed thin-skinned thrust fault is sharply juxtaposing the highest $T_{\max}$ values of its hanging-wall with the lowest values of its footwall. It contrasts with the more gradual decrease of $T_{\max}$ values southwards (values <250 °C 10 km away from the fault). Less obvious features can be observed in the Central Pyrénées within the Tarascon Basin. Restricted between the Axial Zone (North Pyrenean Fault) to the south, the Trois-Seigneurs Massif to the west and the Arize-Saint-Barthélémy massifs to the NW, the Tarascon Basin exposes syn-rift sequences and is significantly less deformed than the Aulus Basin located further to the SW (Fig. 7). The spatial record of the H*T*/L*P* metamorphism indicates that it was
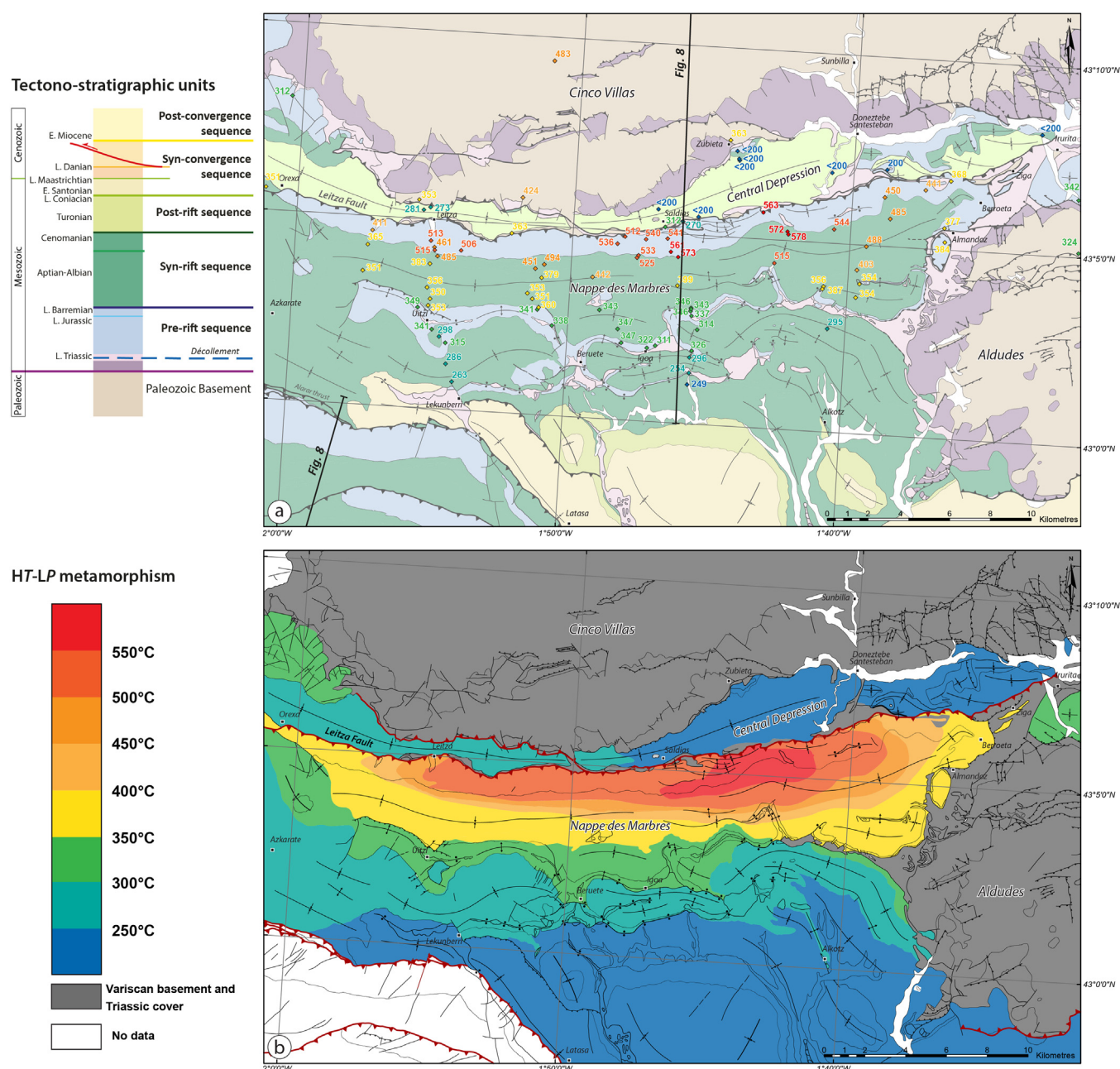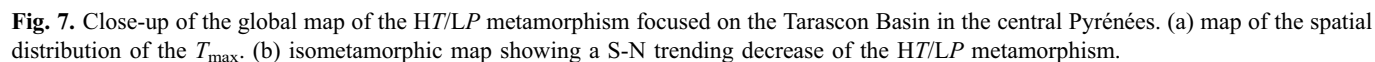
Fig. 6. Close-up of the global map of the H*T*/L*P* metamorphism focused on the eastern part of the Basque-Cantabrian Basin (modified from Ducoux *et al.*, 2019). (a) map of the spatial distribution of the *T*max. (b) isometamorphic map showing a N-S trending decrease of the H*T*/L*P* metamorphism.

more intensively recorded along the southern margin of the basin with *T*max values above 600 °C and then *T*max abruptly drops down to 350 °C toward the north. We also observe an eastward *T*max decrease from 604 ± 20 to 410 ± 16 °C and a westward decrease to ~345 °C along the eastern margin of the Trois-Seigneurs massif and toward the eastern termination of the Aulus Basin. Even though the Tarascon Basin is less documented by *T*max data, it also shows a roughly similar thermal asymmetry than the Basque-Cantabrian Basin but with an opposite direction.

5 Interpretations of the thermal structure *versus* architecture of the Pyrenean-Cantabrian belt

In order to discuss the record of the H*T*/L*P* metamorphism in depth along the Pyrenean-Cantabrian belt, we projected available *T*max data from the RSCM method and R$_o$ values along three N-S cross-sections located respectively in the Eastern Basque-Cantabrian Basin, in the Western Pyrénées and

Fig. 7. Close-up of the global map of the H*T*/L*P* metamorphism focused on the Tarascon Basin in the central Pyrénées. (a) map of the spatial distribution of the *T*$_{max}$. (b) isometamorphic map showing a S-N trending decrease of the H*T*/L*P* metamorphism.

in the Central Pyrénées (Figs. 8–10). It should be acknowledged that this section is dedicated to discuss the 3D spatial distribution of metamorphism at first order and not to make an exhaustive description of the structure of the Pyrenean-Cantabrian belt, already documented by previous studies (*e.g.* DeFelipe *et al.*, 2017; Labaume and Teixell, 2020; Lescoutre and Manatschal, 2020; Mouthereau *et al.*, 2014; Pedrera *et al.*, 2017; Roca *et al.*, 2011; Tugend *et al.*, 2014).

5.1 The Basque Cantabrian Basin

The Basque-Cantabrian Basin, relatively well preserved from pervasive collisional deformations, results from the shortening of a former hyperextended rift system that recorded mantle exhumation (DeFelipe *et al.*, 2017, 2018; Lescoutre and Manatschal, 2020; Pedrera *et al.*, 2017; Roca *et al.*, 2011; Tugend *et al.*, 2014). The sedimentary cover of the basin consists in a bivergent thin-skinned fold and thrust belt,
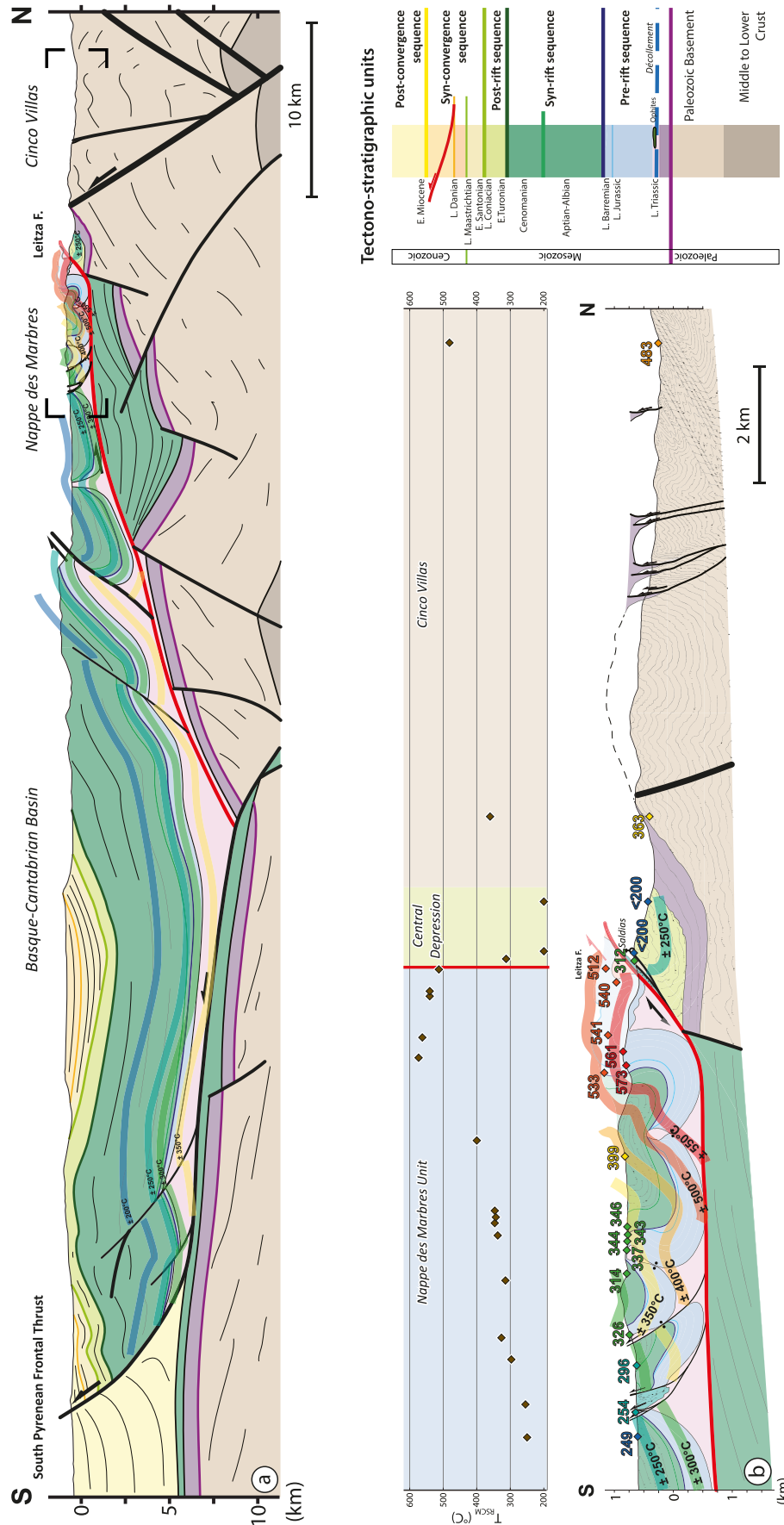
Fig. 8. N-S-striking geological cross-section (see location on Fig. 1) across the eastern Basque-Cantabrian Basin associated with measured T_{max} data. (a) N-S cross-section from the South Pyrenean Frontal Thrust to the south to the Cinco Villas to the north (modified after Lescoutre and Manatschal, 2020). Higher T_{max} are restricted close to the northern part of the Nappe des Marbres along the Leitza Fault in the Nappe des Marbres (see location on Fig. 1) (b) Close-up on the Nappe des Marbres Basin with the distribution of the HT/LP metamorphism (modified after Ducoux *et al.*, 2019) and relevant graph (T_{max} versus distance). The isograds were plotted with a margin of error.

Fig. 9. N-S geological cross-section across the Western Pyrénées (see location on Fig. 1) associated with measured T_{max} and Vitrinite Reflectance data. The southern part of the section drawn from surface geology is modified from Labaume and Teixell (2020). According to the seismic reflection data, the vertical scale of the whole section is in two-way traveltime (second). To preserved coherency within the whole section, the southern part of the section constructed with surface geology was drawn in the prolongation of the seismic data based on TWT vertical-scale. (a) 100 km-long N-S stiking geological cross-section through the Chaînons Béarnais, Grand Rieu ridge, Arzacq Basin and the Aquitaine platform, built form a 2D reflection seismic composite line available in Figure S1. (b) close-up focused on the Chaînons Béarnais and the Grand Rieu ridge. (c) close-up focused on the Aquitaine platform.

thrusted southward above the Iberian continental crust along the South Pyrenean Frontal Thrust and northward on top of the European continental crust represented by the Cinco Villas massif along the Leitza Fault (Fig. 8a). The Upper Triassic evaporites act as the main décollement layer located at the interface between the Mesozoic sedimentary series and the underlying basement. As pointed out in the previous section, this basin is anequivaly and homogeneously affected by the HT/LP metamorphism (Fig. 8). Only specific areas expose metamorphic rocks, especially the Nappe des Marbres Unit located in the NE termination of the Basque-Cantabrian Basin (Ducoux *et al.*, 2019). As paleo-isogrades crosscut the pre-orogenic geometry of the basin at large-scale (Fig. 8), these authors suggested that a significant part of the folding in the Nappe des Marbres Unit, and more widely of the Basque-Cantabrian Basin, predated the regional HT/LP peak metamorphism conditions and resulted from the interaction between salt tectonics and rifting processes. Paleo-isograds are well constrained in the northern part of the cross-section but

are extrapolated for the southern part. At basin-scale only a small strip of the basin is affected by temperatures exceeding 500 °C along its northern boundary affecting both pre- and syn-rift sediments. It structurally corresponds to the basal and more deeply buried part of the basin today exposed along the Leitza Fault. It should be noticed that the highest T_{max} coincides with the reported occurence of mantle rocks (serpentinites and ophicalcites) observed along the north-eastern margin of the Nappe des Marbre Unit (DeFelipe *et al.*, 2017; Mendia and Gil Ibarguchi, 1991) demonstrating that the rifting came to a mantle exhumation stage. Toward the south, T_{max} gently decreases below 250 °C, as shown by the distance-temperature diagram and the geometry of the isograds (Fig. 8b). Isograds are only deformed by collision-related folds and faults. The rest of the basin shows relatively low to moderate metamorphic grade with temperatures on the order of 300 °C, suggested at its base, much lower than the thermal peak recorded at the northern border of the Nappe des Marbres unit. The Leitza Fault abruptly juxtaposes two units of contrasted thermal
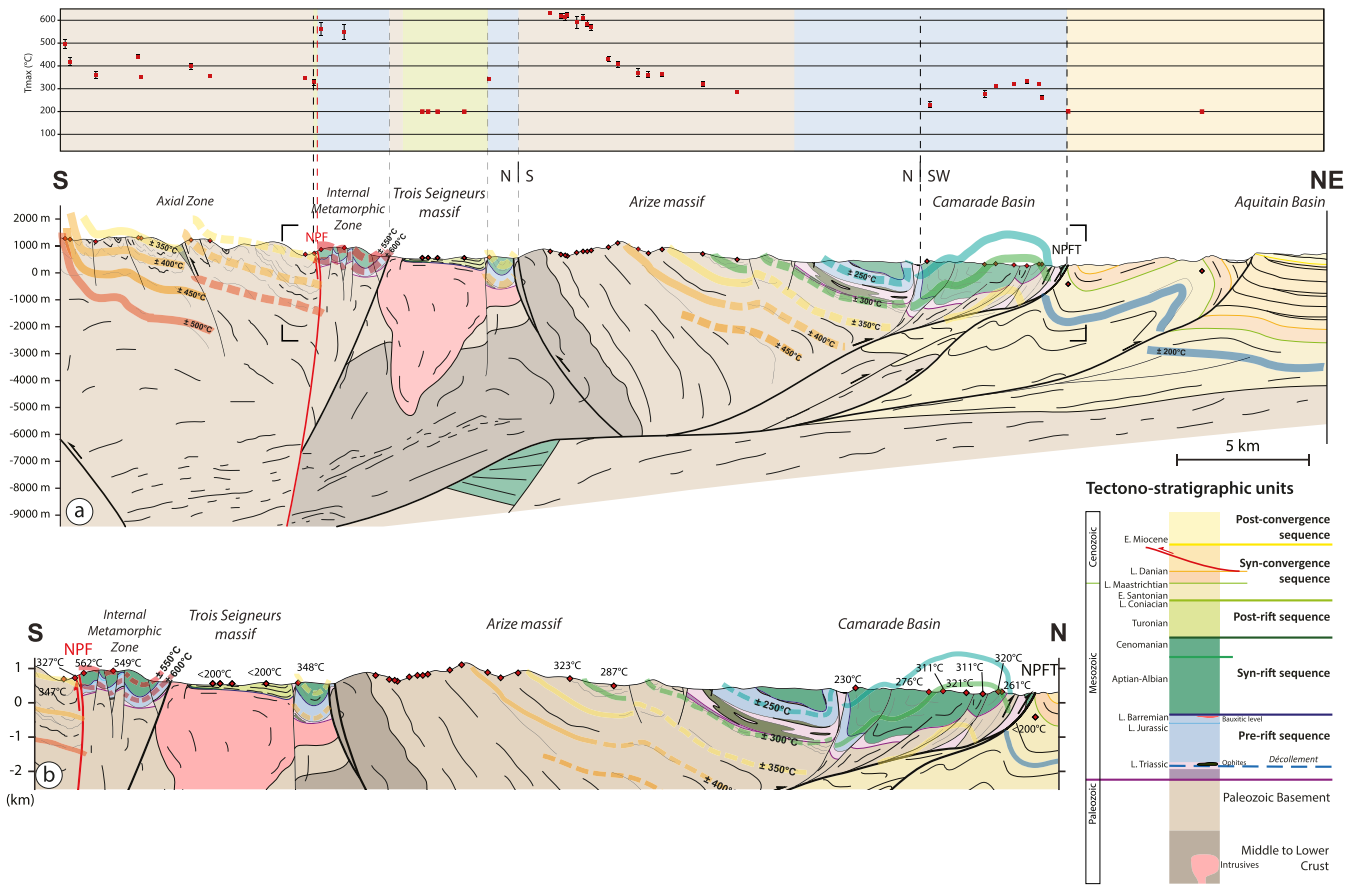
Fig. 10. N-S-striking geological cross-section (see location on Fig. 1) across the Central Pyrénées from the Axial Zone to the south to the Aquitaine Foreland Basin to the north. (a) Geologic cross-section associated with the distribution of the H*T*/L*P* metamorphism and relevant graph (T_{max} versus distance). The isograds were plotted with a margin of error. (b) Close-up on the Mesozoic basins.

records; the lowest conditions being experienced by the so-called Central Depression mostly made of post-rift sediments (with thin and discontinuous syn-rift sequence) unconformably lying on the Paleozoic basement (Fig. 8b). This abrupt lateral decrease in intensity of the metamorphism is shown by the dip of isograds and plotted T_{max} in the isometamorphic map (Figs. 6 and 8).

5.2 The Western Pyrénées: the eastern Mauléon-Arzacq rift system across the Chaînons Béarnais area

By using 2D seismic reflection composite line (Fig. S1, courtesy of TOTAL R&D), we constructed a ca. 100 km-long geological cross-section through the western part of the Chaînons Bearnais area corresponding to the Eastern Mauléon Basin, going across the Arzacq/Aquitaine foreland basins in the north. All of the nearby available T_{max} and R_o values were then projected on this section considering their depth and stratigraphic levels (Fig. 9). As for the Basque-Cantabrian Basin, the Chaînons Béarnais area results from the thin-skinned shortening of the pre- and syn-rift cover above the Upper Triassic main décollement. It was also paleogeographi-cally corresponding to the former distalmost part of the hyperextended rift basin as shown by outcropping occurrences

of deep basin syn-rift sedimentary facies associated with late syn-rift magmatic intrusions and mantle rocks exposures. Even thought it was more or less intensively deformed during orogenesis as a function of the still debated structural interpretations, it still preserves its first order proximal to distal relationships with its neighboring underthrusted Iberian and European crustal necking zones to the south and the north respectively (Izquierdo-Llavall *et al.*, 2020; Labaume and Teixell, 2020; Teixell *et al.*, 2016; Tugend *et al.*, 2014).

In the southern part of the section, the Chaînons Béarnais display an alternation of salt walls enclosing tightened and inverted minibasins during the collision (Izquierdo-Llavall *et al.*, 2020; Labaume and Teixell, 2020). As for the Nappe des Marbres Unit, salt tectonics may have therefore strongly influenced the pre-orogenic structure of the rift basin, mostly composed of pre- and syn-rift sediments lying above the Upper Triassic salt décollement level and hyperextended rift crust. Thus, a significant part of the folding should predate H*T*/L*P* metamorphism in this case too (Izquierdo-Llavall *et al.*, 2020; Labaume and Teixell, 2020). This observation is in agreement with T_{max} values mostly around 350 °C obtained from surface outcrops. Local higher temperatures within pre- and syn-rift metasediments are observed in the Tres Crouts area as well as in the central and southern parts of the

Chaînons Bearnais (Corre, 2017; Izquierdo-Llavall *et al.*, 2020; Villard, 2016). Even though there is no direct calibration for the T_{max} reached at the bottom part of the Chaînons Béarnais, high T_{max} values up to 480 °C were measured in the vicinity of some of the mantle exposures, *i.e.* the basement underneath the basin. At a first order, it indicates that T_{max} may have been significantly higher in depth close to the basin floor where the syn-rift sedimentary burial may have been higher too. The restored geometry of paleo-isograds that we propose also use the T_{max} estimate temperatures from R_o values from the nearby Oloron-1 borehole that penetrated >5 km thick syn-rift sequence (Fig. 9a, b). This range of T_{max} is actually similar to those obtained from in the central and eastern part of the belt along the IMZ. According to the estimated temperatures obtained from R_o measurements at depth in the different wells located north of the Oloron-1 well, the metamorphism intensity shows a northward moderate to rapid decrease until the North Pyrenean Frontal Thrust that crosscut metamorphic isograds (Fig. 9b). The Chaînons Béarnais unit thrust the Paleozoic basement of the Axial Zone towards the south by reactivating a rift-related north-dipping detachment fault surface (Labaume and Teixell, 2020). It is noteworthy that the underlying basement of the Chaînons Béarnais is poorly exposed on our section as the deformation is essentially thin-skinned. However, two first order observations are providing insights on its variable nature and structural context spatially: (1) the central and northern parts of the Chaînons Béarnais unit bear mantle outcrops indicating that they were lying ontop of an extremely thinned continental crust and/or exhumed mantle rocks; (2) a shortcut of the southern Chaînons Béarnais basement is exposed on the eastern side of the Aspe valley a few kilometers east of our section. It is made of Paleozoic basement rocks covered by its pre-salt autochthonous Lower Triassic cover. Of course, the rift paleogeography should not have been cylindrical, but these observations regionally indicate the occurrence of preserved blocks of upper crust located in the hanging-wall of the reactivated detachment of Labaume and Teixell (2020) but located south of exhumed mantle domains, *i.e.* as the extended basement of the southern Chaînons Béarnais as well as the Mauléon Basin (*e.g.* Lescoutre and Manatschal, 2020; Masini *et al.*, 2014; Saspiturry *et al.*, 2020; Tugend *et al.*, 2014). As direct constraints on the basement are not numerous in the area, we therefore choose to use structural observations in addition of T_{max} in our Western Pyrénées section (Fig. 9a, b). Whatever the detailed syn-rift structure, it is unconformably overlain the post-rift deposits showing moderate T_{max} of ~320 °C. This range of T_{max} indicates a persisting moderate to high geothermal gradient as recently proposed by recent study in the area (Caldera *et al.*, 2021).

Toward the north and underneath the North Pyrenean Frontal Thrust, the Grand Rieu ridge belonging to the European border of the inverted rift basin corresponds to a former palaeo-high limiting the Mauléon from the Arzacq Basin located farther north. This rift-related setting is indicated by the onlapping post-rift and syn-convergence deposits above a major erosional unconformity which truncates discontinuous remnants of syn- and pre-rift deposits if not directly the basement (Biteau *et al.*, 2006; Canérot *et al.*, 2005, see La Commande-101 borehole). In this area, the post-rift sequence show a moderate to high thermal maturity of organic matter

with R_o of 1.21% until 2.7%, corresponding to temperatures between 180 to 280 °C eq, observed respectively in Cardesse-2 and Le Rouat-1 boreholes (Fig. 9a, b and Tab. S4). Underlying Permian-Lower Triassic sediments preserved on top of the Grand Rieu ridge recorded similar R_o values with 2.3 and 3.1%, whereas the basement shows higher R_o of 4.7% (~350 °C). The Pau anticline, penetrated by the Pont-d'As-5 well (Fig. 9a, b) is well imaged by the seismic data. As there is no evidence for a significant top-basement décollement south of this thin-skinned fold neither on seismic data nor in wells, we interpret this structure as the surface expression of the orogenic tightening of the Arzacq Basin located further north (*i.e.* frontal triangular-shape structure). At equivalent burial, recorded R_o values within the post-rift sequence show a large lateral variation ranging from 2.5–2.7% for the Le Rouat-1 borehole in the south to 1.0 and 0.7% respectively for La Commande-101 and Pont d'As-5 boreholes (Fig. 9a, b). As for the post-rift sequence, syn-convergence deposits display values of R_o ~0.6–0.7% in the La Commande-101 and ~0.5–0.6% in the Pont-d'As-5 boreholes, while it recorded 1.7% in the Le Rouat-1 borehole. These values characterize a lower thermal maturity of organic matter and are similar to R_o documented by Pont-d'As-5 borehole in the younger post-convergence sediments with values of R_o ~0.4% (Fig. 9b). It is interesting to note that this decrease from post-rift to syn-convergence deposits and from south to north corresponds, as a paradox, to the maximum syn-orogenic sedimentary burial underneath and along the North Pyrenean Frontal Thrust. On the northern margin of the Grand Rieu ridge, pre-rift sediments show moderate to high values of R_o ~2.5% corresponding to a temperature of 270 °C eq. A thermal maturity break is observed within the overlying syn-rift sediments with R_o of 0.7%. This specific point is discussed below.

The northern slope of the Grand Rieu ridge is flanked by a north-dipping low-angle fault which accommodated the formation of the Arzacq Basin northwards (Ducoux *et al.*, 2021b). This syncline-shaped basin highlighted by the pre-rift units above the salt décollement level is infilled by a thick sequence of syn-rift sediments (~2 s TWT). By using estimated temperatures from R_o, we suggest that the deepest part of this basin filled by ~5 km of compacted pre- and syn-rift sediments, recorded temperatures exceeding 250 °C (Fig. 9a), at the depocenter that may explain the significant quantity of dry gas discovered in this oil and gas province (*e.g.* Biteau *et al.*, 2006). Further north, the top basement and the pre-rift sequence get shallower along the gently rising northern margin of the Arzacq Basin until the Aquitaine platform. The northern edge of this section represents the Aquitaine Platform where the pre-rift units is covering a thin layer of Upper Triassic evaporitic level which accommodate its underlying slightly faulted basement. The syn-rift sequence appears thinner in this more proximal area (<1 s TWT) and is pinching out toward the north similarly than the pre-rift sequence (Fig. 9a, c). A succession of boreholes penetrating the Aquitaine Platform documents the thermal maturity of organic matter in the overall stratigraphic column (see above and Fig. 9c). Average R_o values in the pre-rift sediments are ~1%. In the Theze-1 borehole R_o values ranging between 0.8 to 1.27% contrast with R_o values exceeding 2.5% on the southern side of the Arzacq Basin (*e.g.* Pont-d'As-5) with a similar burial (Fig. 9a). The rest of the drilled sediments on the northern side of the

Arzacq Basin (post-convergence to syn-rift) show low to very low thermal maturity with R$_o$ values <0.5%, decreasing upsection to 0.3% (Fig. 9c). This range of values corresponds to estimated temperatures <60 °C.

5.3 The Central Pyrénées

Unlike the Basque-Cantabrian Basin and the Western Pyrénées, the Central Pyrénées were intensively affected by a collisional overprint (*e.g.* Choukroune and the ECORS Team, 1989; Ford *et al.*, 2016; Mouthereau *et al.*, 2014). Only discontinuous remnants of the Mesozoic sediments belonging to the IMZ are preserved between the Axial Zone and the North Pyrenean Massifs. Further north, the Camarade basin, located at the northern margin of the Arize massif, overthrusted the Aquitaine Foreland Basin, which is mainly filled with syn-convergence sediments (Fig. 10). Along this transect, T_{max} values were measured in all units from the Axial Zone in the south to the Camarade Basin in the north. This transcect documents both the T_{max} recorded within the Mesozoic sediments affected by the Cretaceous rift-related metamorphism only and Paleozoic rocks that were also affected by earlier Variscan metamorphism.

The Axial Zone records a gentle decrease of temperature from 495 °C in the south to 347 ± 2 °C close to the North Pyrenean Fault, its northern limit (Fig. 10a). Pinched between the Axial Zone and the IMZ, deformed post-rift sediments show relatively high T_{max} of 327 ± 14 °C. Further north across the North Pyrenean Fault, the IMZ records very high T_{max} of 549 ± 35 and 562 ± 30 °C. T_{max} observed in the post-rift sediments directly overlying the Trois-Seigneurs massif contrast with the IMZ, with values <200 °C. This massif formed a basement high during the rifting event, as suggested by the lack of pre- and syn-rift sediments. As for the IMZ, a second small basin filled by Mesozoic sediments is pinched between the Trois-Seigneurs and Arize massifs further north. The recorded T_{max} of 348 ± 7 °C in this area indicates a lower intensity of the HT/LP metamorphism within this basin compared to the IMZ (Fig. 10b).

The southern margin of the Arize Massif, composed of metasediments, shows T_{max} exceeding 600 °C. A thermal break can be observed in the central part of the massif where T_{max} rapidly decrease to ~400 °C. From this break, T_{max} gently decreases under 300 °C, in agreement with the T_{max} close to 300 °C recorded in the syn-rift sediments of the Camarade Basin in the syn-rift sediments (Fig. 10). Interestingly, measured T_{max} in the northern margins of the Arize Massif composed of Devonian sediments are significantly lower than the T_{max} observed in the same stratigraphic levels of the Axial Zone. The Aquitaine Foreland Basin has not recorded the HT/LP metamorphism, with T_{max} <200 °C measured in the early syn-convergence sediments (Santonian to Maastrichtian in age).

6 Discussion

6.1 Time constraints on the HT/LP metamorphic event

The most constraining observations regarding the timing of the HT/LP metamorphic event come from the Vitrinite

Reflectance values obtained from boreholes data. They provide crucial information on the vertical maturation trends within both the Mauléon and Arzacq basins located in the Western Pyrénées (Figs. 2, 3 and 4). The depth evolution of R$_o$ values generally shows a break between two linear trends corresponding to the late syn-rift and the early post-rift sequences (Cenomanian). The lower trend affects the pre- and syn-rift depositional sequences and represents a higher thermal maturity gradient in comparison with the upper trend. Such a vertical evolution in the absence of a major erosional unconformity can be interpreted as a decrease of the thermal gradient in between the two sequences (*i.e.* syn-rift/post-rift and syn-orogenic time, *e.g.* Allen and Allen, 2013; Dow, 1977). It can also be noticed that the vertical trends of the R$_o$ values are affected by the Pyrenean orogenic deformation. This is first demonstrated by the Bellevue-1 well where the vertical trend of the R$_o$ is not depth-dependent along the drilled vertical fold limb (base of the well; Fig. 2b). Isovalues of R$_o$ seem to be bed-parallel and subsequently folded during the tectonic inversion. In the Orthez well, it can also be shown from the sudden vertical decrease of R$_o$ values across the NPFT that the maximum maturity was locally reached before thrusting (Saspiturry *et al.*, 2020). From the map in Figure 4a displaying the spatial distribution of R$_o$ data as a function of the stratigraphic interval (*i.e.* not burial-dependent), a strip of high values anomalies (ranging between 0.9 to 2.29%) can also be reported within early syn-orogenic deposits in the vicinity of the NPFT (*i.e.* along the Grand-Rieu ridge, Figs. 4a and 9). This narrow strip of high temperatures will be discussed in more detail in the following section as a likely signature for early orogenic hydrothermal circulations (Bahnan *et al.*, 2020; Renard *et al.*, 2019; Salardon *et al.*, 2017).

These new data are in general agreement with the literature that directly or indirectly suggests that the HT/LP metamorphic event is Upper Cretaceous in age throughout the Pyrénées (Albarède and Michard-Vitrac, 1978a, 1978b; Casquet *et al.*, 1992; Chelalou *et al.*, 2016; Clerc *et al.*, 2015; Golberg and Maluski, 1988; Golberg *et al.*, 1986; Montigny *et al.*, 1986). The timing of the HT/LP metamorphic event is also supported by the subsidence analyses from the Aquitaine Basin showing that a part of the syn-orogenic subsidence is related to thermal relaxation and require a late rift residual thermal anomaly reaching the Aquitaine Basin (Angrand *et al.*, 2018; Brunet, 1984).

6.2 Intensity and spatial distribution of the HT/LP event

Generally, it has been reported that the HT/LP metamorphic oveprint is restricted to the NPZ and that the maximum intensities (>500 °C on pre-rift strata by RSCM) was reached within the IMZ (*e.g.* Clerc *et al.*, 2015). It has also been proposed, based on these maximum values collected at the present-day surface, that there is a progressive decrease of the intensity of the thermal anomaly from east to west along the Pyrénées reaching a minimum in the Mauléon Basin (Clerc and Lagabrielle, 2014; Clerc *et al.*, 2015). Our dataset is nuancing these conclusions. Similar high T_{max} measurements were undifferently obtained from the Eastern and Central Pyrénées as well as from the Basque-Cantabrian Basin (Nappe des

Marbres unit) located at the SW edge of the study area (>500 °C on RSCM data), *i.e.* further west from the Mauléon Basin. Moreover, once considering wells data from the Mauléon Basin, a downward increase of T_{max} values is revealed by R_o measurements traduce a much higher T_{max} values at the base of the basin (∼400–500 °C) from which the deepest (and hotter) levels have never been reached by drillholes. These high temperatures are consistently reached by pre- to syn-rift strata deeply buried underneath the northern (and deepest) part of the Mauléon Basin, partly outcropping in the Chaînons Béarnais fold and thrust belt, at the easternmost termination of the Western Pyrénées (Fig. 9). Such palaeo-temperatures also explain why oil and gas exploration has been generally discarded from the NPZ. These results are in agreement with Saspiturry *et al.* (2020) proposing similar maximum temperatures distribution within the Mauléon Basin. In order to enlarge this spatial distribution at the scale of the entire rift system and for the whole Pyrenean-Cantabrian belt, we propose in this study an interpolated map combining surface and subsurface data to better locate T_{max} values reached at the base of the Pyrenean rift basin (Fig. 11). From this dataset, it can be proposed that the E-W variations of surface T_{max} values may not be due to the intensity of the thermal anomaly itself (*i.e.* "hot" *versus* "cold" rifting as addressed by Clerc and Lagabrielle, 2014) but are rather due to the burial conditions of outcropping pre- and syn-rift sediments along the NPZ. In other words, as observed in the geological cross-sections (Figs. 8–10), Eastern and Central Pyrénées outcrops are mostly made of discontinuous remnants of the former basal part of deeply buried rift basins and its exposed underlying basement (*i.e.* younger deposits were eroded) whereas the Western Pyrénées do preserve a more complete, less deformed and shallower rift sedimentary succession that were located closer to the seabed at the thermal climax. In the Western Pyrénées former rift basins were sampled as a pop-up above the colliding European and Iberian continents. This situation is partly due to the low frictional Upper Triassic evaporites that acted as a basal décollement that efficiently decoupled thick-skinned from thin-skinned deformations during basin inversion. It partly explains the preservation of rift architecture like in the Chaînons Béarnais characterized by tightened salt diapirs/ walls bracketting inverted minibasins on top of the forming thick-skinned orogen (*e.g.* Izquierdo-Llavall *et al.*, 2020; Labaume and Teixell, 2020). According to our field observations, the outcropping rocks in the Chaînons Béarnais mostly represent the shallow part of the basin made of a succession of tightened minibasins and salt walls above a thick pile of Mesozoic sediments (Fig. 9) (Labaume and Teixell, 2020). Further west, the Mauléon Basin mainly exposed at the surface even more preserved late syn-rift to post-rift sediments above up to 5 km of syn-rift sediments at the depocenter as suggested by wells (*e.g.* Lescoutre *et al.*, 2019; Saspiturry *et al.*, 2020). From this point of view, the Western Pyrénées contrasts with the Central and Eastern Pyrénées from the exposed structural level at the present-day surface (deep *versus* shallow parts of rift basin infill) (*e.g.* Ford *et al.*, 2016; Mouthereau *et al.*, 2014). Such a difference may be due to different orogenic processes (orogenic non-cylindricity, *e.g.* Muñoz, 2002; Roca *et al.*, 2011), to a lateral change in the pre-orogenic rift geometry (rift non-cylindricity, *e.g.* lateral change

in the rift polarity of Tugend *et al.*, 2015), or a combination of these two with different modes of rift inversion along strike (*e.g.* Chevrot *et al.*, 2018). Because of this preservation issue, reaching the N-S thermal architecture within the former rift basins can be done in detail within the Western Pyrénées, where the thermal record is preserved at depth. From our dataset, it can be shown that the Vitrinite Reflectance maturity profiles with depth are much steeper across the Arzacq Basin (*e.g.* Thèse well in Fig. 9) than along the Grand Rieu ridge and the northern slope of the Mauléon Basin (Fig. 11) with similar burial depth. The Grand Rieu ridge record is even more discriminant. As shown by onlapping post-rift sediments above the erosional surface truncating the pre- and syn-rift sequences along this rift relief (Biteau *et al.*, 2006; Canérot *et al.*, 2005; Labaume and Teixell, 2020; Masini *et al.*, 2014; Teixell *et al.*, 2016), the syn- and post-rift burial was extremely limited. From the Grand Rieu ridge southwards, high T_{max} values are rapidly increasing toward the juxtaposed deepest part of the Mauléon Basin. In agreement with Lescoutre *et al.* (2019) conclusions, this dataset further indicates that syn-rift heat flow may have been significantly higher toward the more distal and more extended rifted domains. This latter sampled by the NPZ was characterized by exhumed mantle (Debroas *et al.*, 2010; Fortané *et al.*, 1986; Jammes *et al.*, 2009; Lagabrielle *et al.*, 2010; Masini *et al.*, 2014) and late Albian/ Cenomanian alkaline magma intrusions (*e.g.* Azambre and Rossy, 1976; Azambre *et al.*, 1992; Montigny *et al.*, 1986; Rossy *et al.*, 1992). Such a thermal climax may reflect the increased lithospheric thinning in this direction as well as the spatial migration of deformation from rift borders inward (Lescoutre *et al.*, 2019; Tugend *et al.*, 2015). This interpretation is in agreement with the former width of the rifted domain affected by the Pyrenean H*T*/L*P* event revealed by our dataset (Fig. 12) including both the Southern Arzacq and the Mauléon basins as well as the northern part of the Axial zone It should be noticed that evidence for a hot thermal gradient were also discovered in the northern border of the Axial zone (less intense than the former hyperextended rift domain, *e.g.* Airaghi *et al.*, 2020; Bellahsen *et al.*, 2019). At present, this area is ∼60 km wide in the N-S section in the Western Pyrénées (Figs. 9 and 12a, b) not considering the orogenic shortening accommodated within the Mauléon Basin. Accounting for the Pyrenean shortening accommodated within this domain, the initial N-S width of the metamorphic domain should have been in the order of 80–100 km (Figs. 12a, b) (Jammes *et al.*, 2009; Labaume and Teixell, 2020; Teixell *et al.*, 2016).

Replacing the IMZ in respect of the entire rift system may also be meaningful to address rift to orogenic processes. For this purpose, it should be first acknowledged that the zone affected by the H*T*/L*P* metamorphism within the Western Pyrénées does not corresponding to an entire rift section between the stable European and Iberian crusts. The entire N-S rift section within the Western Pyrénées (Fig. 12e, f) is made of two juxtaposed rift depocenters overlying thinned crustal (and locally mantle) domains: the Mauléon and Arzacq basins. The Mauléon Basin, in the southern half of the rifted section, is entirely recording the H*T*/L*P* metamorphism that increasing northwards and with an increased sedimentary burial along the tapering Iberian crust from South to North. The basement of the Mauléon Basin was made of the crustal necking zone
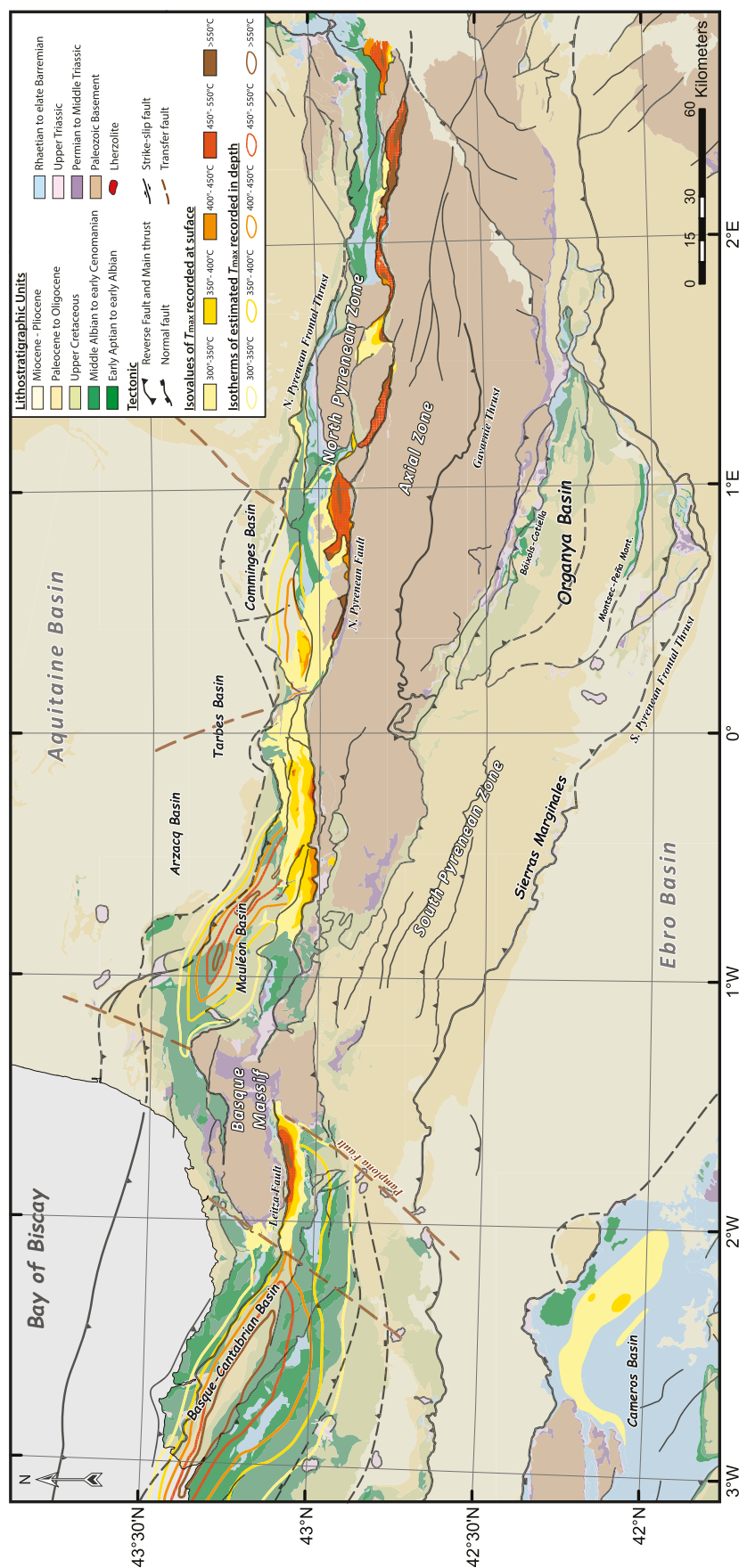
Fig. 11. Interpretative map of the H*T*/L*P* metamorphism in the overall Pyrenean-Cantabrian belt and Cameros Basin, combining measured *T*max data at surface and estimated *T*max data at the base of former rift basins. Estimated *T*max were calculated from R$_o$ values measured in boreholes. The H*T*/L*P* metamorphism mapping of the Cameros Basin is from Rat *et al.* (2019).
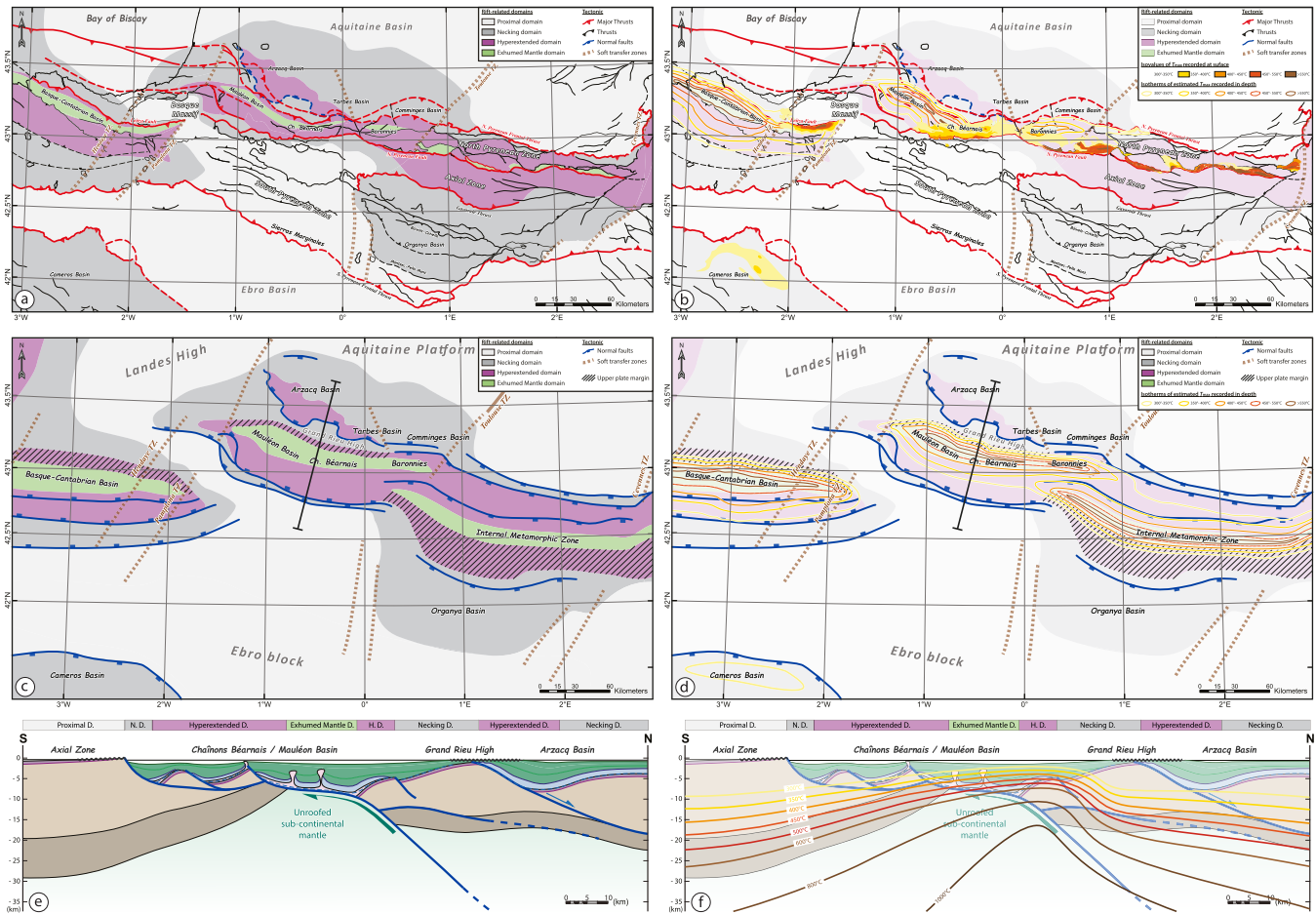
Fig. 12. Comparison of rift-related domains with the spatial distribution of the H*T*/L*P* metamorphism for the present-day structure and for the end of rifting restoration. (a) Rift-related map of the Pyrenean-Cantabrian belt modified from Tugend *et al.* (2014) and Lescoutre and Manatschal (2020). (b) The same rift-related map associated with the distribution of the H*T*/L*P* metamorphism shown in the Figure 11. (c) map of the restored Pyrenean-Cantabrian rift system modified from Tugend *et al.* (2014) and Lescoutre and Manatschal (2020). (d) The same map of the restored rift associatedwith the distribution of the H*T*/L*P* metamorphism. (e) Crustal-scale cross-section restored at the end of the rifting modified from Masini *et al.* (2014), Gomez-Romeu *et al.* (2019) and Ducoux *et al.* (2021b), (f) associated with isotherms of the H*T*/L*P* metamorphism.

(represented by the northern tip of the Axial zone, the Lakhora thrust sheet and the Aldudes massif), the hyper-thinned crust and the exhumed mantle domain (Chaînons Béarnais and Northern Mauléon Basin) from south to north. Thermochronological results performed along the Iberian necking zone of the Mauléon Basin document geothermal gradients up to 80 °C/km (Hart *et al.*, 2017) in agreement with the recent T_{max} dataset of Saspiturry *et al.* (2020). This thermal record contrasts with the European side of the rift system. From north to south, the European necking zone (zone of crustal thinning *sensu* Manatschal, 2004) corresponds to the southward tapering continental crust underneath the Arzacq Basin that form coevally to its Iberian conjugate during the Aptian − Early Albian phase of rifting (Masini *et al.*, 2014; Tugend *et al.*, 2014). Both subsidence analysis (*e.g.* Brunet, 1984) and more recent geophysical images (Chevrot *et al.*, 2018; Wang *et al.*, 2016) indicate that the European crust thins by a factor of 2 from the Aquitaine plateform in the north to the Grand Rieu ridge in the south (made itself of a thinned piece of European

crust). Despite the intensity of crustal thinning, our dataset shows that the European necking zone was not significantly affected by the H*T*/L*P* metamorphic event showing that the northern half of the rift section was located away from the rift thermal anomaly. Whatever the underlying rift-related process, it indicates a first order thermal asymmetry at the scale of the complete rift system. From the available pure shear-dominated rift models (*e.g.* Labaume and Teixell, 2020; Lagabrielle *et al.*, 2020; Saspiturry *et al.*, 2020; Teixell *et al.*, 2016), similar thermal records would be expected for equivalent stretching/thinning factors (*i.e.* equivalent structural domains for conjugate pairs of rifted margins). They cannot easily explain the diverging thermal evolutions recorded by the European and Iberian necking zones and thinned crustal domains arising from our dataset. Former authors were reporting that there is a misfit between the upper crustal stretching (limited number of normal faults) and the observed crustal thinning along the Arzacq Basin (*e.g.* Masini *et al.*, 2014; Saspiturry *et al.*, 2019). If they disagree on the

regional rift geometry, they all converge on proposing depth-dependent processes to thin the European crust from north to south, that is a diagnostic criterion for a simple shear component of rifting (heterogenous vertical thinning) and fits with an upper plate relative position at the considered location (*e.g.* Lister *et al.*, 1986). As for the thermal record, these structural observations within the Arzacq Basin therefore diverge with those from the Mauléon Basin too, where evidence for high-strain top-basement extensional structures (detachment faulting) and exhumation of deep crustal rocks make a large consensus at present (*e.g.* Lagabrielle *et al.*, 2020; Masini *et al.*, 2014; Saspiturry *et al.*, 2020). Both the structural and thermal observations were recently simulated by thermo-mechanical modeling experiments (Lescoutre *et al.*, 2019) and is in good agreement with our palaeothermal dataset. These models generally predict a persisting and high lateral thermal gradient at the tip of the upper plate margin what is best exemplified by the Grand Rieu ridge tectono-thermal record (Figs. 9, 11 and 12). Therefore, we think that the varying spatial tectono-thermal record across the Western Pyrénées are indicating a rift asymmetry where the Iberian side would represent a lower plate evolution whereas Europe would represent its upper plate counterside (Gómez-Romeu *et al.*, 2019; Masini *et al.*, 2014; Tugend *et al.*, 2014). The total initial width of the entire rift system, including the lower and upper plate crustal tapers may therefore be >140 km in the Western Pyrénées. It falls into similar numbers regarding the Pyrenean-like Porcupine Basin (NW Ireland) where hyperextension rifting was presumably stopping at a mantle exhumation stage (Reston *et al.*, 2001; Watremez *et al.*, 2018). A similar asymmetric thermal architecture is also revealed from the Basque-Cantabrian Basin data (Ducoux *et al.*, 2019) located further to the SE. Even more heavily affected by Pyrenean deformations, the same first order thermal asymmetry can also be unraveled from the Central and Eastern Pyrénées dataset where the sharp lateral thermal gradient is however switching on the opposite border of the rift as the highest T_{max} values are located along the southern side of the NPZ juxtaposed to the North Pyrenean Fault (*e.g.* Tarascon Basin, Figs. 11 and 12). Already known for its present-day non-cylindricity of the orogenic structure (*e.g.* Chevrot *et al.*, 2018), such a lateral shift of the rift thermal structure may further support that the non cylindricity may also be inherited from the Pyrenean rift history (*e.g.* reversal of rift polarity of Tugend *et al.*, 2015 and Chevrot *et al.*, 2018; Fig. 12).

6.3 Evidence for a significant role of hydrothermal fluids for the Pyrenean thermal record

The regional scale of the HT anomaly discussed above is further complicated by smaller-scale spatial variations recorded in the T_{max} values. First, a small strip of high R$_o$ values (1.0 to 2.58%; 150 to 250 °C eq) is observed can be reported from the post-rift and early syn-orogenic deposits along the NPFT above the Grand Rieu ridge of the Western Pyrénées (Figs. 4a and 9). A likely possibility is that this area may have been anomalously buried underneath a thick pile of sediments emplaced by either sedimentation or thrusting (or a combination of both) which was subsequently eroded. It should be noticed that much lower T_{max} values are recorded both northward (La Commande-101 and Pont-d'As-5 wells) and southward (Cardesse-2 well) in spite of a deeper burial depth indicated by the local Pyrenean tectono-stratigraphic architecture (Fig. 9). As it is geometrically related to the NPFT, an alternative scenario is that this HT imprint is rather due to hydrothermal circulations along the NPFT that was channeling rising hot fluids to this precise location (Fig. 9). Contrasting with the rest of the area, this thermal record is early orogenic as it affects latest Cretaceous deposits but no younger units. Therefore, this HT is coeval with the northward underthrusting of a part of the former hyperextended basement of the Mauléon Basin underneath Europe below the Grand Rieu Ridge (*e.g.* Gómez-Romeu *et al.*, 2019; Tugend *et al.*, 2014). From the record of the Mauléon Basin as well as the rest of the NPZ, it was demonstrated that this basement was made of highly hydrated minerals (serpentinized mantle, altered continental crust, Clerc *et al.*, 2013; Corre *et al.*, 2018; DeFelipe *et al.*, 2017; Incerpi *et al.*, 2020b; Monchoux, 1970; Quesnel *et al.*, 2019). Thus, we further speculate that those fluids may have been sourced by the syn-orogenic dehydration of these rocks during their prograde metamorphic evolution at depth. Such a complex fluid-controlled thermal regime was already well identified within syn-rift times (Bernus-Maury, 1984; Clerc *et al.*, 2015; Corre *et al.*, 2016; Golberg, 1987; Incerpi *et al.*, 2020a; Lagabrielle *et al.*, 2019a; Motte *et al.*, 2021; Mukonzo *et al.*, 2021; Renard *et al.*, 2019; Salardon *et al.*, 2017). Scapolites observed in the syn-rift sequence are evidence for salt-rich fluids having circulated through the sedimentary succession, which originated from Upper Triassic evaporites (Clerc *et al.*, 2015; Golberg and Leyreloup, 1990).

In the hotter and more distal part of the rift located north of the Mauléon Basin and south of the Grand Rieu ridge, it has already been noticed that the HT record is spatially associated with occurences of late rift alkaline magma (the so-called "Episyenites"), hyperthinned continental crust and exhumed mantle rocks (serpentinites and ophicalcites, Clerc *et al.*, 2013; DeFelipe *et al.*, 2017). All of those rocks imply a significant magmatic heat advection and hydrothermal activity that should strongly impact the thermal regime of the rift system. We cannot exclude that the syn-convergence HT record may relate to the remaining rift-related heat-flow and the delay of thermal relaxation (*e.g.* Bellahsen *et al.*, 2019; Caldera *et al.*, 2021; Vacherat *et al.*, 2014). All of these observations in pre- and syn-rift sequences are commonly indicating a major role of fluids influencing the thermal record. These syn-tectonic thermal regimes (either under rifting or early orogenesis) were not entirely conductive but also imply fluid flow. In such a context, the resulting geotherm may not have been a linear depth-dependent function but should strongly vary both vertically and laterally as a function of the geometries of convection cells (*e.g.* Incerpi *et al.*, 2020a, 2020b; Pinto *et al.*, 2015), what could explain the apparent rapid lateral variations of measured T_{max} values in our dataset at a more local/sub-basin scale.

Different thermal records of the Mauléon and Arzacq basins may also be related to different fluid-related thermal regimes and may be due to different structural settings with respect to hyperextension rifting. As proposed by Pinto *et al.* (2015) and Incerpi *et al.* (2020b) in the Alps and by Incerpi *et al.* (2020a) in the Pyrénées, hydrothermal fluids along hyperextended domains of rifts transport the heat from the

active part of detachment faults along the fault plane and therefore reach the exhumed domain and the supra-detachment rift basin. This asymmetric situation makes that the thermal effect of incoming "hot" fluids is more favorably recorded within supra-detachment basins (along the footwall of the detachment faults) than within basins located in the hanging-wall of detachment systems, as for instance the Arzacq Basin (Fig. 12e, f). If valid, this model strongly supports a supra-detachment thermal record for the Mauléon Basin along which fluids may have intensively interacted with the sediments south of the Grand Rieu ridge (Fig. 12e, f). As discussed by Lavier *et al.* (2019) and proposed in the Pyrénées by Clerc *et al.* (2015), it may indicate that the thermal maximum could be delayed because of the decrease of hydrothermal circulations through time. While decreasing, the thermal regime becomes more conductive, implying a heating phase because of the low thermal conductivity of sediments (*i.e.* blanketing effect) that could exceed and erase the older thermal record.

The Arzacq Basin thermal record would rather fits, by contrast, with an upper plate situation record as only its southern tip records a late thermal H*T* event. The more limited effect of fluid circulations in this area may have promoted a continuous and progressive conduction-dominated syn to post-rift thermal regime. As being mostly conductive, an upper plate situation with respect to the detachment systems of late rifting (above the "exhumation channel" of Brune *et al.*, 2014) would imply a maximum delay in the recorded T_{max} (*i.e.* post-rift) in respect of active rifting. Such a post-rift thermal maximum is documented in this area along the southern end of the Arzacq Basin as well as along the Grand Rieu ridge and further supported by an "anomalous" late to post-rift uplift (in the order of ~2 km, see Renard *et al.*, 2019 for more details).

6.4 Role of sediments for hyperextended rift thermal record

Of course, sediment burial is needed to record a T_{max}, whatever the gradient and thermal regime in space and time. More than a thermal tape-recorder, sedimentation also actively interacts with the thermal regime of rift systems. As globally discussed by Lavier *et al.* (2019) for hyperextended rifting, sediments induce a so-called blanketing effect (*e.g.* Blackwell and Steele, 1989; Callies *et al.*, 2018; Lucazeau and Le Douaran, 1985; Nunn and Lin, 2002; Pollack and Cercone, 1994; Wangen, 1995) resulting from their low initial heat-flow and their low thermal conductivity above a thinned lithosphere and a high basement heat-flow. This effect widely described for the Pyrenean rift (*e.g.* Asti *et al.*, 2019; Clerc and Lagabrielle, 2014; Clerc *et al.*, 2015; Lagabrielle *et al.*, 2019b), is characterized by progressive heating and a delayed thermal climax during heat conduction across a rift basin. While interacting with hyper-extension processes, the blanketing effect could lead to an extremely complex spatial thermal structure (Lavier *et al.*, 2019). During hyperextension, this is mostly due to the spatial tectonic migration toward the rift axis forced by detachment faulting (*i.e.* toward the future ocean if a breakup is recorded, *e.g.* Brune *et al.*, 2014; Péron-Pinvidic and Manatschal, 2019 and references therein). Accounting for thermal blanketing with tectonic migration and increased

lithospheric thinning, the recorded T_{max} are expected to get younger and more intense toward the rift axis, and therefore might even post-date rifting in the younger and more distal part of a hyperextended rift because of the conduction delay. This tendency should even be reinforced by higher sedimentation rates and/or thicker sedimentary cover. In the Pyrénées, despite rift basins were underfilled as shown by the development of deepwater conditions, the distal part of the hyperextended rift was likely covered by a pre-, syn- and post-rift sedimentary cover locally exceeding 5 km in thickness before the onset of shortening (Debroas, 1990; Ducoux *et al.*, 2021b; Labaume and Teixell, 2020; Rougier *et al.*, 2016). Effectively corresponding to a sedimented hyperextended rift system and in agreement with former studies (*e.g.* Angrand *et al.*, 2018; Clerc *et al.*, 2015; Hart *et al.*, 2017; Jourdon *et al.*, 2019; Saspiturry *et al.*, 2020; Ternois *et al.*, 2019; Vacherat *et al.*, 2014), our dataset strongly confirms that a late to post-rift (and a likely early orogenic) H*T* record is consistently recorded along the entire NPZ of the Pyrénées and the northern side of the Cantabrian belt (Ducoux *et al.*, 2019). It is noteworthy that such a delayed Mid-Cretaceous thermal climax is not only restricted to the Pyrenean record sensu stricto but was also reported from the nearby but slightly older Cameros Basin located further south (Rat *et al.*, 2019) (Fig. 11). In this case, an even thicker sedimentary cover accumulated within the rift basin during and after the rifting (Omodeo-Salé *et al.*, 2017) and could have contributed to further delay the recorded T_{max} with respect to its initial rifting evolution.

The effect of sediments for the rift-related thermal record is also evidenced while comparing the Pyrenean record to its Alpine analogue. Of Jurassic age, the Alpine Tethys rifting came to an even more mature stage of divergence as it experienced, at least, an incipient seafloor spreading stage as recorded by the presence of ophiolites (*e.g.* Bernoulli *et al.*, 2003; Decandia and Elter, 1972; Froitzheim and Manatschal, 1996; Lagabrielle and Cannat, 1990; Lemoine *et al.*, 1986; McCarthy *et al.*, 2018, 2020; Picazo *et al.*, 2016). However, with the exception of direct indicators within basement rocks or indirect diagenetic/fluid inclusion contents of syn- and post-rift sediments (*e.g.* European necking zone: Barale *et al.*, 2016; Beltrando *et al.*, 2012, Beltrando *et al.*, 2014; Decarlis *et al.*, 2017; Ewing *et al.*, 2013; Rossetti *et al.*, 2015; Seymour *et al.*, 2016; Adriatic supra-detachment distal margin units: Coltat *et al.*, 2020; Incerpi *et al.*, 2020b; Pinto *et al.*, 2015), there is little evidence for a Pyrenean-like H*T*-L*P* rift-related metamorphism in the Alpine Tethys rift systems. Even though it could have been overprinted by subduction and collisional overprints (Gabalda *et al.*, 2009), it should be noticed that hyperextension rifting ahead of the Alpine necking zones was under a severe sediment starvation during and after rifting across the different segments of the Alpine Tethys (*e.g.* Lemoine *et al.*, 1986; Manatschal, 2004; Manatschal and Bernoulli, 1999; Masini *et al.*, 2012, 2013; Mohn *et al.*, 2010; Ribes *et al.*, 2020). This characteristic is primarily shown by long-standing hiatuses and condensed levels on rift-related palaeo-highs (*e.g.* Dumont *et al.*, 1984; Lemoine and Trümpy, 1987; Trümpy, 1949), directly overlained by radiolarian cherts or marbles above the Alpine ocean-continent transition (*e.g.* Alpine European margin: Florineth and Froitzheim, 1994; Lemoine *et al.*, 1987; Alpine Adriatic margin: Hermann and Müntener, 1996; Manatschal and Nievergelt, 1997; Ligurian
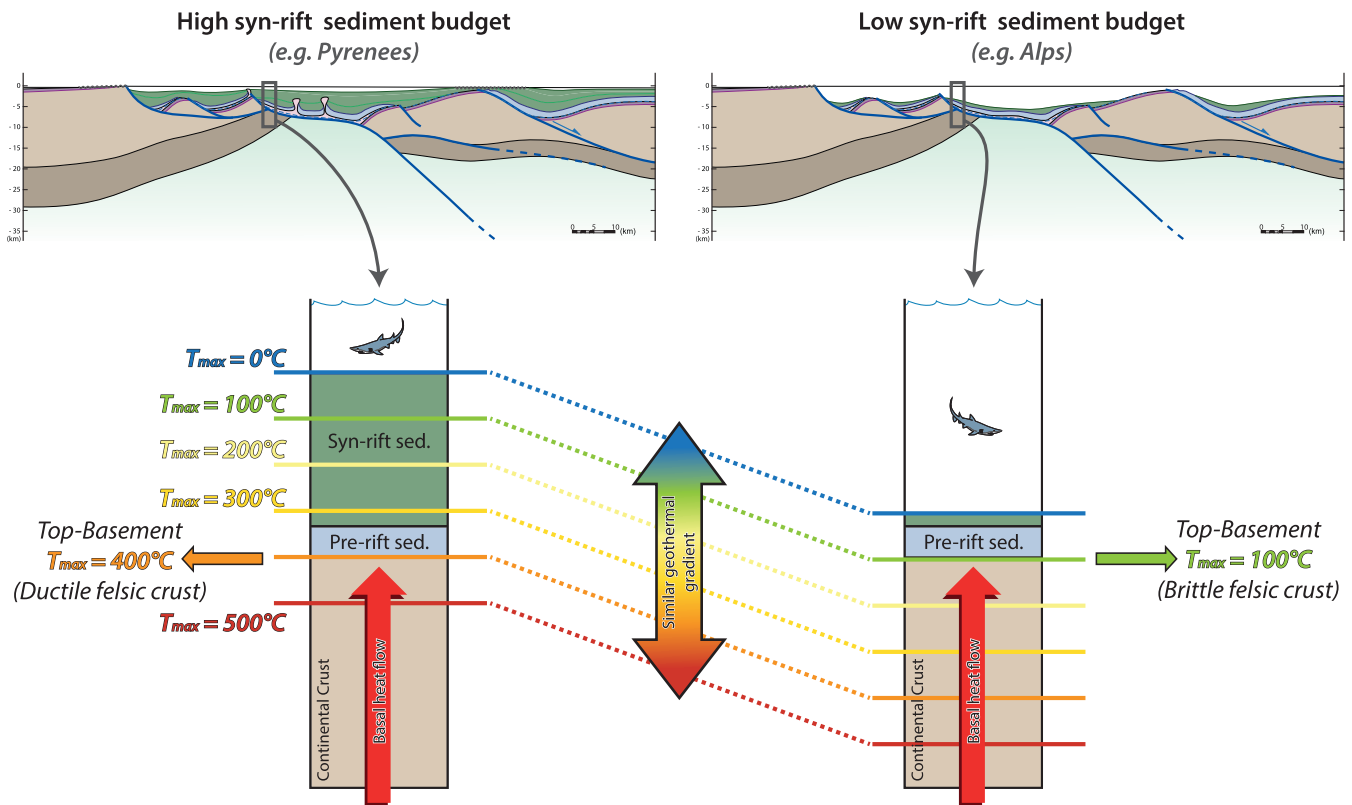
Fig. 13. Comparison between two conceptual models displaying respectively a high sedimentary budget rifted margin (*e.g.* the Pyrenean belt) and a low sedimentary budget rifted margin (*e.g.* the Alps). Associated logs display recorded T_{max} at equivalent heat flow and lithospheric thinning. Observed T_{max} influence the rheology of the basement which becomes ductile beyond of 350 °C for a typical felsic continental crust. In the case of high sedimentary budget, the recorded T_{max} at the top basement exceeds 400 °C, while for the case of low sedimentary budget, the recorded T_{max} are close to 100 °C.

Tethyan margins: Brovarone *et al.*, 2011; Marroni *et al.*, 1998; Molli, 1996) and discontinuous layers of pre- and syn-rift sedimentary slivers along hyperthinned crustal domains (Beltrando *et al.*, 2014). This low-sedimentation rate is partly due to the persisting syn- and post-rift marine environments along sourcing areas and the occurrence of more proximal troughs trapping detrital sedimentation. It should also be replaced in the context of a wider Alpine oceanic basin (hundreds of kilometers wide, Vissers *et al.*, 2013) with respect to the ∼100 km wide aborted Pyrenean rift system (McCarthy *et al.*, 2020). Although the Alpine margins may have recorded similar heat flows and hydrothermal circulations at the top of the basement, it cannot be efficiently recorded within a thin if not simply absent sedimentary cover, most of the syn-rift heat being directly brought to the seawater (Pinto *et al.*, 2015). Thus, the comparison between the Pyrenean and Alpine examples strongly highlights that the top-basement T_{max} during rifting is obviously influenced by the syn-rift sedimentary budget within the hyperextended domain (Fig. 13). For similar thinning factors, it also implies that a felsic crust under hyperextension can easily reach and stay longer in the ductile field (*i.e.* >350 °C) for a highly-sedimented rift system than for a poorly-sedimented scenario, as suggested by recent studies (Asti *et al.*, 2019; Clerc and

Lagabrielle, 2014; Clerc *et al.*, 2015; Lagabrielle *et al.*, 2019b). In other words, high sedimentary budgets for similar top-basement heat flows should delay the crustal embrittlement during hyperextension. The resulting ∼10 km crustal thickness considered as a "thinning threshold" allowing the crustal embrittlement required for mantle exhumation proposed from both the Alpine and Iberia-Newfoundland sediment-poor cases (Manatschal *et al.*, 2001; Müntener *et al.*, 2000; Pérez-Gussinyé *et al.*, 2003) may not be applicable for higher syn-rift sedimentary budgets like in the Pyrénées. Out of Western Europe and from this point of view, the observed extremely thinned (<5 km) but still mantle-decoupled crust of the distal part of the Lower Congo rift basin of the South Atlantic (Congo and Angola margins) described by Clerc *et al.* (2018) may not only be related to an abnormal late rift thermal gradient (*i.e.* hot *versus* cold rifting) but rather to an extremely high sedimentary budget as shown by its 7–8 km thick syn-rift burial.

7 Conclusions

This study provides an unprecedented database of thermal constraints of the entire Pyrenean hyperextended rift system

inverted and passively integrated in the Pyrenean orogenesis. This database is made of a compilation of surface and subsurface measurements of peak metamorphism temperatures (T_{max}) archived by the organic matter originating from pre-rift to syn-orogenic sedimentary deposits of different rift-related and alpine structural units. Temperature constraints all derived from RSCM and Vitrinite Reflectance (R_o) methods harvested from all current available academic and industrial studies. The database described and analysed in this study enables investigating the spatial and temporal thermal record of a hyperextended rift system reaching a mantle exhumation stage, but which failed to reach a seafloor spreading stage. If its so-called HT/LP Pyrenean metamorphism is its most famous evidence, the spatial and temporal resolution of our study considerably refines its spatial and stratigraphic distribution and provides new data on its intensity, which can be then replaced in a rift and orogenic tectonic context after decades of research in the area. From our analysis we show that:

– at the rift scale, the depth T_{max} profiles recorded by R_o values along drillholes generally show a thermal break between the end of the syn-rift and the early post-rift sequences (*i.e.* at post-rift time) that is affected by Pyrenean deformations. It indicates that the effect of the HT/LP metamorphic event is mostly recorded within pre- and syn-rift sediments;

– this regional trend is however not respected along a small HT-strip within early orogenic sediments along the North Pyrenean Frontal Thrust and above the Grand Rieu ridge. Linked to previous studies, we attribute this HT-stripe to the percolation of hot hydrothermal fluids sourced from the dehydration of underthrust basement and/or sediment rocks at depth during the early orogenic stage ("continental subduction");

– the same intensity of the HT/LP metamorphism (reaching ~500 °C) is recorded all along the Pyrénées from the Boucheville and Bas-Agly areas in the east to the Cantabrian belt in the west for similar burial and rift-related structural settings. They are consistently recorded at the basement-sediment interface underneath the most distal part of the hyperextended domain (in the vicinity of exhumed crustal or mantle rocks). This thermal peak is recorded underneath the northern border of the Mauléon Basin (calibrated by wells) and is shifted across transfer zone on the opposite side of the NPZ along the Central and Eastern Pyrénées where it outcrops at the surface. It suggests that all of the Pyrenean rift system can reach equally "hot" T_{max} from east to west and that the rift system may have recorded a major change in the rift paleogeography (*e.g.* Chevrot *et al.*, 2018; Tugend *et al.*, 2015), that in turn played a role during their orogenic shortening;

– along N-S-striking sections and at the scale of the entire rift system (*i.e.* necking zone to necking zone), the thermal structure appears asymmetric and reveals different horizontal thermal gradients between the northern and southern borders of rift basins as observed in the Basque-Cantabrian, Mauléon-Arzacq and Tarascon rift segments. This may be linked with an asymmetry of the former hyperextended rift system as proposed by former studies (Lescoutre *et al.*, 2019);

– by comparing the Pyrenean and Alpine hyperextended rift systems, we can conclude that this high thermal imprint is strongly influenced by fluid advection during hyperextension and may be a characteristic feature of hyperextended rift settings with a high sedimentation rate promoting thermal blanketting. Because of tectonic migration or cessation, the persisting late to post-rift Pyrenean HT record suggests that the decrease of heat convection led to a more conductive post-rift thermal regime and a delay of peak metamorphism.

Supplementary material

Fig. S1. N-S seismic composite line (82-BUZ-11, 2005-Rontignon-Lacq-Merge, 82-SVG-08, 82-SVG-008, 82 SVG-03, Pecorade and AG1-V9 seismic lines provided by Total, R&D) across the Western Pyrénées as well as the location of the different used wells (at the top). Line drawing and geological interpretation of the seismic composite line with all tectono-stratigraphic units presented in the paper (at the bottom).

Table S1. R_o values from the Les Cassières-2 borehole and estimated temperatures calculated with the formulas provide by Barker and Pawlewicz (1994).

Table S2. R_o values from the Bellevue-1 borehole and estimated temperatures calculated with the formulas provide by Barker and Pawlewicz (1994).

Table S3. R_o values from the Orthez-102 borehole and estimated temperatures calculated with the formulas provide by Barker and Pawlewicz (1994).

Table S4. All R_o data used to build maps of spatial distribution of thermal maturity of organic matter by each tectonostratigraphic unit.

Table S5. RSCM peak temperatures from this study measured in the Pyrenean-Cantabrian belt. The parameters RA1$_{Lahfid}$ (Lahfid *et al.*, 2010) and R2$_{Beyssac}$ (Beyssac *et al.*, 2002) are used to estimate temperatures <320 and >330 °C, respectively. RA1$_{Lahfid}$, R2$_{Beyssac}$ and T are expressed in terms of mean values and SD of all the data obtained for each of the 208 samples from the whole Pyrénées. The total number of spectra and the number of used spectra is detailed. Standard errors (SE) are given for all the temperatures (SD divided by the square root of the number of measurements).

The Supplementary Material is available at https://www.bsgf.fr/10.1051/bsgf/2021029/olm.

References

Airaghi L, Bellahsen N, Dubacq B, Chew D, Rosenberg C, Janots E, *et al.* 2020. Pre-orogenic upper crustal softening by lower greenschist facies metamorphic reactions in granites of the central Pyrenees. *J Metamorph Geol* 38(2): 183–204.

Albarède F, Michard-Vitrac A. 1978a. Age and significance of the North Pyrenean metamorphism. *Earth Planet Sci Lett* 40: 327–332.

Albarède F, Michard-Vitrac A. 1978b. Datation du metamorphisme des terrains secondaires des Pyrenees par les methodes (super 39) Ar- (super 40) Ar et (super 87) Rb- (super 87) Sr; ses relations avec les peridotites associees. *Dating Metamorph Mesoz Terrains* 20: 681–687.

Allen PA, Allen JR. 2013. Basin analysis: Principles and application to petroleum play assessment. John Wiley & Sons.

Angrand P, Ford M, Watts AB. 2018. Lateral variations in foreland flexure of a rifted continental margin: The Aquitaine Basin (SW France). *Tectonics* 37(2): 430–449.

Angrand P, Ford M, Ducoux M, de Saint Blanquat M. 2021. Extension and early orogenic inversion along the basal detachment of a hyper-extended rifted margin: an example from the Central Pyrenees (France). *J Geol Soc*.

Arche A, López-Gómez J. 1996. Origin of the Permian-Triassic Iberian basin, central-eastern Spain. *Tectonophysics* 266(1–4): 443–464.

Asti R, Lagabrielle Y, Fourcade S, Corre B, Monié P. 2019. How do continents deform during mantle exhumation? Insights from the northern Iberia inverted paleopassive margin, western Pyrenees (France). *Tectonics* 38(5): 1666–1693.

Autran A, Cogne EJ. 1980. La zone interne de l'orogène varisque dans l'Ouest de la France et sa place dans le développement de la chaîne hercynienne. In: Cogne J, Slansky M, eds. Géologie de l'Europe. *Mémoires du BRGM* 108: 90–111.

Azambre B, Rossy M. 1976. Le magmatisme alcalin d'age cretace, dans les Pyrenees occidentales et l'Arc basque; ses relations avec le metamorphisme et la tectonique. *Bull Soc Geol Fr* S7-XVIII: 1725–1728. https://doi.org/10.2113/gssgfbull.S7-XVIII.6.1725.

Azambre B, Rossy M, Albarede F. 1992. Petrology of the alkaline magmatism from the Cretaceous North-Pyrenean rift zone (France and Spain). *Eur J Miner* 4: 813–834.

Bahnan AE, Carpentier C, Pironon J, Ford M, Ducoux M, Barre G, *et al.* 2020, Impact of geodynamics on fluid circulation and diagenesis of carbonate reservoirs in a foreland basin: Example of the Upper Lacq reservoir (Aquitaine basin, SW France). *Mar Pet Geol* 111: 676–694.

Barale L, Bertok C, Talabani NS, D'Atri A, Martire L, Piana F, *et al.* 2016. Very hot, very shallow hydrothermal dolomitization: An example from the Maritime Alps (north-west Italy-south-east France). *Sedimentology* 63: 2037–2065. https://doi.org/10.1111/sed.12294.

Barker CE, Pawlewicz MJ. 1994. Calculation of vitrinite reflectance from thermal histories and peak temperatures: A comparison of methods. In: Mukhopadhyay PK, Dow WG, eds. Vitrinite Reflectance as a Maturity Parameter (Vol. 570). Washington,

DC: American Chemical Society, pp. 216–229. https://doi.org/10.1021/bk-1994-0570.ch014.

Barnett-Moore N, Hosseinpour M, Maus S. 2016. Assessing discrepancies between previous plate kinematic models of Mesozoic Iberia and their constraints. *Tectonics* 35: 2015TC004019. https://doi.org/10.1002/2015TC004019.

Beaumont C, Muñoz JA, Hamilton J, Fullsack P. 2000. Factors controlling the Alpine evolution of the central Pyrenees inferred from acomparison of observations and geodynamical models, *J Geophys Res* 105(B4): 8121–8145. https://doi.org/10.1029/1999JB900390.

Bellahsen N, Bayet L, Denele Y, Waldner M, Airaghi L, Rosenberg C, *et al.* 2019. Shortening of the axial zone, pyrenees: Shortening sequence, upper crustal mylonites and crustal strength. *Tectonophysics* 766: 433–452.

Beltrando M, Frasca G, Compagnoni R, Vitale Brovarone A. 2012. The Valaisan controversy revisited: multi-stage folding of a Mesozoic hyper-extended margin in the Petit St. Bernard pass area (Western Alps). *Tectonophysics* 579: 17–36. https://doi.org/10.1016/j.tecto.2012.02.010.

Beltrando M, Manatschal G, Mohn G, Dal Piaz GV, Brovarone AV, Masini E. 2014. Recognizing remnants of magma-poor rifted margins in high-pressure orogenic belts: the Alpine case study. *Earth Sci Rev* 131: 88–115. https://doi.org/10.1016/j.earscirev.2014.01.001.

Bernoulli D, Desmurs L, Manatschal G, Muentener O. 2003. Mantle exhumation, ophicalcites and incipient magmatism in an alpine ocean-continent-transition. *GeoActa* 2(Suppl.): 13–17.

Bernus-Maury C. 1984. Étude des paragenèses caractéristiques du métamorphisme mésozoïque dans la partie orientale des Pyrénées (French). Paris 6.

Beyssac O, Goffé B, Chopin C, Rouzaud JN. 2002a. Raman spectra of carbonaceous material in metasediments: a new geothermometer. *J Metamorph Geol* 20: 859–871. https://doi.org/10.1046/j.1525-1314.2002.00408.x.

Beyssac O, Rouzaud J-N., Goffé B, Brunet F, Chopin C. 2002b. Graphitization in a high-pressure, low-temperature metamorphic gradient: a Raman microspectroscopy and HRTEM study. *Contrib Miner Petrol* 143: 19.

Beyssac O, Bollinger L, Avouac JP, Goffé B. 2004. Thermal metamorphism in the lesser Himalaya of Nepal determined from Raman spectroscopy of carbonaceous material. *Earth Planet Sci Lett* 225(1–2): 233–241.

Biteau JJ, Le Marrec A, Le Vot M, Masset JM. 2006. The aquitaine basin. *Petrol Geosci* 12(3): 247–273.

Blackwell DD, Steele JL. 1989. Thermal Conductivity of Sedimentary Rocks: Measurement and Significance. In: Naeser ND, McCulloh TH, eds. Thermal History of Sedimentary Basins. New York: Springer. http://link.springer.com.biblioplanets.gate.inist.fr/chapter/10.1007/978-1-4612-3492-0_213–36.

Boillot G, Dupeuble PA, Malod J. 1979. Subduction and Tectonics on the continental margin off northern Spain. *Mar Geol* 32: 53–70.

Boillot G. 1984. Le Golfe de Gascogne et les Pyrénées. In: Boillot G, Montadert L, Lemoine M, Biju-Duval B, eds. Les marges continentales actuelles et fossiles autour de la France. Paris: Masson, pp. 249–334.

Bois C, Gariel O. 1994. Deep seismic investigation in the Parentis Basin (Southwestern France). In: Mascle A, ed. Hydrocarbon and Petroleum Geology of France. Berlin, Heidelberg: Springer. *Spec Publ Eur Assoc Petrol Geosci* 4: 173–186.

Bollinger L, Avouac JP, Beyssac O, Catlos EJ, Harrison TM, Grove M, *et al.* 2004. Thermal structure and exhumation history of the Lesser Himalaya in central Nepal. *Tectonics* 23(5).

Boulvais P, de Parseval P, D'Hulst A, Paris P. 2006. Carbonate alteration associated with talc-chlorite mineralization in the eastern Pyrenees, with emphasis on the St. Barthelemy Massif. *Miner Petrol* 88: 499–526. https://doi.org/10.1007/s00710-006-0124-x.

Boulvais P, Ruffet G, Cornichet J, Mermet M. 2007. Cretaceous albitization and dequartzification of Hercynian peraluminous granite in the Salvezines Massif (French Pyrénées). *Lithos* 93: 89–106. https://doi.org/10.1016/j.lithos.2006.05.001.

Boulvais P. 2016. Fluid generation in the Boucheville Basin as a consequence of the North Pyrenean metamorphism. *C R Geosci* 348(From rifting to mountain building: the Pyrenean Belt): 301–311. https://doi.org/10.1016/j.crte.2015.06.013.

Brovarone AV, Beltrando M, Malavieille J, Giuntoli F, Tondella E, Groppo C, *et al.* 2011. Inherited ocean-continent transition zones in deeply subducted terranes: insights from Alpine Corsica. *Lithos* 124(3–4): 273–290.

Brune S, Heine C, Pérez-Gussinyé M, Sobolev SV. 2014. Rift migration explains continental margin asymmetry and crustal hyper-extension. *Nat Commun* 5: 4014.

Brunet MF. 1984. Subsidence history of the Aquitaine Basin determined from the subsidence curves, *Geol Mag* 121(5): 421–428.

Buck WR, Martinez F, Steckler MS, Cochran JR. 1988. Thermal consequences of lithospheric extension: pure and simple. *Tectonics* 7: 213–234.

Cadenas P, Fernández-Viejo G, Pulgar JA, Tugend J, Manatschal G, Minshull TA. 2018. Constraints imposed by rift inheritance on the compressional reactivation of a hyperextended margin: mapping rift domains in the North Iberian margin and in the Cantabrian Mountains. *Tectonics* 37. https://doi.org/10.002/2016TC004454.

Cadenas P, Manatschal G, Fernández-Viejo G. 2020, Unravelling the architecture and evolution of the inverted multi-stage North Iberian-Bay of Biscay rift. *Gondwana Res* 88: 67–87.

Caldera N, Teixell A, Griera A, Labaume P, Lahfid A. 2021. Recumbent folding in the Upper Cretaceous Eaux-Chaudes massif: A Helvetic-type nappe in the Pyrenees? *Terra Nova* 00: 1–0. https://doi.org/10.1111/ter.12517.

Callies M, Filleaudeau PY, Dubille M, Lorant F. 2018. How to predict thermal stress in hyperextended margins: Application of a new lithospheric model on the Iberia margin. *AAPG Bull* 102(4): 563–585.

Canérot J. 1988. Manifestations de l'halocinèse dans les chaînons béarnais (zone Nord-Pyrénéenne) au Crétacé inférieur. *C R Acad Sci*. Série 2, Mécanique, Physique, Chimie, Sciences de l'univers, Sciences de la Terre 306: 1099–1102.

Canérot J. 1989. Early Cretaceous rifting and salt tectonics on the Iberian margin of the Western Pyrenees (France). *Struct Conseq* 13: 87–99.

Canérot J, Lenoble JL. 1993. Diapirisme crétacé sur la marge ibérique des Pyrénées occidentales: Exemple du Pic de Lauriolle, comparaisons avec l'Aquitaine, les Pyrénées centrales et orientales. *Bull Soc Géol Fr* 164: 719–726.

Canérot J, Hudec MR, Rockenbauch K. 2005. Mesozoic diapirism in the Pyrenean orogen: Salt tectonics on a transform plate boundary. *AAPG Bull* 89(2): 211–229.

Cardott BJ, Lambert MW. 1985. Thermal maturation by vitrinite reflectance of Woodford Shale, Anadarko basin, Oklahoma. *AAPG Bull* 69(11): 1982–1998.

Casas-Sainz AM, Gil-Imaz A. 1998. Extensional subsidence, contractional folding and thrust inversion of the eastern Cameros Basin, northern Spain. *Geologische Rundschau* 86(4): 802–818.

Casquet C, Galindo Francisco M, González Casado JM, Alonso Millán Á. 1992. El metamorfismo en la cuenca de los Cameros. Geocronología e implicaciones tectónicas. *Geogaceta* 11: 22–25.

Chelalou R, Nalpas T, Bousquet R, Prevost M, Lahfid A, Poujol M, *et al.* 2016. Tectonics, tectonophysics: New sedimentological, structural and paleo-thermicity data in the Boucheville Basin (eastern North Pyrenean Zone, France). *C R Géosci* 348(3–4): 312–321. https://doi.org/10.1016/j.crte.2015.11.008.

Chenin P, Manatschal G, Picazo S, Müntener O, Karner G, Johnson C, *et al.* 2017. Influence of the architecture of magma-poor hyperextended rifted margins on orogens produced by the closure of narrow versus wide oceans. *Geosphere* 13(2): 559–576.

Chevrot S, Sylvander M, Diaz J, Martin R, Mouthereau F, Manatschal G, *et al.* 2018. The non-cylindrical crustal architecture of the Pyrenees. *Sci Rep* 8(1): 1–8.

Choukroune P. 1976. Strain patterns in the Pyrenean Chain. *Philos Trans R Soc Lond Ser Math Phys Sci* 283: 271–280.

Choukroune P. 1972. Relations entre tectonique et métamorphisme dans les terrains secondaires de la zone nord-pyreneenne centrale et orientale. *Relatsh Tecton Metamorph Mesoz Terrains Cent Orient North Pyr* 14: 3–11.

Choukroune P, ECORS Team. 1989. The ECORS Pyrenean deep seismic profile reflection data and the overall structure of an orogenic belt. *Tectonics* 8: 23–39.

Clerc C, Lagabrielle Y, Neumaier M, Reynaud JY, de Saint Blanquat M. 2012, Exhumation of subcontinental mantle rocks: evidence from ultramafic-bearing clastic deposits nearby the Lherz peridotite body, French Pyrenees. *Bull Soc Géol Fr* 183(5): 443–459.

Clerc C, Boulvais P, Lagabrielle Y, de Saint Blanquat M. 2013. Ophicalcites from the northern Pyrenean belt: a field, petrographic and stable isotope study. *Int J Earth Sci* 103: 141–163. https://doi.org/10.1007/s00531-013-0927-z.

Clerc C, Lagabrielle Y. 2014. Thermal control on the modes of crustal thinning leading to mantle exhumation: Insights from the Cretaceous Pyrenean hot paleomargins. *Tectonics* 33: 2013TC003471. https://doi.org/10.1002/2013TC003471.

Clerc C, Lagabrielle Y, Neumaier M, Reynaud J-Y, de Saint Blanquat M. 2012. Exhumation of subcontinental mantle rocks: evidence from ultramafic-bearing clastic deposits nearby the Lherz peridotite body, French Pyrenees. *Bull Soc Geol Fr* 183: 443–459.

Clerc C, Lahfid A, Monie P, Lagabrielle Y, Chopin C, Poujol M, *et al.* 2015. High-temperature metamorphism during extreme thinning of the continental crust: a reappraisal of the North Pyrenean passive paleomargin. *Solid Earth* 6: 643–668. https://doi.org/10.5194/se-6-643-2015.

Clerc C, Ringenbach JC, Jolivet L, Ballard JF. 2018. Rifted margins: Ductile deformation, boudinage, continentward-dipping normal faults and the role of the weak lower crust. *Gondwana Res* 53: 20–40.

Cloix A. 2017. Bréchification de la série prérift Nord-Pyrénéenne: Mécanismes tectoniques ou/et sédimentaires et place dans l'histoire tectono-métamorphique de la marge extensive crétacée et de son inversion pyrénéenne (Chaînons Béarnais, Zone Nord-Pyrénéenne). Master Géosciences, Mémoire de Master 2. Université de Montpellier. http://rgf.brgm.fr/sites/default/files/upload/documents/productionscientifique/Masters/rgf_amipyr2016_ma12_memoire_cloix.pdf.

Coltat R, Branquet Y, Gautier P, Boulvais P, Manatschal G. 2020. The nature of the interface between basalts and serpentinized mantle in oceanic domains: Insights from a geological section in the Alps. *Tectonophysics* 797: 228646.

Conand C, Mouthereau F, Ganne J, Lin AT-S, Lahfid A, Daudet M, *et al.* 2020. Strain partitioning and exhumation in oblique Taiwan collision: Role of rift architecture and plate kinematics. *Tectonics* 38. https://doi.org/10.1029/2019TC005798.

Corre B. 2017. La bordure nord de la plaque ibérique à l'Albo-Cénomanien: architecture d'une marge passive de type ductile

(Chaînons Béarnais, Pyrénées Occidentales). Doctoral dissertation. Rennes 1.

Corre B, Boulvais P, Boiron MC, Lagabrielle Y, Marasi L, Clerc C. 2018. Fluid circulations in response to mantle exhumation at the passive margin setting in the north Pyrenean zone, France. *Miner Petrol* 1–24.

Corre B, Lagabrielle Y, Labaume P, Fourcade S, Clerc C, Ballèvre M. 2016. Deformation associated with mantle exhumation in a distal, hot passive margin environment: new constraints from the Saraillé Massif (Chaînons Béarnais, North-Pyrenean Zone). *C R Géosci* 348(3–4): 279–289.

Dauteuil O, Ricou LE. 1989. Une circulation de fluides de haute-temperature a l'origine du metamorphisme cretace nord-pyreneen. *Circ High-Temp Fluids Orig North Pyrenean Cretac Metamorph* 3: 237–250.

Debroas EJ. 1990. Le flysch noir albo-cenomanien temoin de la structuration albienne a senonienne de la Zone nord-pyreneenne en Bigorre (Hautes-Pyrenees, France). *Bull Soc Géol Fr* 6: 273–285.

Debroas EJ, Canérot J, Billote M. 2010. Les brèches d'Urdach, témoins de l'exhumation du manteau pyrénéen dans un escarpement de faille vraconien-cénomanien inférieur (Zone Nord Pyrénéenne, Pyrénées Atlantiques, France). *Géol Fr* 2: 53–65.

Decandia FA, Elter P. 1972. La "zona" ofiolitifera del Bracco nel settore compreso fra Levento e la Val Graveglia (Appenino ligure). *Mem Soc Geol Ital* 11: 503–530.

Decarlis A, Fellin MG, Maino M, Ferrando S, Manatschal G, Gaggero L, *et al.* 2017. Tectono-thermal Evolution of a Distal Rifted Margin: Constraints From the Calizzano Massif (Prepiedmont-Briançonnais Domain, Ligurian Alps). *Tectonics* 36(12): 3209–3228.

DeFelipe I, Pedreira D, Pulgar JA, Iriarte E, Mendia M. 2017. Mantle exhumation and metamorphism in the Basque-Cantabrian Basin (NSpain): Stable and clumped isotope analysis in carbonates and comparison with ophicalcites in the North-Pyrenean Zone (Urdach and Lherz). *Geochem Geophys Geosyst* n/a-n/a. https://doi.org/10.1002/2016GC006690.

DeFelipe Martín I, Álvarez Pulgar FJ, Pedreira Rodríguez D. 2018. Crustal structure of the Eastern Basque-Cantabrian Zone-western Pyrenees: from the Cretaceous hyperextension to the Cenozoic inversion. *Revista de la Sociedad Geológica de España* 31(2).

Dérégnaucourt D, Boillot G. 1982. New structural map of the Bay of Biscay (In). *C R Acad Sci* 294: 219–222.

de Saint Blanquat M, Bajolet F, Grand'Homme A, Proietti A, Zanti M, Boutin A, *et al.* 2016. Cretaceous mantle exhumation in the central Pyrenees: new constraints from the peridotites in eastern Ariège (North Pyrenean zone, France). *C R Géosci* 348(3–4): 268–278.

Desegaulx P, Brunet MF. 1990. Tectonic subsidence of the Aquitaine basin since Cretaceous times. *Bull Soc Géol Fr* 8: 295–306.

Dielforder A, Frasca G, Brune S, Ford M. 2019. Formation of the Iberian-European Convergent Plate Boundary Fault and Its Effect on Intraplate Deformation in Central Europe. *Geochem Geophy Geosyst* 20(5): 2395–2417.

Dow WG. 1977. Kerogen studies and geological interpretations. *J Geochem Explor* 7: 79–99.

Ducoux M. 2017. Structure, thermicité et évolution géodynamique de la Zone Interne Métamorphique des Pyrénées. Thèse de Doctorat, Université d'Orléans.

Ducoux M, Jolivet L, Callot J-P, Aubourg C, Masini E, Lahfid A, *et al.* 2019. The Nappe des Marbres Unit of the Basque-Cantabrian Basin: The tectono-thermal evolution of a fossil hyperextended rift basin. *Tectonics* 38. https://doi.org/10.1029/2018TC005348.

Ducoux M, Jolivet L, Cagnard F, Baudin T. 2021a. Basement-cover decoupling during the inversion of a hyperextended basin: insights

from the Eastern Pyrenees. *Tectonics* 40: e2020TC006512. https://doi.org/10.1029/2020TC006512.

Ducoux M, Masini E, Tugend J, Gómez-Romeu J, Calassou S. 2021b. Basement-decoupled hyperextension rifting: the tectono-stratigraphic record of the salt-rich Pyrenean necking zone (Arzacq Basin, SW France). *GSA Bull*. https://doi.org/10.1130/B35974.1.

Dumont T, Lemoine M, Tricart P. 1984. Tectonique synsédimentaire triasico-jurassique et rifting téthysien dans l'unité prépiémontaise de Rochebrune au Sud-Est de Briançon. *Bull Soc Géol Fr* 7(5): 921–933.

Duretz T, Asti R, Lagabrielle Y, Brun JP, Jourdon A, Clerc C, *et al.* 2020. Numerical modelling of Cretaceous Pyrenean Rifting: The interaction between mantle exhumation and syn-rift salt tectonics. *Basin Res* 32(4): 652–667.

Elders WA, Rex RW, Robinson PT, Biehler S, Meidav T. 1972. Crustal spreading in Southern California: The Imperial Valley and the Gulf of California formed by the rifting apart of a continental plate. *Science* 178(4056): 15–24.

Espurt N, Angrand P, Teixell A, Labaume P, Ford M, de Saint Blanquat M, *et al.* 2019. Crustal-scale balanced cross-section and restorations of the Central Pyrenean belt (Nestes-Cinca transect): Highlighting the structural control of Variscan belt and Permian-Mesozoic rift systems on mountain building. *Tectonophysics* 764: 25–45.

Etheve N, Mohn G, Frizon de Lamotte D, Roca E, Tugend J, *et al.* 2018. Extreme Mesozoic Crustal Thinning in the Eastern Iberia Margin: The Example of the Columbrets Basin (Valencia Trough). *Tectonics* 37(2): 636–662.

Ewing TA, Hermann J, Rubatto D. 2013. The robustness of the Zr-in-rutile and Ti-in-zircon thermometers during high-temperature metamorphism (Ivrea-Verbano Zone, northern Italy). *Contrib Miner Petrol* 165(4): 757–779.

Fabriès J, Lorand J-P, Bodinier J-L, Dupuy C. 1991. Evolution of the Upper Mantle beneath the Pyrenees: Evidence from Orogenic Spinel Lherzolite Massifs. *J Petrol* Special_Volume: 55–76. https://doi.org/10.1093/petrology/Special_Volume.2.55.

Fabriès J, Lorand J-P, Bodinier J-L. 1998. Petrogenetic evolution of orogenic lherzolite massifs in the central and western Pyrenees. *Tectonophysics* 292: 145–167. https://doi.org/10.1016/S0040-1951(98)00055-9.

Fallourd S, Poujol M, Boulvais P, Paquette J-L, de Saint Blanquat M, Remy P. 2014. In situ LA-ICP-MS U-Pb titanite dating of Na-Ca metasomatism in orogenic belts: the North Pyrenean example. *Int J Earth Sci* 103: 667–682. https://doi.org/10.1007/s00531-013-0978-1.

Ferrer O, Roca E, Benjumea B, Muñoz JA, Ellouz N, MARCONI Team. 2008. The deep seismic reflection MARCONI-3 profile: role of extensional Mesozoic structure during the Pyrenean contractional deformation at the eastern part of the Bay of Biscay. *Mar Pet Geol* 25: 714–730. https://doi.org/10.1016/j.marpetgeo.206.002.

Ferrer O, Roca E, Jackson MPA, Muñoz JA. 2009. Effects of Pyrenean contraction on salt structures of the offshore Parentis Basin (Bay of Biscay). *Trabajos de Geología* 29(29).

Florineth D, Froitzheim N. 1994. Transition from continental to oceanic basement in the Tasna nappe (Engadine window, Graubunden, Switzerland): evidence for early Cretaceous opening of the Valais Ocean. *Schweiz Mineral Petrogr Mitt* 74: 437–448.

Ford M, Hemmer L, Vacherat A, Gallagher K, Christophoul F. 2016. Retro-wedge foreland basin evolution along the ECORS line, eastern Pyrenees, France. *J Geol Soc* 173: 419–437. https://doi.org/10.1144/jgs2015-129.

Fortané A, Duée G, Lagabrielle Y, Coutelle A. 1986. Lherzolites and the western "Chainons béarnais"(French Pyrenees): Structural and paleogeographical pattern. *Tectonophysics* 129(1–4): 81–98.

Froitzheim N, Manatschal G. 1996. Kinematics of Jurassic rifting, mantle exhumation, and passive-margin in the Austroalpine and Penninic nappes (eastern Switzerland). *Geol Soc Am Bull* 108: 1120–1133.

Gabalda S, Beyssac O, Jolivet L, Agard P, Chopin C. 2009. Thermal structure of a fossil subduction wedge in the Western Alps. *Terra Nova* 21(1): 28–34.

García-Mondéjar J. 1996. Plate reconstruction of the Bay of Biscay. *Geology* 24: 635–638.

García-Senz J. 2002. Cuencas extensivas del Cretacico Inferior en los Pireneos Centrales − formacion y subsecuente inversion. PhD thesis. Barcelona: University of Barcelona.

García-Senz J, Pedrera A, Ayala C, Ruiz-Constán A, Robador A, Rodríguez-Fernández LR. 2019. Inversion of the north Iberian hyperextended margin: the role of exhumed mantle indentation during continental collision. In: Hammerstein JA, ed. Fold and Thrust Belts: Structural Style, Evolution and Exploration. *Geol Soc Lond Spec Publ*: 490. https://doi.org/10.1144/SP490-2019-112.

Garrido-Megias A, Rios Aragues LM. 1972. Sintesis geologica del Secundario y Terciario entre los rios Cinca y Segre (Pirineo Central de la vertiente sur pirenaica, provincias de Huesca y Lerida). *Summ Mesoz Tert Geol Cinca Segre Rivers Souther* 83: 1–47.

Golberg JM, Maluski H, Leyreloup AF. 1986. Petrological and age relationship between emplacement of magmatic breccia, alkaline magmatism, and static metamorphism in the North Pyrenean Zone. *Tectonophysics* 129: 275–290. https://doi.org/10.1016/0040-1951(86)90256-8.

Golberg JM. 1987. Le métamorphisme mésozoique dans la partie orientale des Pyrénées ; relations avec l'évolution de la chaîne au crétacé. Montpellier, France: Université des Sciences et Techniques du Languedoc, Centre Géologique et Géophysique.

Golberg JM, Leyreloup AF. 1990. High temperature-low pressure Cretaceous metamorphism related to crustal thinning (Eastern North Pyrenean Zone, France). *Contrib Miner Pet* 104: 194–207. https://doi.org/10.1007/BF00306443.

Golberg JM, Maluski H. 1988. Donnees nouvelles et mise au point sur l'age du metamorphisme pyreneen. *New Data Discuss Age Pyrenean Metamorph* 306: 429–435.

Gómez-Romeu J, Masini E, Tugend J, Ducoux M, Kusznir N. 2019. Role of rift structural inheritance in orogeny highlighted by the Western Pyrenees case-study. *Tectonophysics* 766: 131–150.

González-Acebrón L, Goldstein R, Mas R, Arribas J. 2011. Criteria for recognition of localization and timing of multiple events of hydrothermal alteration in sandstones illustrated by petrographic, fluid inclusion, and isotopic analysis of the Tera Group, Northern Spain. *Int J Earth Sci* 100(8): 1811–1826. https://doi.org/10.1007/s00531-010-0606-2.

Gorini C, Le Marrec A, Mauffret A. 1993. Contribution to the structural and sedimentary history of the Gulf of Lions (western Mediterranean), from the ECORS profiles, industrial seismic profiles and weII data. *Bull Geol Soc. Fr* 164: 353–363.

Gorini C, Mauffret A, Guennoc P, Le Marrec A. 1994. Structure of the Gulf of Lions (Northwestern Mediterranean Sea): a review. In: Mascle A, ed. Hydrocarbon and Petroleum Geology of France. Springer-Verlag, pp. 223–243.

Grool AR, Ford M, Vergés J, Huismans RS, Christophoul F, Dielforder A. 2018. Insights into the crustal-scale dynamics of a doubly vergent orogen from a quantitative analysis of its forelands: A case study of the eastern Pyrenees. *Tectonics* 37(2): 450–476.

Hantschel T, Kauerauf AI. 2009. Fundamentals of Basin and Petroleum Systems Modeling. https://doi.org/10.1007/978-3-540-72318-9.

Hart NR, Stockli DF, Lavier LL, Hayman NW. 2017. Thermal evolution of a hyperextended rift basin, Mauléon Basin, western Pyrenees. *Tectonics* 36: 1103–1128. https://doi.org/10.1002/2016TC004365.

Hermann J, Müntener O. 1996. Exhumation-related structures in the Malenco- Margna system: implications for paleogeography and its consequences for rifting and Alpine tectonics. *Schweizerische Mineralogische und Petrographische Mitteilungen* 76: 501–520.

Hogan PJ, Burbank KDW. 1996. Evolution of the Jaca piggy-back basin and emergence of the External Sierras, southern Pyrenees. In: Friend PF, Dabrio CJ, eds. Tertiary Basins of Spain. Cambridge, UK: Cambridge Univ. Press, pp. 153–160.

Incerpi N, Manatschal G, Martire L, Bernasconi SM, Gerdes A, Bertok C. 2020a. Characteristics and timing of hydrothermal fluid circulation in the fossil Pyrenean hyperextended rift system: new constraints from the Chaînons Béarnais (W Pyrenees). *Int J Earth Sci* 1–23.

Incerpi N, Martire L, Manatschal G, Bernasconi SM, Gerdes A, Czuppon G, *et al.* 2020b. Hydrothermal fluid flow associated to the extensional evolution of the Adriatic rifted margin: Insights from the pre-to post-rift sedimentary sequence (SE Switzerland, N ITALY). *Basin Res* 32(1): 91–115.

Izquierdo-Llavall E, Menant A, Aubourg C, Callot JP, Hoareau G, Camps P, *et al.* 2020. Preorogenic folds and syn-orogenic basement tilts in an inverted hyperextended margin: The Northern Pyrenees case study. *Tectonics* 39(7): e2019TC005719.

Jagoutz O, Müntener O, Manatschal G, Rubatto D, Péron-Pinvidic G, Turrin BD, *et al.* 2007. The rift-to-drift transition in the North Atlantic: a stuttering start of the MORB machine? *Geology* 35: 1087–1090. https://doi.org/10.1130/G23613A.1.

James V, Canerot J. 1999. Diapirisme et structuration post-triasique des Pyrénées occidentale et de l'Aquitaine méridionale (France). *Eclogae Geologicae Helvetiae* 63. https://doi.org/10.5169/seals-168647.

Jammes S, Manatschal G, Lavier L, Masini E. 2009. Tectonosedimentary evolution related to extreme crustal thinning ahead of a propagating ocean: Example of the western Pyrenees. *Tectonics* 28: TC4012. https://doi.org/10.1029/2008TC002406.

Jammes S, Lavier L, Manatschal G. 2010a. Extreme crustal thinning in the Bay of Biscay and the Western Pyrenees: From observations to modeling. *Geochem Geophys Geosyst* 11: Q10016. https://doi.org/10.1029/2010GC003218.

Jammes S, Manatschal G, Lavier L. 2010b. Interaction between prerift salt and detachment faulting in hyperextended rift systems: The example of the Parentis and Mauléon basins (Bay of Biscay and western Pyrenees). *AAPG Bull* 94(7): 957–975.

Jammes S, Tiberi C, Manatschal G. 2010c. 3D architecture of a complex transcurrent rift system: the example of the Bay of Biscay-Western Pyrenees. *Tectonophysics* 489(1–4): 210–226.

Jolivet M, Labaume P, Monié P, Brunel M, Arnaud N, Campani M. 2007. Thermochronology constraints for the propagation sequence of the south Pyrenean basement thrust system (France-Spain). *Tectonics* 26: TC5007. https://doi.org/10.1029/2006TC002080.

Jolivet L, Romagny A, Gorini C, Maillard A, Thinon I, Couëffé R, *et al.* 2020. Fast dismantling of a mountain belt by mantle flow: Late-orogenic evolution of Pyrenees and Liguro-Provençal rifting. *Tectonophysics* 776: 228312.

Jourdon A, Le Pourhiet L, Mouthereau F, Masini E. 2019. Role of rift maturity on the architecture and shortening distribution in mountain belts. *Earth Planet Sci Lett* 512: 89–99.

Labaume P, Teixell A. 2020. Evolution of salt structures of the Pyrenean rift (Chaînons Béarnais, France): From hyper-extension to tectonic inversion. *Tectonophysics* 785: 228451.

Labaume P, Meresse F, Jolivet M, Teixell A, Lahfid A. 2016. Tectonothermal history of an exhumed thrust-sheet-top basin: an example from the south Pyrenean thrust belt. *Tectonics* 35: 1280–1313. https://doi.org/10.1002/2016TC004192.

Lagabrielle Y, Cannat M. 1990. Alpine Jurassic ophiolites resemble the modern central Atlantic basement. *Geology* 18: 319–322.

Lagabrielle Y, Bodinier J-L. 2008. Submarine reworking of exhumed subcontinental mantle rocks; field evidence from the Lherz peridotites, French Pyrenees. *Terra Nova* 20: 11–21. https://doi.org/10.1111/j.1365-3121.2007.00781.x.

Lagabrielle Y, Clerc C, Vauchez A, Lahfid A, Labaume P, Azambre B, *et al.* 2016. Very high geothermal gradient during mantle exhumation recorded in mylonitic marbles and carbonate breccias from a Mesozoic Pyrenean palaeomargin (Lherz area, North Pyrenean Zone, France). *C R Geosci* 348(From rifting to mountain building: the Pyrenean Belt): 290–300. https://doi.org/10.1016/j.crte.2015.11.004.

Lagabrielle Y, Asti R, Duretz T, Clerc C, Fourcade S, Teixell A, *et al.* 2020. A review of cretaceous smooth-slopes extensional basins along the Iberia-Eurasia plate boundary: How pre-rift salt controls the modes of continental rifting and mantle exhumation. *Earth-Science Reviews* 201: 103071.

Lagabrielle Y, Asti R, Fourcade S, Corre B, Poujol M, Uzel J, *et al.* 2019a. Mantle exhumation at magma-poor passive continental margins. Part I. 3D architecture and metasomatic evolution of a fossil exhumed mantle domain (Urdach lherzolite, north-western Pyrenees, France) Exhumation du manteau au pied des marges passives pauvres en magma. Partie 1. Architecture 3D et évolution métasomatique du domaine fossile à manteau exhumé (lherzolite d'Urdach, Pyrénées NW, France). *Bull Soc Géol Fr* 190(1).

Lagabrielle Y, Asti R, Fourcade S, Corre B, Labaume P, Uzel J, *et al.* 2019b. Mantle exhumation at magma–poor passive continental margins. Part II: Tectonic and metasomatic evolution of large–displacement detachment faults preserved in a fossil distal margin domain (Saraillé lherzolites, northwestern Pyrenees, France). *Bull Soc Géol Fr* 190(1).

Lagabrielle Y, Labaume P, de Saint Blanquat M. 2010. Mantle exhumation, crustal denudation, and gravity tectonics during Cretaceous rifting in the Pyrenean realm (SW Europe): Insights from the geological setting of the lherzolite bodies. *Tectonics* 29: TC4012. https://doi.org/10.1029/2009TC002588.

Lahfid A, Beyssac O, Deville E, Negro F, Chopin C, Goffe B. 2010. Evolution of the Raman spectrum of carbonaceous material in low-grade metasediments of the Glarus Alps (Switzerland). *Terra Nova* 22: 354–360. https://doi.org/10.1111/j.1365-3121.2010.00956.x.

Larsen HC, Mohn G, Nirrengarten M, Sun Z, Stock J, Jian Z, *et al.* 2018. Rapid transition from continental breakup to ig-neous oceanic crust in the South China Sea. *Nat Geosci* 11: 782–789. https://doi.org/10.1038/s41561-018-0198-1.

Lavier L, Manatschal G. 2006. A Mechanism to Thin the Continental Lithosphere at Magma-Poor Margins. *Nature* 440: 324–328. https://doi.org/10.1038/nature04608.

Lavier LL, Ball PJ, Manatschal G, Heumann MJ, MacDonald J, Matt VJ, *et al.* 2019. Controls on the Thermomechanical Evolution of Hyperextended Lithosphere at Magma-Poor Rifted Margins: The Example of Espirito Santo and the Kwanza Basins. *Geochem Geophys Geosyst* 20(11): 5148–5176.

Lemoine M, Trümpy R. 1987. Pre-oceanic rifting in the Alps. *Tectonophysics* 133: 305–320.

Lemoine M, Bas T, Arnaud-Vanneau A, Arnaud H, Dumont T, Gidon M, *et al.* 1986. The continental margin of the Mesozoic Tethys in the Western Alps. *Mar Pet Geol* 3: 179–199.

Lemoine M, Tricart P, Boillot G. 1987. Ultramafic and gabbroic ocean floor of the Ligurian Tethys (Alps, Corsica, Apennines). In search of a genetic model. *Geology* 15: 622–625.

Lescoutre R, Tugend J, Brune S, Masini E, Manatschal G. 2019. Thermal evolution of asymmetric hyperextended magma-poor rift systems: results from numerical modelling and Pyrenean field observations. *Geochem Geophys Geosyst* 20(10): 4567–4587. https://doi.org/10.1029/2019gc008600.

Lescoutre R, Manatschal G. 2020. Role of rift-inheritance and segmentation for orogenic evolution: example from the Pyrenean-Cantabrian system. *Bull Soc Géol Fr* 191(1).

Lister GS, Etheridge MA, Symonds PA. 1986. Detachment faulting and the evolution of passive continental margins. *Geology* 14(3): 246–250.

López-Mir B, Muñoz JA, Senz JG. 2014. Restoration of basins driven by extension and salt tectonics: Example from the Cotiella Basin in the central Pyrenees. *J Struct Geol* 69: 147–162.

Lucazeau F, Le Douaran S. 1985. The blanketing effect of sediments in basins formed by extension: A numerical model. Application to the Gulf of Lion and Viking graben. *Earth Planet Science Lett* 74(1): 92–102. https://doi.org/10.1016/0012-821X(85)90169-4.

Macchiavelli C, Vergés J, Schettino A, Fernàndez M, Turco E, Casciello E, *et al.* 2017. A new southern North Atlantic isochron map: Insights into the drift of the Iberian plate since the Late Cretaceous. *J Geophys Res Solid Earth* 122: 9603–9626. https://doi.org/10.1002/2017JB014769.

Manatschal G. 2004. New models for evolution of magma-poor rifted margins based on a review of data and concepts from West Iberia and the Alps. *Int J Earth Sci* 93: 432–466. https://doi.org/10.1007/s00531-004-0394-7.

Manatschal G, Nievergelt P. 1997. A continent-Ocean transition recorded in the Err and Platta nappes (Eastern Switzerland). *Eclog Geol Helv* 90: 3–28.

Manatschal G, Bernoulli D. 1999. Architecture and tectonic evolution of nonvolcanic margins: Present-day Galicia and ancient Adria. *Tectonics* 18(6): 1099–1119.

Manatschal G, Froitzheim N, Rubenach M, Turrin BD. 2001. The role of detachment faulting in the formation of an ocean-continent transition; insights from the Iberia abyssal plain. *Geol Soc Lond Spec Publ* 187: 405–428.

Mantilla Figueroa LC, Galindo C, Mas R, Casquet C. 2002. El metamorfismo hidrotermal cretácico y paleógeno en la cuenca de Cameros (Cordillera Ibérica, España). *Zubía* 14: 143–154.

Marroni M, Molli G, Montanini A, Tribuzio R. 1998. The association of continental crust rocks with ophiolites in the Northern Apennines (Italy): implications for the continent-ocean transition in the Western Tethys. *Tectonophysics* 292: 43–66.

Martinez-Torres LM. 1989. El Manto de los Marmoles (Pirineo occidental): geologia estructural y evolucion geodinamica. Thesis. Leioa: Universidad del Pais Vasco.

Masini E, Manatschal G, Mohn G, Unternehr P. 2012. Anatomy and tectono-sedimentary evolution of a rift-related detachment system: The example of the Err detachment (central Alps, SE Switzerland). *Bulletin* 124(9–10): 1535–1551.

Masini E, Manatschal G, Mohn G. 2013. The Alpine Tethys rifted margins: Reconciling old and new ideas to understand the stratigraphic architecture of magma-poor rifted margins. *Sedimentology* 60(1): 174–196.

Masini E, Manatschal G, Tugend J, Mohn G, Flament J-M. 2014. The tectono-sedimentary evolution of a hyper-extended rift basin; the example of the Arzacq-Mauleon rift system (western Pyrenees, SW

France). *Int J Earth Sci Geol Rundsch* 103: 1569–1596. https://doi.org/10.1007/s00531-014-1023-8.

Mauffret A, Pascal G, Maillard A, Gorini C. 1995. Tectonics and deep structure of the north-western Mediterranean basin. *Mar Pet Geol* 12: 645–666.

Mauffret A, Durand de Grossouvre B, Dos Reis AT, Gorini C, Nercessian A. 2001. Structural geometry in the eastern Pyrenees and western Gulf of Lion (Western Mediterranean). *J Struct Geol* 23: 1701–1726.

McCarthy A, Chelle-Michou C, Müntener O, Arculus R, Blundy J. 2018. Subduction initiation without magmatism: The case of the missing Alpine magmatic arc. *Geology* 46(12): 1059–1062.

McCarthy A, Tugend J, Mohn G, Candioti L, Chelle-Michou C, Arculus R, *et al.* 2020. A case of Ampferer-type subduction and consequences for the Alps and the Pyrenees. *Am J Sci* 320(4): 313–372.

McClay K, Munoz J-A, Garcia-Senz J. 2004. Extensional salt tectonics in a contractional orogen; a newly identified tectonic event in the Spanish Pyrenees. *Geol Boulder* 32: 737–740. https://doi.org/10.1130/G20565.1.

McDowell SD, Elders WA. 1980. Authigenic layer silicate minerals in borehole Elmore 1, Salton Sea Geothermal Field, California, USA. *Contrib Miner Pet* 74: 293–310. https://doi.org/10.1007/BF00371699.

McDowell SD, Elders WA. 1983. Allogenic layer silicate minerals in borehole Elmore Salton Sea geothermal field, California. *Am Miner* 68: 1146–1159.

McKenzie D. 1978. Some remarks on the formation of sedimentary basins. *Earth Planet Sci Lett* 40: 25–32.

Mendia MS. 1987. Estudio petrológico de las rocas metamórfica prealpinas asociadas a la Falla de Leiza (Navarra). Tesis de Licenciatura. Universidad del País Vasco, UPV/EHU.

Mendia MS, Gil Ibarguchi JI. 1991. High-grade metamorphic rocks and peridotites along the Leiza Fault (Western Pyrenees, Spain). *Geol Rundsch* 80: 93–107.

Millán Garrido H. 2006. Estructura y cinemática del frente de cabalgamiento surpirenaico en las Sierras Exteriores aragonesas. In: Colección de Estudios Altoaragoneses, vol. 53. Huesca, Spain: Instituto de Estudios Altoaragoneses.

Millán Garrido H, Pueyo Morer EL, Aurell Cardona M, Aguado Luzón A, Oliva Urcia B, Martínez Peña MB, *et al.* 2000. Actividad tectonica registrada en los depósitos terciarios del frente meridional del Pirineo central. *Rev Soc Geol Esp* 13: 279–300.

Mohn G, Manatschal G, Müntener O, Beltrando M, Masini E. 2010. Unravelling the interaction between tectonic and sedimentary processes during lithospheric thinning in the Alpine Tethys margins. *Int J Earth Sci* 99: 75–101. https://doi.org/10.1007/s00531-010-0566-6.

Molli G. 1996. Pre-orogenic tectonic framework of the northern Appennine ophiolites. *Eclogae Geologicae Helveticae* 89/1: 163–180.

Monchoux P. 1970. Les Lherzolites pyrénéennes : contribution à l'étude de leur minéralogie, de leur genèse et de leurs transformations. Doctoral dissertation. Toulouse : Universite Paul Sabatier.

Montadert L, Roberts DG, De Charpal O, Guennoc P. 1979. Rifting and subsidence of the northern continental margin of the Bay of Biscay. In: Montardet L, Roberts DG, *et al.*, eds. Initial Reports of the Deep Sea Drilling Project, 48. Washington, DC: US Government Printing Office, pp. 1025–1060.

Montigny R, Azambre B, Rossy M, Thuizat R. 1986. K-Ar study of Cretaceous magmatism and metamorphism in the Pyrenees; age

and length of rotation of the Iberian Peninsula. *Tectonophysics* 129: 257–273.

Motte G, Hoareau G, Callot JP, Révillon S, Piccoli F, Calassou S, *et al.* 2021. Rift and salt-related multi-phase dolomitization: example from the northwestern Pyrenees. *Mar Pet Geol* 126: 104932.

Moutthereau F, Filleaudeau PY, Vacherat A, Pik R, Lacombe O, Fellin MG, *et al.* 2014. Placing limits to shortening evolution in the Pyrenees: Role of margin architecture and implications for the Iberia/Europe convergence. *Tectonics* 33: 2283–2314. https://doi.org/10.1002/2014TC003663.

Muffler LJP, White DE. 1969. Active Metamorphism of Upper Cenozoic Sediments in the Salton Sea Geother mal Field and the Salton Trough, Southeastern California. *Geol Soc Am Bull* 80: 157–182. https://doi.org/10.1130/0016-7606(1969)80[157:AMOUCS]2.0.CO;2.

Mukonzo JN, Boiron MC, Lagabrielle Y, Cathelineau M, Quesnel B. 2021. Fluid-rock interactions along detachment faults during continental rifting and mantle exhumation: the case of the Urdach lherzolite body (North Pyrenees). *J Geol Soc* 178(2).

Muñoz JA. 1992. Evolution of a continental collision belt; ECORS-Pyrenees crustal balanced cross-section. In: McClay KR, ed. Thrust tectonics. London, United Kingdom: Chapman & Hall, pp. 235–246.

Muñoz JA. 2002. The Pyrenees. In: Gibbons W, Moreno T, eds. The Geology of Spain. The Geological Society of London, pp. 370–385.

Müntener O, Hermann J, Trommsdorff V. 2000. Cooling history and exhumation of lower-crustal granulite and upper mantle (Malenco, Eastern Central Alps). *J Petrol* 41: 175–200.

Neres M, Miranda JM, Font E. 2013. Testing Iberian kinematics at Jurassic-Cretaceous times. *Tectonics* 32: 1312–1319. https://doi.org/10.1002/tect.20074.

Nirrengarten M, Manatschal G, Tugend J, Kusznir NJ, Sauter D. 2017. Nature and origin of the J-magnetic anomaly offshore Iberia–Newfoundland: implications for plate reconstructions. *Terra Nova* 29(1): 20–28.

Nirrengarten M, Manatschal G, Tugend J, Kusznir N, Sauter D. 2018. Kinematic evolution of the southern North Atlantic: Implications for the formation of hyperextended rift systems. *Tectonics* 37(1): 89–118.

Nirrengarten M, Mohn G, Schito A, Corrado S, Gutiérrez-García L, Bowden SA, et al. 2020. The thermal imprint of continental breakup during the formation of the South China Sea. *Earth Planet Sci Lett* 531: 115972.

Nunn JA, Lin G. 2002. Insulating effect of coals and organic rich shales: implications for topography-driven fluid flow, heat transport, and genesis of ore deposits in the Arkoma Basin and Ozark Plateau. *Basin Res* 14: 129–145. https://doi.org/10.1046/j.1365-2117.2002.00172.x.

Olivet J-L. 1996. La cinematique de la plaque Iberique. *Bull Cent Rech Explor Prod Elf-Aquitaine* 20: 131–195.

Oliva-Urcia B, Beamud E, Garcés M, Arenas C, Soto R, Pueyo EL, *et al.* 2015. New magnetostratigraphic dating in the Palaeogene syntectonic sediments of the west-central Pyrenees: Tectonostratigraphic implications. In: Pueyo EL, ed. Palaeomagnetism in Fold and Thrust Belts: New Perpectives. *Geol Soc Spec Publ* 425. https://doi.org/10.1144/SP425.5.

Omodeo-Salé S, Salas R, Guimerà J, Ondrak R, Mas R, Arribas J, *et al.* 2017. Subsidence and thermal history of an inverted Late Jurassic-Early Cretaceous extensional basin (Cameros, North-central Spain) affected by very low-to-low-grade metamorphism. *Basin Res* 29: 156–174.

Ortiz A, Guillocheau F, Lasseur E, Briais J, Robin C, Serrano O, *et al.* 2020. Sediment routing system and sink preservation during the post-orogenic evolution of a retro-foreland basin: The case example of the North Pyrenean (Aquitaine, Bay of Biscay) Basins. *Mar Pet Geol* 112: 104085.

Osmundsen PT, Péron-Pinvidic G, Ebbing J, Erratt D, Fjellanger E, Bergslien D, *et al.* 2016. Extension, hyperextension and mantle exhumation offshore Norway: a discussion based on 6 crustal transects. *Nor J Geol* 96: 343–372. https://doi.org/10.17850/njg96-4-05.

Pasteris J, Wopenka B. 1991. Raman-Spectra of Graphite as Indicators of Degree of Metamorphism. *Can Miner* 29: 1–9.

Pasteris JD. 1989. In situ analysis in geological thin-sections by laser Raman microprobe spectroscopy; a cautionary note. *Appl Spectrosc* 567–570.

Peace A, McCaffrey K, Imber J, Hobbs R, van Hunen J, Gerdes K. 2017. Quan-tifying the influence of sill intrusion on the thermal evolution of organic-rich sedimentary rocks in nonvolcanic passive margins: an example from ODP 210–1276, offshore Newfoundland, Canada. *Basin Res* 29: 249–265. https://doi.org/10.1111/bre.12131.

Pedrera A, García-Senz J, Ayala C, Ruiz-Constán A, Rodríguez-Fernández LR, Robador A, *et al.* 2017. Reconstruction of the exhumed mantle across the North Iberian Margin by crustal-scale 3-D gravity inversion and geological cross section. *Tectonics* 36. https://doi.org/10.1002/2017TC004716.

Pedreira D, Pulgar JA, Gallart J, Torné M. 2007. Three-dimensional gravity and magnetic modeling of crustal indentation and wedging in the western Pyrenees-Cantabrian Mountains. *J Geophys Res Solid Earth* 112: B12405. https://doi.org/10.1029/2007JB005021.

Pérez-Gussinyé M, Ranero CR, Reston TJ, Sawyer D. 2003. Mechanisms of extension at nonvolcanic margins: Evidence from the Galicia interior basin, west of Iberia. *Journal of Geophysical Research: Solid Earth* 108(B5).

Péron-Pinvidic G, Manatschal G. 2009. The final rifting evolution at deep magma-poor passive margins from Iberia-Newfoundland: a new point of view. *Int J Earth Sci* 98: 1581–1597. https://doi.org/10.1007/s00531-008-0337-9.

Péron-Pinvidic G, Manatschal G. 2019. Rifted margins: State of the art and future challenges. *Front Earth Sci* 7: 218.

Péron-Pinvidic G, Osmundsen PT. 2016. Architecture of the distal and outer domains of the Mid-Norwegian rifted margin: Insights from the Rån-Gjallar ridges system. *Mar Pet Geol* 77: 280–299. https://doi.org/10.1016/j.marpetgeo.2016.06.014.

Picazo S, Müntener O, Manatschal G, Bauville A, Karner G, Johnson C. 2016. Mapping the nature of mantle domains in Western and Central Europe based on clinopyroxene and spinel chemistry: Evidence for mantle modification during an extensional cycle. *Lithos* 266: 233–263.

Pin C, Paquette JL, Monchoux P, Hammouda T. 2001. First fieldscale occurrence of Si-Al-Na-rich low-degree partial melts from the upper mantle. *Geology* 29: 451–454

Pin C, Monchoux P, Paquette J-L, Azambre B, Wang RC, Martin RF. 2006. Igneous albitite dikes in orogenic lherzolites, Western Pyrenees, France: a possible source for corundum and alkali feldspar xenocrysts in basaltic terrenes. II. Geochemical and petrogenetic considerations. *Can Miner* 44:843–856

Pinet B, Montadert L, Curnelle R, Cazes M, Marillier F, Rolet J, *et al.* 1987. Crustal thinning on the Aquitaine shelf Bay of Biscay, from deep seismic data. *Nature* 325: 513–516.

Pinto VH, Manatschal G, Karpoff AM, Viana A. 2015. Tracing mantle-reacted fluids in magma-poor rifted margins: the example of Alpine Tethyan rifted margins. *Geochem Geophys Geosyst* 16: 3271–3308. https://doi.org/10.1002/2015GC005830.

Pollack HN, Cercone KR. 1994. Anomalous thermal maturities caused by carbonaceous sediments. *Basin Res* 6: 47–51.

Poprawski Y, Basile C, Agirrezabala LM, Jaillard E, Gaudin M, Jacquin T. 2014. Sedimentary and structural record of the Albian growth of the Bakio salt diapir (the Basque Country, northern Spain). *Basin Res* 26(6): 746–766. https://doi.org/10.1111/bre.12062.

Poprawski Y, Basile C, Jaillard E, Gaudin M, Lopez M. 2016. Halokinetic sequences in carbonate systems: An example from the middle Albian Bakio breccias formation (Basque Country, Spain). *Sediment Geol* 334: 34–52. https://doi.org/10.1016/j.sedgeo.2016.01.013.

Poujol M, Boulvais P, Kosler J. 2010. Regional-scale Cretaceous albitization in the Pyrenees: evidence from in situ U-Th-Pb dating of monazite, titanite and zircon. *J Geol Soc* 167: 751–767. https://doi.org/10.1144/0016-76492009-144.

Pross J, Pletsch T, Shillington DJ, Ligouis B, Schellenberg F, Kus J. 2007. Ther-mal alteration of terrestrial palynomorphs in mid-Cretaceous organic-rich mud-stones intruded by an igneous sill (Newfoundland Margin, ODP Hole 1276A). *Int J Coal Geol* 70: 277–291. https://doi.org/10.1016/j.coal.2006.06.005.

Quesnel B, Boiron MC, Cathelineau M, Truche L, Rigaudier T, Bardoux G, *et al.* 2019. Nature and origin of mineralizing fluids in hyperextensional systems: The case of cretaceous Mg metasoma-tism in the Pyrenees. *Geofluids* 2019.

Rat P. 1988. The Basque-Cantabrian Basin between the Iberian and European plates, some facts but still many problems. *Rev Soc Geol Esp* 1: 327–348.

Rat J, Mouthereau F, Brichau S, Crémades A, Bernet M, Balvay M, *et al.* 2019. Tectonothermal evolution of the Cameros basin: Implications for tectonics of North Iberia. *Tectonics* 38(2): 440–469.

Ravier J. 1959. Le metamorphisme des terrains secondaires des Pyrenees. *Mem Soc Geol Fr Nouv Ser* 38.

Renard S, Pironon J, Sterpenich J, Carpentier C, Lescanne M, Gaucher EC. 2019. Diagenesis in Mesozoic carbonate rocks in the North Pyrénées (France) from mineralogy and fluid inclusion analysis: Example of Rousse reservoir and caprock. *Chem Geol* 508: 30–46.

Reston TJ, Pennell J, Stubenrauch A, Walker I, Pérez-Gussinyé M. 2001. Detachment faulting, mantle serpentinization, and serpen-tinite-mud volcanism beneath the Porcupine Basin, southwest of Ireland. *Geology* 29(7): 587–590.

Revelli N. 2013. Structuration de la Zone Nord-Pyrénéenne dans la région de Bessède de Sault, Pyrénées Orientales. Master Sciences de la Terre et de l'Environnement, Mémoire de Master 2. Université d'Orléans.

Ribes C, Ghienne JF, Manatschal G, Dall'Asta N, Stockli DF, Galster F, *et al.* 2020. The Grès Singuliers of the Mont Blanc region (France and Switzerland): stratigraphic response to rifting and crustal necking in the Alpine Tethys. *Int J Earth Sci* 109(7): 2325–2352.

Robert P. 1971. Étude petrographique des matieres organiques insolubles par la mesure de leur pouvoir reflecteur; contribution a l'exploration petroliere et a la connaissance des bassins sedimen-taires. *Petrogr Insoluble Org Mater Based It* 26: 105–135.

Roca E, Sans M, Cabrera L, Marzo M. 1999. Oligocene to Middle Miocene evolution of the central Catalan margin (northwestern Mediterranean). *Tectonophysics* 315: 209–229. https://doi.org/10.1016/S0040-1951(99)00289-9.

Roca E. 2001. The Northwest Mediterranean Basin (Valencia Trough, gulf of Lions and Liguro-Provençal basins): structure and geodynamic evolution. In: Ziegler PA, Cavazza W, Robertson AHF, Crasquin-Soleau S, eds. Peri-Tethys Memoir 6: Pery-Tethyan Rift/Wrench Basins and Passive Margins. Paris: Mémoires Muséum National d'Histoire Naturelle 186, pp. 671–706.

Roca E, Muñoz JA, Ferrer O, Ellouz N. 2011. The role of the Bay of Biscay Mesozoic extensional structure in the configuration of the Pyrenean orogen: Constraints from the MARCONI deep seismic reflection survey. *Tectonics* 30: TC2001. https://doi.org/10.1029/2010TC002735.

Roest WR, Srivastava S. 1991. Kinematics of the plate boundaries between Eurasia, Iberia and Africa in the North Atlantic from the late Cretaceous to the present. *Geology* 19: 613–616.

Roigé M, Gómez-Gras D, Stockli DF, Teixell A, Boya S, Remacha E. 2019. Detrital zircon U-Pb insights into the timing and provenance of the South Pyrenean Jaca basin. *J Geol Soc* 176(6): 1182–1190.

Rosenbaum G, Lister GS, Duboz C. 2002. Relative motions of Africa, Iberia and Europe during Alpine orogeny. *Tectonophysics* 359: 117–129. https://doi.org/10.1016/S0040-1951(02)00442-0.

Rossetti P, Barale L, Bertok C, D'Atri AR, Gerdes A, Martire L, *et al.* 2015. Metamorphic recrystallization related to the circulation of CO_2-rich hydrothermal fluids: the case of the Valdieri marbles (Maritime Alps). In: Il Pianeta Dinamico: sviluppi e prospettive a 100 anni da Wegener Congresso congiunto SIMP-AIV-SoGeI-SGI (Vol. 35, No. 2), pp. 116–116.

Rossy M, Azambre B, Albarède F. 1992. REE and Sr/1bNd isotope geochemistry of the alkaline magmatism from the Cretaceous North Pyrenean Rift Zone (France-Spain). *Chem Geol* 97: 33–46. https://doi.org/10.1016/0009-2541(92)90134-Q.

Rougier G, Ford M, Christophoul F, Bader AG. 2016. Stratigraphic and tectonic studies in the central Aquitaine Basin, northern Pyrenees: Constraints on the subsidence and deformation history of a retro-foreland basin. *C R Geosci* 348(3–4): 224–235.

Roure F, Choukroune P, Berastegui X, Munoz JA, Villien A, Matheron P, *et al.* 1989. ECORS deep seismic data and balanced cross sections; geometric constraints on the evolution of the Pyrenees. *Tectonics* 8: 41–50. https://doi.org/10.1029/TC008i001p00041.

Royden L, Sclater JG, von Herzen RP. 1980. Continental margin subsidence and heat flow: important parameters in formation of petroleum hydrocarbons. *Am Assoc Pet Geol Bull* 64: 173–187. https://doi.org/10.1306/2F91894B-16CE-11D7-8645000102C1865D.

Salardon R, Carpentier C, Bellahsen N, Pironon J, France-Lanord C. 2017. Interactions between tectonics and fluid circulations in an inverted hyper-extended basin: example of Mesozoic carbonate rocks of the western North Pyrenean Zone (Chaînons Béarnais, France). *Mar Pet Geol* 80:563–586

Saspiturry N, Lahfid A, Baudin T, Guillou-Frottier L, Razin P, Issautier B, *et al.* 2020. Paleogeothermal Gradients across an Inverted Hyperextended Rift System: Example of the Mauléon Fossil Rift (Western Pyrenees). *Tectonics* 39(10): e2020TC006206.

Saspiturry N, Razin P, Baudin T, Serrano O, Issautier B, Lasseur E, *et al.* 2019. Symmetry *vs.* asymmetry of a hyper-thinned rift: example of the Mauléon Basin (Western Pyrenees, France). *Marine and Petroleum Geology* 104: 86–105.

Saura E, Ardèvol i Oró L, Teixell A, Vergés J. 2016. Rising and falling diapirs, shifting depocenters, and flap overturning in the Cretaceous Sopeira and Sant Gervàs subbasins (Ribagorça Basin, southern Pyrenees). *Tectonics* 35(3): 638–662.

Scharf A, Handy MR, Ziemann MA, Schmid SM. 2013. Peak-temperature patterns of polyphase metamorphism resulting from accretion, subduction and collision (eastern Tauern Window, European Alps); a study with Raman microspectroscopy on carbonaceous material (RSCM). *J Metamorph Geol* 31: 863–880. https://doi.org/10.1111/jmg.12048.

Sclater JG, Jaupart C, Galson D. 1980. The heat flow through oceanic and conti-nental crust and the heat loss of the Earth. *Rev. Geophys* 18: 269–311. https://doi.org/10.1029/RG018i001p00269.

Seymour NM, Stockli DF, Beltrando M, Smye AJ. 2016. Tracing the thermal evolution of the Corsican lower crust during Tethyan rifting. *Tectonics* 35: 2439–2466. https://doi.org/10.1002/2016TC004178.

Sibuet J-C, Srivastava SP, Spakman W. 2004. Pyrenean orogeny and plate kinematics. *J Geophys. Res Solid Earth* 109: B08104. https://doi.org/10.1029/2003JB002514.

Srivastava SP, Sibuet JC, Cande S, Roest WR, Reid ID. 2000. Magnetic evidence for slow seafloor spreading during the formation of the Newfoundland and Iberian margins. *Earth Planet Sci Lett* 182: 61–76.

Sutra E, Manatschal G, Mohn G, Unternehr P. 2013. Quantification and restoration of extensional deformation along the Western Iberia and Newfoundland rifted margins. *Geochem Geophys Geosystems* 14: 2575–2597. https://doi.org/10.1002/ggge.20135.

Tavani S, Bertok C, Granado P, Piana F, Salas R, Vigna B, *et al.* 2018. The Iberia-Eurasia plate boundary east of the Pyrenees. *Earth Sci Rev* 187: 314–337.

Taylor GH, Teichmüller M, Davis A, Diessel C, Littke R, Robert P. 1998. Organic petrology. Stuttgart, Germany: Gebriider Born-traeger, 704 p.

Teixell A. 1996. The Ansó transect of the southern Pyrenees: Basement and cover thrust geometries. *J Geol Soc* 153: 301–310.

Teixell A. 1998. Crustal structure and orogenic material budget in the west central Pyrenees. *Tectonics* 17: 395–406. https://doi.org/10.1029/98TC00561.

Teixell A, Labaume P, Lagabrielle Y. 2016. The crustal evolution of the west-central Pyrenees revisited: Inferences from a new kinematic scenario. *C R Géosci* 348: 257–267. https://doi.org/10.1016/j.crte.2015.10.010.

Teixell A, Labaume P, Ayarza P, Espurt N, de Saint Blanquat M, Lagabrielle Y. 2018. Crustal structure and evolution of the Pyrenean-Cantabrian belt: A review and new interpretations from recent concepts and data. *Tectonophysics* 724: 146–170.

Ternois S, Odlum M, Ford M, Pik R, Stockli D, Tibari B, *et al.* 2019. Thermochronological evidence of early orogenesis, eastern Pyrenees, France. *Tectonics* 38: 1308–1336. https://doi.org/10.1029/2018TC005254.

Tissot BP, Welte DH. 1984. From kerogen to petroleum. In Petroleum formation and occurrence. Berlin, Heidelberg: Springer, pp. 160–198.

Tomassino A, Marillier F. 1997. Processing and interpretation in the tau-p domain of the ECORS Bay of Biscay expanding spread profiles. *Mem Soc Geol Fr* 171: 31–43.

Trümpy R. 1949. Der Lias der Glarner Alpen. Denkschr. Schweiz. Nat. forsch. Ges., E.T.H. Zuerich, Switzerland, 193 p.

Tugend J, Manatschal G, Kusznir NJ. 2015. Spatial and temporal evolution of hyperextended rift systems: Implication for the nature, kinematics, and timing of the Iberian-European plate boundary. *Geology* 43(1): 15–18.

Tugend J, Manatschal G, Kusznir NJ, Masini E, Mohn G, Thinon I. 2014. Formation and deformation of hyperextended rift systems; insights from rift domain mapping in the Bay of Biscay-Pyrenees. *Tectonics* 33: 1239–1276. https://doi.org/10.1002/2014TC003529.

Ungerer P, Burrus J, Doligez B, Chenet PY, Bessis F. 1990. Basin evaluation by integrated two-dimensional modeling of heat transfer, fluid flow, hydrocarbon generation, and migration. In: AAPG Bulletin. USA: American Association of Petroleum Geologists. http://www.osti.gov/scitech/servlets/purl/6990099.

Vacherat A, Mouthereau F, Pik R, Bernet M, Gautheron C, Masini E, *et al.* 2014. Thermal imprint of rift-related processes in orogens as recorded in the Pyrenees. *Earth Planet Sci Lett* 408: 296–306. https://doi.org/10.1016/j.epsl.2014.10.014.

Vauchez A, Clerc C, Bestani L, Lagabrielle Y, Chauvet A, Lahfid A, *et al.* 2013. Pre-orogenic exhumation of the north Pyrenean Agly Massif (eastern Pyrenees, France). *Tectonics* 32: 95–106. https://doi.org/10.1002/tect.20015.

Vergés J, García-Senz J. 2001. Mesozoic evolution and Cainozoic inversion of the Pyrenean rift. In: Ziegler PA, *et al.*, eds. Peri-Tethyan Rift/Wrench Basins and Passive Margins. Mémoire, pp. 187–212.

Vergés J, Fernàndez M, Martìnez A. 2002. The Pyrenean orogen: pre-, syn-, and post-collisional evolution. *Journal of the Virtual Explorer* 8: 55–74.

Vergés J, Millán H, Roca E, Muñoz JA, Marzo M, Cirés J, *et al.* 1995. Eastern Pyrenees and related foreland basins: pre-, syn- and post-collisional crustal-scale cross-sections. *Mar Pet Geol Integr Basin Stud* 12: 903–915. https://doi.org/10.1016/0264-8172(95)98854-X.

Villard J. 2016. Déformation et thermicité de la couverture mésozoïque dans une structure salifère des Chaînons Béarnais (Zone Nord Pyrénéenne). Master Géosciences, Mémoire de Master 2. Université de Montpellier. http://rgf.brgm.fr/sites/default/files/upload/documents/productionscientifique/Masters/rgf_amipyr2015_ma7_memoire_villard.pdf.

Vissers RLM. 1992. Variscan extension in the Pyrenees. *Tectonics* 11 (6): 1369–1384.

Vissers RLM, Meijer PT. 2012. Mesozoic rotation of Iberia: Subduction in the Pyrenees? *Earth Sci Rev* 110: 93–110. https://doi.org/10.1016/j.earscirev.2011.11.001.

Vissers RL, van Hinsbergen DJ, Meijer PT, Piccardo GB. 2013. Kinematics of Jurassic ultra-slow spreading in the Piemonte Ligurian ocean. *Earth Planet Sci Lett* 380: 138–150.

Vissers RL, van Hinsbergen DJ, van der Meer DG, Spakman W. 2016. Cretaceous slab break-off in the Pyrenees: Iberian plate kinematics in paleomagnetic and mantle reference frames. *Gondwana Research* 34: 49–59.

Wang Y, Chevrot S, Monteiller V, Komatitsch D, Mouthereau F, Manatschal G, *et al.* 2016. The deep roots of the western Pyrenees revealed by full waveform inversion of teleseismic P waves. *Geology* 44(6): 475–478.

Wangen M. 1995. The blanketing effect in sedimentary basins. *Basin Res* 7: 283–298.

Watremez L, Prada M, Minshull T, O'Reilly B, Chen C, Reston T, *et al.* 2018. Deep structure of the Porcupine Basin from wide-angle seismic data. In: Geological Society, London, Petroleum Geology Conference series (Vol. 8, No. 1). Geological Society of London, pp. 199–209.

Winnock E. 1974. Le Bassin d'Aquitaine. In: Debelmas J, ed., Géologie de la France - Vieux massifs et grands bassins sédimentaires. Paris, France: Doin, v. 1, pp. 255–293.

Wopenka B, Pasteris JD. 1993. Structural characterization of kerogens to granulite-facies graphite: applicability of Raman microprobe spectroscopy. *Am Miner* 78: 533–557.

Ziegler PA, Dèzes P. 2006. Crustal evolution of Western and Central Europe. In: Gee DG, Stephenson RA, eds. *European Lithosphere Dynamics* 32: 43–56.